MOLECULAR MODELLING STUDIES ON STRUCTURE AND REACTIVITY OF CATION EXCHANGED AND ISOMORPHOUSLY SUBSTITUTED ZEOLITES

A THESIS SUBMITTED IN PARTIAL FULFILLMENT OF
THE REQUIREMENTS FOR THE DEGREE OF

DOCTOR OF PHILOSOPHY

By
PARITOSH MONDAL

Registration No.: 016 0f 2008

Department of Chemical sciences
School of Science and Technology
Tezpur University
Napaam, Tezpur-784 028
Assam, India

December 2008

Dedicated to -

my parents, my wife and my daughter Kripa

Abstract

MOLECULAR MODELLING STUDIES ON STRUCTURE AND REACTIVITY OF CATION EXCHANGED AND ISOMORPHOUSLY SUBSTITUTED ZEOLITES

ABSTRACT

The goal of the present thesis is to investigate the structure and reactivity of cation exchanged and isomorphously substituted zeolites using quantum chemical methods. We used density functional based reactivity descriptors such as global hardness, global softness, electrophilicity etc. as reactivity parameters of the active sites of zeolites. Zeolites are microporous aluminosilicates that have been extensively used as eco-friendly catalysts in petrochemical industries. The catalytic activity of zeolites can be modified by ion exchange and isomorphous substitution of framework Si atoms with trivalent (Al, B, Ga, etc.) and tetravalent (Ti, Zr, Ge, Sn, etc.) cations. With the aim of exploring the fundamentals of catalytic activity of zeolites, we have made a theoretical investigation on structures of the active sites of catalytically important zeolites such as ZSM-5, faujasite etc. The structure and reactivity of these zeolites are compared with the available experimental results in the literatures. The contents of the thesis have been distributed into eight chapters:

⇒ **In Chapter 1**, we present a brief introduction to zeolites and their catalytic activities towards organic reactions. Zeolites are crystalline, micro-porous aluminosilicates made up of edge-sharing SiO_4 and AlO_4 tetrahedra. Pure silicate structure is charge-neutral; however, the substitution of Si atoms of the zeolite framework with trivalent cations like Al^{3+}, Ga^{3+}, B^{3+} etc. creates negative charges in the framework, which can be compensated by protons, metal cations or both. Catalytic activity of zeolites is highly dependent on the nature of the substituting elements as well as the nature of the exchanged cations. After a brief introduction to zeolites, we discuss the fundamentals of density functional theory (DFT) in this chapter. We present the details of the global and local reactivity descriptors which have been extensively used to study catalytic activity of zeolitic systems. The DFT based reactivity parameters have been used for analyzing the thermodynamic aspects of chemical reactions which provide information related to the reaction paths. We presented the usefulness of the hybrid quantum mechanics/molecular mechanics (QM/MM) method, ONIOM (Our-own-N-layer Integrated molecular Orbital + molecular Mechanics) in the zeolites systems. The region of the system where the chemical process takes place, for example bond breaking and formation, is treated with an appropriately accurate QM method, while the remainder of the system is treated at the lower level, MM method. ONIOM method has been used successfully to study the reaction mechanism of alkylation of aromatic compounds on acidic zeolites.

⇒ **In Chapter 2**, we describe the Lewis acidity of alkali and alkaline-earth cation exchanged faujasite zeolites. Faujasite (FAU) framework structure is composed of four- and six-membered rings. There are five different types of cationic sites in FAU structure which are

designated as SI, SI', SII, SII' and SIII. The SI, SI', SII and SII' are situated at six member rings while in site SIII the cation is coordinated to a four-ring. However, only site SII from the first group of the cationic positions is accessible to guest molecules because it is located in the supercage, while the other three sites are blocked by zeolite framework. The site SIII is also in the supercage, but it is occupied by the cations only when the Al content in the zeolites is high. In the cation exchanged zeolites, the charge compensating cations behave as Lewis acidic sites while the framework oxygen atoms bearing partial negative charges act as Lewis basic sites. Alkali and alkaline earth exchanged faujasite zeolites promotes selective oxidation of hydrocarbon with molecular oxygen. The activation of hydrocarbon and oxygen molecule in cation exchanged zeolites is different from conventional processes. The Lewis acid strength of the exchanged cations play important role in directing guest molecules for chemical activation. DFT calculation on 6T ring cluster of alkali and alkaline earth cation exchanged faujasite zeolite show a significant change in geometric parameters around the cations. The smaller cations have significant effect in changing the geometric parameters around the cations. In this chapter, we have presented that DFT based global reactivity descriptors, *viz.* chemical potential, chemical hardness and softness and electrophilicity values of the cation exchanged zeolites and local reactivity descriptors, relative electrophilicity of the exchanged cation are reliable in predicting Lewis acidity of zeolites.

⇒ **In Chapter 3**, we report density functional studies of the effect of alkali and alkaline earth metal cation on Brönsted acidity of bridging hydroxyl groups present in their close vicinity of mixed form of zeolites (containing two types of charge compensating cations). Brönsted acidity of zeolite materials containing both metal cations and protons as charge

compensating cations is a subject of continued interest. This type of charge compensation is restricted to high Al content in the zeolite framework. We performed cluster model calculations of zeolite in this study. The zeolite framework was modelled with a 9T (T=tetrahedral unit of zeolite) cluster containing six-member ring (SII site) of the supercage of faujasite structure and three other Si atoms in the wall of the supercage. This model cluster is appropriate for investigation of Brönsted acidity which generates the possibility of having a cation and a bridging OH group simultaneously in the material. Strength of Brönsted acid site depends on a number of factors including the structure and the presence of extra framework cations in the proximity of acidic sites. Therefore, understanding the effects of metal cations on the structure and acidity of active sites of H-M-zelites (M=exchanged cation) is a crucial step toward rationalization of their chemical and catalytic properties. Our study revealed that location of the cation in six ring cluster depends upon their radii. With the increasing ionic radii, the cation move away from the plane of the T sites. It is also noticed that the smaller alkali as well alkaline earth cations show less number of coordination. The Brönsted acidity sequence derived from DFT calculations are in agreement with the available experimental results.

⇒ **In Chapter 4**, we present the results of our quantum chemical calculations on the variation of Brönsted acidity in isomorphously substituted ZSM-5 (MFI) zeolite. The framework of ZSM-5 zeolite has been modelled with a 11T model cluster. The Brönsted acidity in the zeolites is developed due to isomorphous substitution of tetravalent Si atom by trivalent Al, Fe, Ga or B atoms. These isomorphously substituted zeolites are used in several industrial processes. For example, Fe-ZSM-5 is an active catalyst for the production

methanol from methane and phenol from benzene. Ga-ZSM-5 shows high selectivity in the aromatization of alkanes. B-ZSM-5 has been shown to be an active catalyst for the production of methanol and isobutene from methoxy butane. The intrinsic acid strength of these catalysts has been found to be very important for their activity. Incorporation of hetero atoms in to the zeolite framework not only changes the acidity but also pore structure of zeolites. Our study demonstrated that Ga—O_b (O_b is the bridging oxygen) distance in [Ga-ZSM-5] is larger than that in Al-[ZSM-5]. This is due to large size of Ga atom compared to Al atom. But B—O_b bond distance is found to be much longer for the smaller atom B in B-[ZSM-5]. This indicates that B atom has a tendency to have trigonal coordination instead of tetrahedral coordination when it is isomorphously substituted in zeolites. We demonstrated the usefulness of the DFT based reactivity descriptors in analyzing the acidity of these zeolites.

⇒ **In Chapter 5**, results of DFT calculations on preferential location of titanium, zirconium and tin atoms in MFI structure are presented. Purely siliceous MFI zeolite is catalytically inactive. However, when some of the silicon atoms are isomorphously substituted with Ti, Zr, Sn, etc., the zeolite shows remarkable activity and selectivity towards organic reactions. For example, titanium silicalite (TS-1) has shown to be very an active and highly-selective catalysts in a number of low-temperature oxidation reactions with aqueous H_2O_2 that include phenol hydroxylation, olefin epoxidation, alkane oxidation, oxidation of ammonia to hydroxylamine, cyclohexanone ammoximation, ammoximation of ortho and para-hydroxyacetophenones etc. Although numerous experimental and theoretical methods have been devoted to the catalytic activity and general structure of TS-1 zeolite, the location of titanium atoms in MFI framework remains the subject of considerable debate. The same is

true for the location of zirconium and tin in zeolite framework. We have presented density functional calculation using 10T cluster model to predict the location of Ti atom in the MFI framework. The geometrical parameters around Ti, Zr and Sn sites are found to be in good agreement with the available EXAFS data. We have also evaluated the substitution energy of Ti, Zr and Sn for Si atom using 10T clusters in all the T sites of MFI framework by considering one virtual reaction. Calculated substitution energies at all the 12 crystallograpically distinct T sites are found to be endothermic. Moreover, the substitution energy values are significantly different for some of the T-sites indicating non-random distributions for the preferential location of Ti, Zr and Sn. Sites T4, T8 and T10 are found to be preferred locations for Ti, Zr and Sn.

⇒ **In Chapter 6**, we present the results of our adsorption studies using ONIOM method that mimic zeolite in a more realistic way. We adapted the ONIOM method to calculate the adsorption of small probe molecules viz. water, hydrogen peroxide, methanol and ammonia towards Ti(IV) centers in the framework of TS-1. Adsorption energies and geometrical parameters of TS-1 zeolites calculated with ONIOM have been compared with that derived from the cluster model approach. ONIOM is a Hybrid QM/MM method where active site could be treated with high level quantum mechanical methods and the rest of the environment could be modelled by low level QM or MM methods. Geometry optimization can take the advantage of this partitioning of the material. In our ONIOM calculations we treated the active region with DFT method and environment with low level HF (HF/3-21G) method. The calculated Ti—O bond distance of 5T bare cluster is found to be in the range of 1.796-1.797 Å. However, the Ti—O bond length of 16T bare cluster calculated by ONIOM method is found to be 1.792-1.809 Å. Ti—O distances of adsorption complex of 5T and 16T

cluster with probe molecules are found to be nearly equal. The binding energies of the probe molecules calculated with ONIOM method are higher than that of 5T cluster model calculations. The calculated geometrical parameters and the binding energy values of ONIOM method are very close to the available experimental and theoretical results. We also presented that ammonia molecule is more efficient in distorting the geometrical parameters around the Ti atom in the adsorption complexes.

⇒ **In Chapter 7**, we study the reaction mechanisms of some of the important reactions in catalysis using the cluster method. Here we investigate the alkylation of benzene with alkene over acidic faujasite zeolites. Stepwise and concerted mechanisms of the alkylation reaction are considered. For the stepwise mechanism, the alkylation starts with the protonation of the adsorbed ethylene by an acidic zeolite proton leading to the formation of the ethoxide intermediate and, subsequently, the ethoxide reacts with a benzene molecule forming an ethylbenzene product. For the concerted mechanism, the alkylation of benzene takes place in a single reaction step without prior ethoxide formation.

⇒ **In Chapter 8,** important points emerging out of the present investigation are mentioned on the basis of the results of the work carried out.

Declaration

I hereby declare that the thesis entitled "***Molecular Modelling Studies on Structure and Reactivity of Cation Exchanged and Isomorphously Substituted Zeolites***" being submitted to the Department of Chemical Sciences, Tezpur University, is a record of original research work carried out by me. Any text, figures, results or designs that are not of own devising are appropriately referenced in order to give credit to the original author(s). All sources of assistance have been assigned due acknowledgement I also declare that neither this work as a whole nor a part of it has been submitted to any other university or institute for any other degree, diploma or award.

Date: 30.12.2008

Place: Tezpur

Paritosh Mondal

(Paritosh Mondal)

TEZPUR UNIVERSITY

(A Central University established by an Act of Parliament)

NAPAAM, TEZPUR – 784028

DISTRICT: SONITPUR :: ASSAM:: INDIA

Ph : 03712 – 267004
03712 – 267005
Fax : 03712 – 267006
03712 - 267005
e-mail : adm@agnigarh.tezu.ernet.in

Dr. Ramesh Ch. Deka
Reader
Department of Chemical Sciences

This is to certify that the thesis entitled "***Molecular Modelling Studies on Structure and Reactivity of Cation Exchanged and Isomorphously Substituted Zeolites***" submitted by Mr. Paritosh Mondal for the degree of Doctor of Philosophy of Tezpur University, embodies the record of original investigation carried out by him under my supervision. He has been duly registered, and the thesis presented is worthy of being considered for the Ph. D. Degree. This work has not been submitted for any degree of any other University.

Date: 30-12-2008

Place: Tezpur

Ramesh Ch. Deka
Signature of the Supervisor

Acknowledgement

I would like to express my deep sense of gratitude and respect to all my teachers, past and present, who have contributed immensely at various stages of my life. This is my humble effort to thank them all. I wish to thank my supervisor Dr. Ramesh Chandra Deka, Reader, Department of Chemical Sciences, Tezpur University for his skillful guidance and encouragement during the thesis work. I am very grateful for his readily available discussion and advice.

I would like to extend my thanks to all the faculty members and staff of the department of Chemical Sciences, Tezpur University for their help in various ways during my stay in this department.

I extend my sincere gratitude to Prof S. K, Dolui, Prof. N. S. Islam, Prof. T K Maji, Dr. R.K, Dutta, Dr N. Karak and other faculty members of the Department of Chemical Sciences, Tezpur University, for their help and good wishes.

It is my pleasure to thank my labmates Bulumoni Kalita, Pubalee Sharma, Kalyan Hazarika and Ajanta Deka for their active co-operation.

Special thanks are due to Dr. C. R. Bhattacharjee , Prof. N.V.S. Rao, Prof. M. R. Islam, , Dr. S. B. Paul, and Dr. M. K, Paul, my colleagues of the department of Chemistry,

Assam University, Silchar and my ex. colleagues of the department of Chemistry, Darrang College, Tezpur for their help and encouragement.

The inspiration, blessings and moral support of my Ma, Baba and my brothers Bipul, Dilip and Jayanta boosted me to carry out my research work to completion.

I would like to express deep sense of gratitude to my father-in-law and mother-in-law for their support and good wishes.

I would like to thank my friends and all the research scholars of the Department of Chemical Sciences Gohain da, Pankaj, Raju, Jyotishmoy, Diganta, Rabiul, Jatindranath, Sibdas, Siva Prasad, Harekrishna, Kalyan, Uday, Subrata, Surajit, Laksha, Binod, Lakshi, Suresh, Jeena, Biplap and Buddha for their help and support during the course of my work.

Finally, I want to thank my wife Krishna and my daughter Kripa for their understanding and endless support through encouragement and as a source of inspiration. Without their support, this work would not have been possible.

Department of Chemical Sciences

Tezpur University

Date: 30.12.2008

Paritosh Mondal.

(Paritosh Mondal)

Table OF CONTENTS

List OF TABLES

List OF FIGURES

List OF ABBREVIATIONS

AM1	Austin Model 1 (Semi-emperical methods)
AlPO-5	Aluminophosphate – five
B3LYP	Becke's 3 parameter exchange-correlation functional (Using Lee, Yang and Parr's correlation function)
BEA	Beta (Zeolite structure-type)
CHA	Chabazite (Zeolite structure-type)
DFT	Density Functional Theory
DMol3	Molecular modelling package
DNP	Double Numerical with Polarization basis set
EA	Electron Affinity
f	Fukui function
FAU	faujasite (Zeolite structure type)
Gaussian03	Molecular modelling package
HPA	Hirshfeld Population Analysis
HUMO	Highest Occupied Molecular Orbital
IE	Ionization Energy
IUPAC	International Union Pure and Applied Chemistry
LTA	Linde Type A
LUMO	Lowest Unoccupied Molecular Orbital

m	*meta*
MEL	ZSM-11 (Zeolite structure-type)
MFI	ZSM-5 (Zeolite structure-type)
MNDO	Modified Neglect of Diatomic Overlap
MOR	Mordenite (Zeolite structure-type)
MPA	Mulliken Population Analysis
o	*ortho*
ONIOM	Our-own-N-layered Integrated Molecular Orbital + Molecular Mechanics
p	*para*
QM/MM	Quantum Mechanics/Molecular Mechanics
q_K	atomic charge
S	Global softness
s_k	atomic softness
SBU	Secondary Building Units
TS	Transition State
TS-1	Titano-Silicate-1
Y	Faujasite type zeolite with low Si/Al ratio
η	global hardness

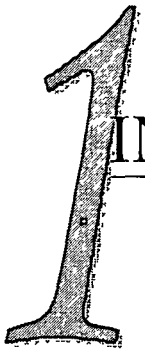

INTRODUCTION

1.1 Zeolites

Zeolites are crystalline aluminosilicates made up of corner-sharing SiO_4 and AlO_4 tetrahedra that adopt verities of three dimensional structures having channels and cavities of molecular dimension.[1-4] The effective pore sizes of zeolites range from ~3Å to aver 10Å, which is sufficient to permit diffusion of catalytically interesting organic molecules through their pores. This fact combined with the possibility of generating active sites inside the channels and cavities of zeolites produces a very unique type of catalyst that by itself can be considered as catalytic micro reactor for various reactions such as hydrocarbon cracking, isomerization, alkylation of hydrocarbons, and alcohol conversion to gasoline in the oil refining and petroleum industries.[5-8]

According to Smith[9], "a zeolite is an aluminosilicate with a framework structure enclosing cavities occupied by large ions and water molecules, both of which have considerable freedom of movement, permitting ion-exchange and reversible dehydration." However, all synthetic zeolites don't obey one or more of these criteria. Zeolites were discovered in 1756 by the Swedish mineralogist Axel Fredrick Cronstedt. The minerals were named zeolites which mean "boiling stones"

in Greek (*Zeo* = boil and *lithos* = stone). Zeolites seem to boil when heated due to loss of water.[10]

The chemical formula of a zeolite is represented by:

$$M^{n+}_{x/n}[(AlO_2)_x(SiO_2)_y]wH_2O$$

where M represents the exchangeable cation of valency n and it is generally Group I or Group II cation, although other metal, non-metal and organic cations can also balance the negative charge created by the presence of $[AlO_4]^-$ units in the framework. The Si/Al ratio of a zeolite is indicated by y/x, and water content inside the side cages and /or channels of the zeolite is represented by w. The square bracket contains framework atoms of a zeolite while the remaining atoms reside in specific sites of the channels. Water molecules present in a zeolite can easily be removed by heating up to about 350°C, which is known as activation.[11]

Zeolites can be divided into two groups: natural and synthetic. Approximately 40 natural zeolites have been found and more than 150 zeolites have been synthesized so far.[12] Natural zeolites are produced by two ways: (1) the most abundant natural zeolites such as clinoptilolites, philipsite, chabazite, mordenite and heulandite are believed to be formed through sedimentary processes at temperatures below 100°C while (2) zeolites such as laumontite and analcime are formed from volcanic materials at temperature above 100°C. Most of the natural zeolites can also be synthesized in laboratory. Synthetic zeolites avoid the problem of impurities and changes in chemical composition depending on the sources and allow to control their properties. Synthetic zeolites have acronyms like zeolite A, zeolite X, zeolite Y, ZSM-5 etc. The IUPAC has suggested a general way to name zeolite frameworks using three capital letter codes.[13] These codes are usually derived from the name of the material. Thus CHA stands for all structures that have a Chabazite framework and FAU stands for all

structures with faujasite framework. Synthetic frameworks are also represented by three capital letter codes, which usually contain the name of the company or institute that synthesized them followed by a number or letter. Thus ZSM-5 and ZSM-11, which are synthesized by Mobil Company, are called MFI (**M**obil **Fi**ve) and MEL (**M**obil **El**even), while those synthesized by Linde are called LT indicating **L**inde **T**ype (LTL, LTA etc.). The IUPAC names of some typical zeolites along with their pore dimensions are listed in Table 1.1. The largest amount of zeolites are used as ion exchangers, e.g. as substitute for phosphates in detergents.

Table 1.1: Pore dimensions of some typical Zeolites

Pore size	Code	Abbreviated name	Full name	Pore (Å)
Small	LTA	**L**inde **T**ype **A**	Zeolite A (Linde Division, Union Carbide)	4.5 × 4.5
	CHA	**Cha**bazite		3.8 × 3.8
	ERI	**Eri**onite		3.6 × 5.2
Medium	MFI	ZSM-5 (**fi**ve)	**Z**eolite **S**ocony **M**obil – five	5.1 × 5.6
	MEL	ZSM-11 (**El**even)	**Z**eolite **S**ocony **M**obil – eleven	5.3 × 5.6
	MTT	ZSM-23 (**t**wenty **t**hree)	**Z**eolite **S**ocony **M**obil – twenty three	4.5 × 5.2
	EUO	**EU**-1 (**o**ne)	**E**dinburg **U**niversity – one	4.1 × 5.7
	AEL	$AlPO_4$-11 (**El**even)	Aluminophosphate – eleven	3.9 × 6.3
Large	MOR	**Mor**denite		6.5 × 7.0
	BEA	Zeolites **Beta**		7.6 × 6.4
	AFI	$AlPO_4$-5 (**fi**ve)	Aluminophosphate – five	7.3
	EMT	**EMC**- 2 (**t**wo)	**E**lf **M**ulhouse **C**himie - two	7.4×6.4
	FAU	**Fau**jasite		7.4

They are also used as drying agents and in gas purification. Nevertheless the most important application of zeolites lies in catalysis. When a tetravalent Si atom is isomorphously substituted by a trivalent cation like Al, a net negative charge is generated in the zeolite framework and this negative charge is compensated by cations like Na^+, K^+, Ca^{2+}, Mg^{2+} and others. These positive ions are rather loosely held and can readily be exchanged for others. When this negative charge of zeolite framework is compensated by a proton, a bridging hydroxyl group is formed and the zeolite behaves as Brönsted acid. In alkali or alkaline-earth metal exchanged zeolites, the metal cations act as Lewis acid sites while the framework oxygen atoms bearing partial negative charges behave as Lewis base sites. A variety of trivalent (B, Ga, Fe, As etc.)[14-17] and tetravalent (Ti, Ge, V, Sn, Zr etc.)[18-23] metal ions have been incorporated in to zeolite structures to modify their catalytic activities. These metallo-silicate analogs of zeolites are commonly referred as molecular sieves.

Zeolites such as ZSM-5, FAU etc. are very important for industrial application because of their pore sizes comparable to that of small organic molecules forming the basis for shape-selective catalysis. The relatively high stability of zeolites towards thermal, hydrothermal and chemical treatment leads to their use as catalysts in oil refining, petrochemical industry and organic synthesis for production of fine chemicals. Moreover, zeolites are (1) shape-selective, (2) tunable, (3) regenerable, (4) non-toxic, (5) long-lasting, (6) easily separated and (7) easily disposed. Thus, zeolites also play a significant role in developing newer green catalysts.

1.1.1 Structure of Zeolites

Three dimensional structures of zeolites are formed by linking tetrahedral primary building units, TO_4, where the central T atoms are either Si or Al surrounded by four

oxygen atoms. Linkage of these tetrahedral building units via oxygen in certain ways produces infinite framework structures of zeolites. A zeolite framework structure is always described in terms of a finite number of specific combination of TO_4 tetrahedra which is called secondary building units (SBU).[1,13,24] These units are simple arrangements of tetrahedral atoms that form four, five, six or eight member rings or a combination of them. Some typical SBU are shown in Figure 1.1. Linkage

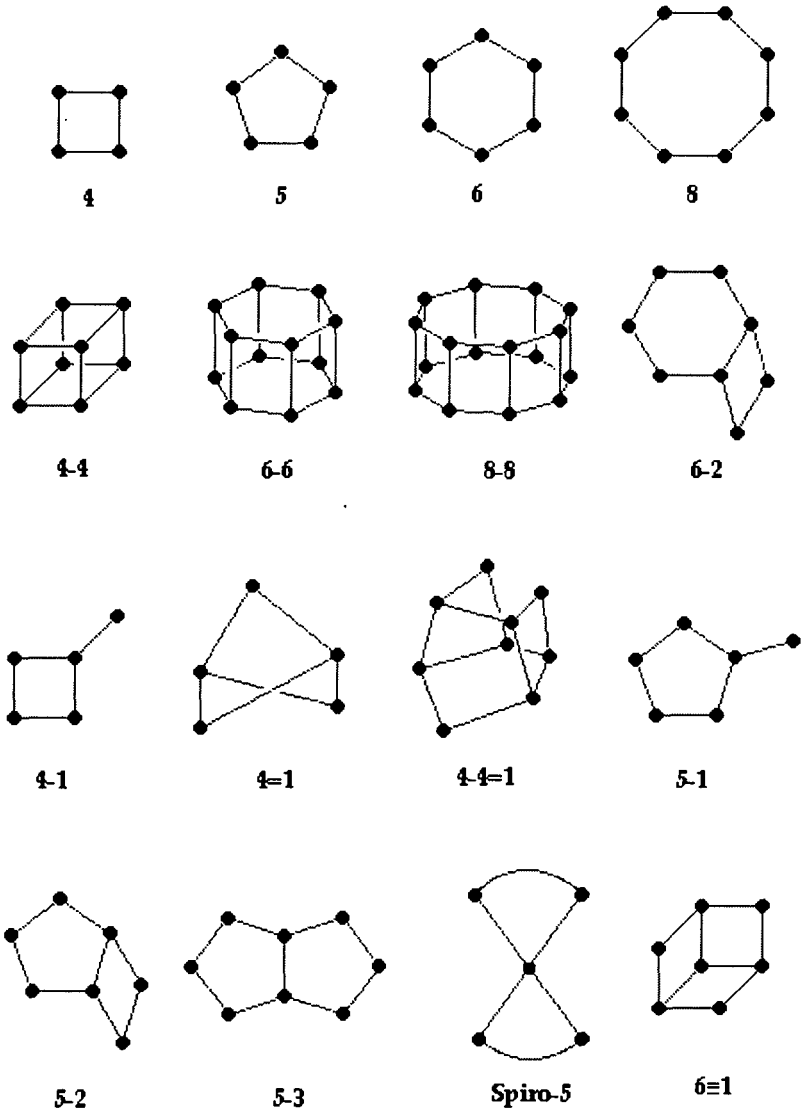

Figure 1.1: Secondary building units (SBU) of zeolites. The corners of the polyhedra represent tetrahedral (T) atoms.

of these SBU via oxygen atoms generates three dimensional structures of zeolites. There are about 20 such SBU identified so far. Usually each zeolite framework is made up of only one type of SBU, although rare, some can have a combination of different SBUs. In fact, a three-dimensional network of a zeolite looks very complicated although it is composed of pretty simple SBUs. Based on their pore sizes, zeolites can be classified into small-pore (pore size < 5 Å, 8-membered ring), medium-pore (pore size 5-6 Å, 10-membered ring) and large-pore (pore size 7-8 Å, 12-membered ring) zeolites. Purely siliceous form of zeolites where all the tetrahedral units are SiO_4 show properties different from aluminosilicates. Because the pure silica frameworks are neutral and have strong hydrophobic surfaces whereas aluminum containing frameworks are negatively charged and strongly hydrophilic.

ZSM-5 zeolite has been extensively studied as it is used in various industrial catalytic processes. Its unit cell has 96 T sites, 192 O sites, and a number of charge compensating cations depending on the Si/Al ratio, which ranges from 10 to infinity. The Si/Al ratio is the fundamental characteristic of zeolites.[26,27] This Si/Al ratio is different for different types of zeolites. However, each framework has a Si/Al range within which it is stable[28]. The distribution of Al in zeolite framework is controlled by the Löwenstein rule,[29] which states that pairs of neighbouring AlO_4^- tetrahedra are forbidden. The lowest possible Si/Al ratio is 1, which has been observed in Zeolite-A.

1.1.2 Shape Selectivity of Zeolites

Since early 1960's the field of petroleum refining has undergone important changes due to the use of zeolite as acid catalysts. Catalysis by zeolites can be applied to most of the reactions that are generally catalyzed by mineral acids. Besides

their acidity, large surface area, uniquely defined pore system, chemical and thermal stability and cation exchanged capacity are important in determining catalytic activity and selectivity.[30] Zeolites have been used as shape selective catalysts in a variety of hydrocarbon reactions, such as cracking, alkylation and isomerization. Catalytic activity of zeolites also depends on proton donor capabilities of the acidic hydroxyl group and the electron donor capabilities of the bridging oxygen.[31] These parameters in turn depend on chemical composition and structure of zeolites, crystallographic siting of oxygens, concentration and distribution of acidic sites in the framework.[32] The shape selectivity of a zeolite is controlled by the pore dimension and position of catalytic sites residing inside the channels.

The concept of shape selectivity was first introduced by Weisz *et al.* from Mobil laboratory.[33,34] Based on the observations of the reactions, three types of shape selectivity models have been proposed to rationalize the observed phenomena in reactions catalyzed by porous catalyst: reactant-shape selectivity, product-shape selectivity and transition state-shape selectivity. Reactant-shape selectivity refers to the selectivity occurring because of the different sizes of the reactants. When a mixture of at least two reactants with different sizes is fed into a reactor, the larger reactant can't enter the zeolite pores to reach most of the active sites in the channel. Those banned bulkier reactants may contact external active sites to undergo the reaction or leave the reactor without being converted to the products. Reactant shape-selectivity for cracking of straight-chain and branched C_7 hydrocarbons is illustrated in Figure 1.2.

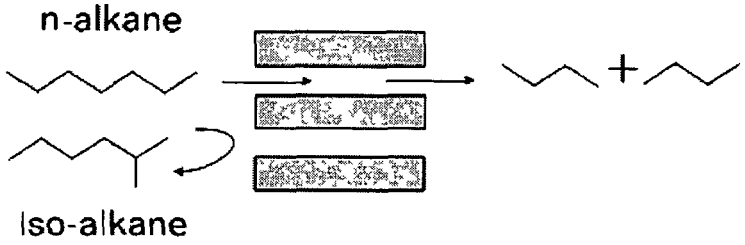

Figure 1.2: Schematic diagram of reactant shape selectivity: branched bulky chains are banned from entering the pores.

In product shape selectivity, all the reactants are so small that they can enter into the channels of the zeolite, where they may form isomers with different sizes inside the channels because the dimension at the intersections are often larger than the pore openings. But only those species that are smaller than pore openings can escape from the channels of zeolites and join the reaction mixture; the bulkier species are unable to escape from the channel and they are therefore excluded from the reaction mixture. The product-shape selectivity can be explained by the product distributions in the alkylation reaction of toluene with methanol over ZSM-5 zeolite;[35] the slimmer *p*-xylene, the main product, diffuses out of the channel 100-1000 times faster than the other two bulkier *o*–, and *m*– isomers. Product selectivity for *p*-xylene over *ortho* and *meta* xylenes are illustrated in Figure 1.3.

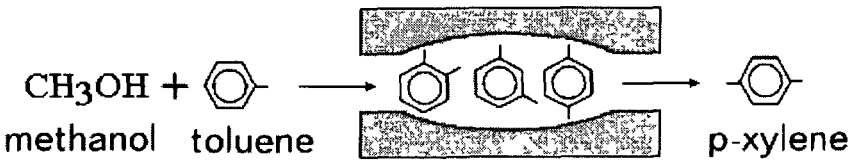

Figure 1.3: Product selectivity for *p*-xylene over *o* – and *m* – forms.

Mass diffusion, which is also called hindered diffusion, is the origin for both reactant- and product-shape selectivity. In a real reaction, it is impossible to completely exclude the bulky reactants from entering the channels of the zeolite or to completely encapsulate the bulky products in the channel of the zeolite. It is generally observed that the rate of disappearance of one of the bulkier reactants, or the rate of formation of one of the bulkier products, is lower than it would have been in the absence of mass diffusion.

Sometimes, the zeolite cavity does not have enough space to accommodate a particular transition state necessary to form a product. This is classified as transition state-shape selectivity. Csicsery [36] reported the first transition state shape selectivity in 1971. A typical example of transition state shape selectivity is *m*-xylene isomerization into *o*-xylene, *p*-xylene and toluene; the *o*-, and *p*-xylene form from a single molecule transition state whereas toluene forms from a twin molecule transition state. As a result, the *o*- and *p*- xylene form favorably whereas the toluene product, which has to go through a bulkier transition state, is suppressed.

Another example of transition state shape selectivity is the disproportionation of *m*-xylene to toluene and trimethylbenzenes in the wide pore zeolites Y and it is illustrated in Figure 1.4. In the large zeolites cavity, bulky diphenylmethane carbenium ion transition states can be formed as precursors for methyl group rearrangement, thereby less bulky carbenium ion B is favored. Thus the product consists mainly unsymmetrical 1, 2, 4-trimethylbenzene rather than mesitylene (case A). In contrast, in ZSM-5, with its medium sized pores, monomolecular xylene isomerization dominates, and the above-mentioned disproportionation is not observed as a side reaction. Sometimes it is difficult to differentiate between the product-shape selectivity and transition-shape selectivity in a reaction. Reactant- and product-shape

selectivities are directly related to their mass diffusion and to the diffusion path length in the zeolite,

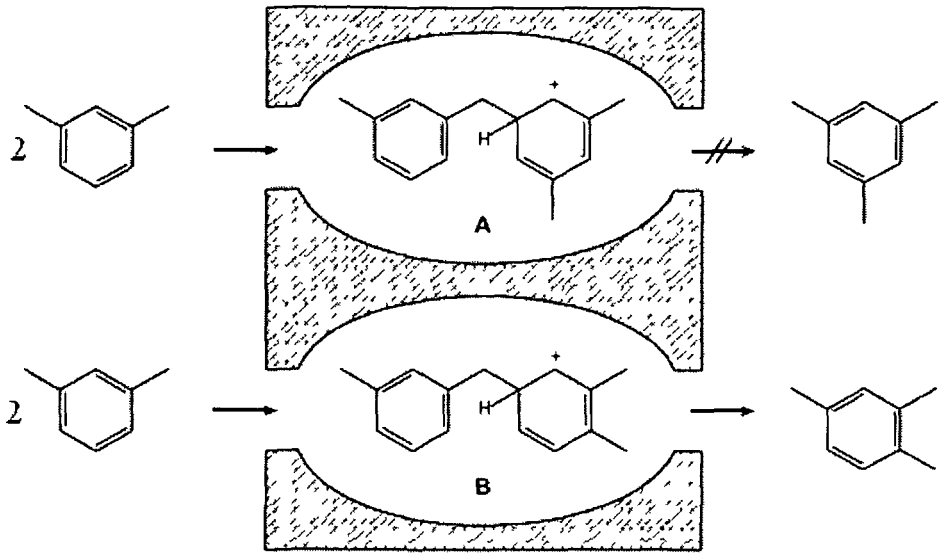

Figure 1.4: Restricted transition state selectivity of disproportionation of *m*-xylene.

which is dependent on the size of the catalyst. In contrast transition state shape selectivity is based on the intrinsic shape of the channels in the zeolite, not on the path length. This is the criterion to distinguish the transition state shape selectivity from product shape selectivity.[37]

1.1.3 Isomorphous substitution of Si

Substitution of Si^{4+} in the tetrahedral positions of a zeolite framework with compatible elements is known as isomorphous substitution. The main purpose of this isomorphous substitution is to modify the catalytic activity making it suitable for a given reaction. Generally the tetrahedral Si^{4+} positions are substituted by trivalent cations like B^{3+}, Al^{3+}, Fe^{3+}, Cr^{3+}, V^{3+}, Ga^{3+}, As^{3+} and tetrahedral cations such as Ti^{4+}, Sn^{4+}, Zr^{4+}, Ge^{4+}, and V^{4+}. There are many reports dealing with isomorphous substitution of zeolites and its effect on the chemical composition with new

applications. A remarkable advancement was achieved with replacement of Si^{4+} by Ti^{4+} in the lattice of silicate-1[38] which is the pure siliceous analog of ZSM-5. The resulting titanosilicate is termed as TS-1. Titanium incorporated ZSM-5 (TS-1) shows excellent catalytic properties in a number of catalytic oxidation reactions with aqueous hydrogen peroxide as the oxidant under mild conditions.[39] When the substitution is carried out on silicalite-2 [40] which is the pure siliceous analog of ZSM-11, the resultant titanosilicate is known as TS-2. The isomorphous substitution of Si^{4+} in a zeolitic framework depends on several factors.

1. Ionic radius of the new cation, greater the differences of the radius of new cation with Si^{4+}, smaller is the possibility of substitution.
2. The new ion should be stable with tetrahedral coordination.
3. Isomorphous substitution is possible when electronegativity and ionizational potential of the new ion are close to Si^{4+} ion.
4. The site and extend of substitution depends on the topology of the zeolitic framework.

Ionic radii of some cations that have been incorporated in the zeolite framework are listed in Table 1.2.

Table 1.2: Cations that exhibit tetrahedral coordination and their ionic radii.

Cation	Radius (Å)	Cation	Radius (Å)
Si^{4+}	0.40	Ga^{3+}	0.61
Al^{3+}	0.53	Ge^{4+}	0.53
B^{3+}	0.25	Ti^{4+}	0.56
Be^{2+}	0.41	V^{5+}	0.49
Fe^{3+}	0.63	Cr^{3+}	0.75

1.2 Importance of Computational Chemistry

Because the generation of active sites in zeolites and their use in catalysis are mainly based on trial and error methods, there is an increasing demand of theoretical predictions of zeolite properties, adsorption, diffusion and interaction of reactants and product molecules. The understanding these properties of zeolites can greatly facilitate the design of new zeolite catalysts. A large intensification of the theoretical studies of zeolites can be seen in the last two decades[41-47].

Accompanying the rapid development of computer science, computational chemistry opens a considerable opportunity in the field of materials science research. Although the developments in experimental techniques have enabled us to obtain highly accurate information of zeolytic materials, most of the techniques are very expensive and it is difficult to make trials-and-errors in experiments for designing new catalysts. Here, computational methods may play a significant role in tailoring materials required for a particular purpose. Computational chemistry may also play a vital role in designing catalyst for various organic reactions in a "green chemistry" way. Computational chemistry can go from description of model system by analytical methods to representation of realistic molecular structures and associated physical and chemical properties by numerical modelling.

The computational chemistry combines all numerical methods based on molecular mechanics (MM), molecular dynamics (MD), Monte Carlo (MC) and quantum chemistry (QC) employed for prediction of the structure, electronic and optical properties of materials[48-56]. The basic principle of these simulations is the accurate determination of the total energy of an investigated system. In this thesis we have mainly used quantum chemical methods, Hartree-Fock, density functional theory and

quantum mechanics/molecular mechanics (QM/MM) that have been discussed briefly in the following sections.

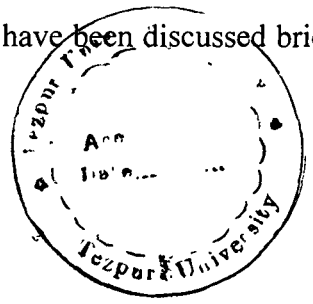

1.2.1 Molecular Mechanics

Molecular mechanics simulations are based on the classical laws of physics to predict the structures and properties of molecules. Molecular mechanics represent the interactions between the atomic species by force field method. The term forcefield arises because the negative of the first derivative of the potential energy of a particle with respect to displacement along some direction is the force on the particle; a forcefield E(x, y, z, coordinates of atoms) can be differentiated to give the force on each atom. Molecular mechanics calculations are performed based on nuclei interactions and don't treat the electrons in a molecular system explicitly. However, electronic effects are included implicitly in force fields through parameterizations. These parameterizations have not been carried out for transition states hindering the study of reaction mechanism using molecular mechanics. The approximations adopted in molecular mechanical calculation make the computations inexpensive. Hence, this method can be applied for large systems containing thousands of atoms, such as bio-molecules. The main disadvantages of molecular mechanics are: first, this method is applicable only for a limited class of molecules for which the force field is parameterized. Secondly, molecular mechanics methods can't be applied for the systems where electronic effects are prominent. For example, this method cannot describe process involving bond formation or bond breaking.

1.2.2 Quantum Chemical Methods

1.2.2.1 Hartree-Fock method

Methods for the calculation of electronic structure of molecules based on quantum mechanics have become important and widespread. The electronic structure and total electronic energy of atoms, molecules and crystals can be obtained by solving the time-independent, non-relativistic Schrödinger equation. However, the electronic structure of molecules and crystals are solved within the Born-Oppenheimer approximation. In this approximation the motion of electrons and nuclei are separated by expanding the total molecular wave function as a product of electronic and nuclear wave functions. The approximation allows us to calculate the wave function for electrons moving in the potential field of the nuclei, treated as fixed point charges. The time-independent Schrödinger equation for the electrons can be written as

$$\hat{H}\psi = E\psi \tag{1.1}$$

The Hamiltonian, $\hat{H}$, is expressed as

$$\hat{H} = -\frac{\hbar^2}{2}\sum_i \frac{1}{m_i}\left(\frac{\delta^2}{\delta x_i^2} + \frac{\delta^2}{\delta y_i^2} + \frac{\delta^2}{\delta z_i^2}\right) + \sum_{i<j}\frac{e_i e_j}{r_{ij}} \tag{1.2}$$

The first quantity on right hand side account for the kinetic energies and the second term accounts for the potential energies, including attractions or repulsions between particles. The equation (1.2) is the time independent Schrödinger equation. However, the time dependent Schrödinger equation used while studying the transient phenomena such as rapidly oscillating electric fields or scattering. Even for the smallest systems, the exact solution of Schrödinger equation is not possible. Various mathematical approximations have been applied for the solution of Schrödinger equation. Quantum chemical methods are divided in to two classes: semi-empirical

methods (such as CNDO, MNDO ete.) and non-empirical (*ab initio*, DFT etc.) methods. Semi-empirical methods neglect many of the differential overlaps. Semi-empirical methods use some parameters derived from experimental data to simply the calculations. Solution of the Schrödinger equation approximately depends upon the availability of appropriate parameters for the chemical system of interest. The semi-empirical methods are less demanding than *ab initio* methods, but may lead to large errors for some systems. *Ab initio* calculations are based on the laws of quantum mechanics and also depend on some physical constants such as speed of light, the masses, charges of the electrons and nuclei, Plank's constant etc. The goal of either method is to obtain the wave function of orbital $\phi(r)$ occupied by each electron, the eigenvalue, ε_i corresponding to that orbital, the total energy, E_{tot} and the atomic force, F on each atom by solving the Schrödinger equation. The quantum chemical calculation is fairly a standard method used for studying chemisorptions and reaction mechanism on zeolite systems. This technique can be used to determine the reaction path and sorbed intermediate species in the cages of zeolites.

1.2.2.2 Density Functional Theory

In 1964, Hohenberg and Kohn proposed DFT [57], which provided an alternative way to solve the Schrodinger equation. They have proven that the ground-state electronic energy is determined completely by the electron density ρ in the system of non-interacting electrons. Their theory is different from the traditional quantum chemical methods based on the wavefunctions. In wavefunction based methods, the wavefunction governs everything, and the electron density results from it. However, in DFT, the picture is reversed. There exists a one-to-one correspondence between the electron density of a system and the energy, that is, there is a map ($v_s(\mathbf{r}) \leftrightarrow \emptyset_s(\mathbf{r}) \leftrightarrow$

$\rho_s(\mathbf{r})$). The ground-state density ρ ($\mathbf{r}$) uniquely determines the external potential $v(\mathbf{r})$ and also the ground-state wave function $\Psi_S(\rho)$. Consequently every observable quantity of a quantum mechanical system is in principle uniquely determined by the electron density alone. In other words, all observables of a many electron system are unique functionals of the electron density. This is the theoretical basis of DFT.

In density functional theory (DFT), quantum chemical calculations can be performed very conveniently in terms of single particle orbitals within the Kohn-Sham formalism[58]. The Kohn-Sham orbitals $\{\phi_i(r)\}$ are given by equation (1.3),

$$\hat{H}_S\phi_i(\mathbf{r}) \equiv \left[-\frac{1}{2}\nabla^2 + v_S(\mathbf{r})\right]\phi_i(\mathbf{r}) = \varepsilon_i\phi_i(\mathbf{r}) \tag{1.3}$$

where, $\mathbf{r}$ is the space vector and $v_{S(\mathbf{r})}$ is external potential. Once accurate Kohn-Sham orbitals $\phi_i(r)$ have been constructed, the electron density can be obtained exactly from a single-particle equation representing an electron moving in an effective field of the other electrons, that is, the electron density $\rho(\mathbf{r})$ is obtained using the following formula by summing over all the occupied orbitals:

$$\rho(\mathbf{r})=\Sigma_i f_i |\phi_i|^2 \tag{1.4}$$

The kinetic, exchange, and correlation energies can be calculated from

$$E^{KS} = \left\langle \Psi_S \middle| \hat{H} \middle| \Psi_S \right\rangle = T_S + V + W_H + E_X \tag{1.5}$$

$$T_S = -\frac{1}{2}\sum_\sigma \sum_{i=1}^{N_\sigma} \int \phi_{i\sigma}^*(\mathbf{r})\nabla^2\phi_{i\sigma}(\mathbf{r})\mathrm{d}\mathbf{r} \tag{1.6}$$

$$E_X = -\frac{1}{2}\sum_{\sigma\sigma'}\sum_{i=1}^{N_\sigma}\sum_{j=1}^{N_\sigma}\iint \frac{\phi_{i\sigma}^*(\mathbf{r})\phi_{j\sigma}(\mathbf{r})\phi_{j\sigma'}^*(\mathbf{r}')\phi_{i\sigma'}(\mathbf{r}')}{|\mathbf{r}-\mathbf{r}'|}\mathrm{d}\mathbf{r}\mathrm{d}\mathbf{r}' \tag{1.7}$$

$$E_C = E_{XC} - E_X = E - E^{KS} \tag{1.8}$$

Obviously, the determination of the KS orbitals is a necessary step, but it turns out that the difficult part in the construction of the accurate KS orbital is the

determination of the KS potential $v_s(\mathbf{r})$ corresponding to accurate target density $\rho_s(\mathbf{r})$. In order to obtain an expression for the Kohn-Sham potential $v_s(\mathbf{r})$, the Hohenberg-Kohn functional for the interacting system is partitioned as follows:

$$F_{HK}[\rho] = T_S[\rho] + \frac{1}{2}\iint \frac{\rho(\mathbf{r}_1)\rho(\mathbf{r}_2)}{|\mathbf{r}_1 - \mathbf{r}_2|} d\mathbf{r}_1 d\mathbf{r}_2 + E_{xc}[\rho] = T_S[\rho] + W_H[\rho] + E_{xc}[\rho] \quad (1.9)$$

Here, the first second and third term is kinetic energy, coulomb interactions between core charges, and exchange-correlation, respectively. Thus the Kohn-Sham potential $v_s(\mathbf{r})$ can be subdivided into the following parts:

$$v_S(\mathbf{r}) = v_{ext}(\mathbf{r}) + v_H(\mathbf{r}) + v_{xc}(\mathbf{r}) \quad (1.10)$$

where, v_{ext} is the external potential (the Coulomb field of the nuclei) and v_H is the Hartree potential, which is the classical Coulomb repulsion between the electrons, and the v_{xc} is the potentials corresponding to the exchange-correlation energy which is the only unknown part. Since v_{ext} is known and v_H calculation is straightforward for any given density, the construction of v_s amounts to the unknown potential $v_{xc}(\mathbf{r})$. Therefore the determination of the accurate KS potential (in particular the exchange-correlation part $v_{xc}(\mathbf{r})$) from the accurate electron density ρ allows us to judge approximations to the energy functional $E_{xc}[\rho]$ by comparing the approximate model potential with the accurate one[59,60].

As the KS potential $v_s(\mathbf{r})$ and the density $\rho(\mathbf{r})$ are interdependent, the equations have to be solved in a Self-Consistent Field (SCF) scheme[61,62], which means that one iteratively adapts the effective potential $v_{xc}(\mathbf{r})$ and the density $\rho(\mathbf{r})$ until the difference in, for example, the energy between two subsequent cycles is sufficiently small. However because the exact force of xc potential is not available in DFT, in order to solve the KS equations an approximation for the xc potential $v_{xc}(\mathbf{r})$ is required. This

xc potential should contain all the many-body effects. Currently, many different $v_{xc}(\mathbf{r})$ functionals have been proposed for practical applications. The important approximations are the local density approximation (LDA) [63], in which it is assumed that, locally, the quantum system under study can be approximated by a homogeneous electron gas. Although this might not seem appropriate for real atoms and molecules, the LDA has been remarkably successful for some systems.

More recently, the generalized gradient approximations (GGA) have been developed[64]. Although the chemical consequences of gradient corrections for correlation are relatively small compared to their exchange counterparts[65], the accurate estimation of correlation energy in GGA has also received considerable attention. The most popular correlation functionals are the LYP (Lee, Yang, and Parr), which includes both local and non-local terms[66], the P86 (Perdew 1986) functional[67], and the PW91 (Perdew and Wang 1991) functional[68] .

Instead of taking only the electron density into account, as in the LDA, the gradient of the density is also considered. This has led to important improvements in accuracy with respect to the LDA. Therefore it is clear that the form of the xc potential determines the accuracy of density functional equation.

1.2.2.3 DFT based reactivity descriptors

Density functional theory (DFT) provides a framework to discuss reactions in terms of changing number of electrons (N) or changing external potential, $v(r)$due to nuclei. The first derivatives of $E(\rho)$with respect to the number of electron N under the constant external potential $v(r)$is defined as the chemical potential μ.

$$\mu = \left(\frac{\delta E}{\delta N}\right)_{v(r)} = -\chi \qquad (1.11)$$

It determines the energy change upon changing the total number of electrons. Therefore μ equals minus the electronegativity[69] χ. Global hardness (η) is defined[70] as the corresponding second derivative of energy.

$$\eta = \frac{1}{2}\left(\frac{\delta^2 E}{\delta N^2}\right)_{v(r)} = \left(\frac{\delta\mu}{\delta N}\right)_{v(\bar{r})} \tag{1.12}$$

The global softness is inverse of global hardness with a factor 1/2:

$$S = \frac{1}{2\eta} = \left(\frac{\delta^2 N}{\delta E^2}\right)_{v(\bar{r})} = \left(\frac{\delta N}{\delta\mu}\right)_{v(\bar{r})} \tag{1.13}$$

By applying finite difference approximation the global hardness and softness are expressed as:

$$\eta = \frac{IE - EA}{2} \tag{1.14}$$

$$S = \frac{1}{IE - EA} \tag{1.15}$$

where IE and EA are the first vertical ionization energy and the electron affinity of the molecule, respectively. Using Koopmans' theorem IE and EA can be approximated as negative of E_{HOMO} and E_{LUMO}, respectively and thus global hardness can be written as:[71]

$$\eta = \frac{E_{LUMO} - E_{HOMO}}{2} \tag{1.16}$$

Recently Parr *et al*[72] proposed a new reactivity descriptor, electrophilicity index (ω), which is defined as

$$\omega = \frac{\mu^2}{2\eta} = \frac{\chi^2}{2\eta} \tag{1.18}$$

The site-selectivity of a chemical system cannot be studied using the global reactivity descriptors. For this purpose, appropriate local reactivity descriptors need

to be defined. Local reactivity descriptors, Fukui function $f(r)$ is defined by Parr and Yang[73] as the mixed second derivative of the energy of the system with respect to the number of electrons, N and the external potential $v(r)$,

$$f(r)=\left(\frac{\delta^2 E}{\delta N \delta v(r)}\right)=\left[\frac{\delta \mu}{\delta v(r)}\right]_N=\left(\frac{\delta \rho(r)}{\delta N}\right)_{v(r)} \tag{1.19}$$

Where, $\rho(r)$ is the electron density. Fukui function is a reactivity index for orbital controlled reactions, the larger the value of the Fukui function, the higher the reactivity. Using left and right derivatives with respect to the number of electrons, electrophilic and nucleophilic Fukui function can be defined. To describe site selectivity or reactivity of an atom in a molecule, it is necessary to condense the values of Fukui function around each atomic site into a single value. This can be achieved by electronic population analysis. Thus for an atom k in a molecule, depending upon the type of electron transfer, we have three different types of condensed Fukui function (f_k^+) ,(f_k^-) and (f_k^0) which correspond to electrophilic, nucleophilic and free radical attack, respectively.

$$f_k^+ = \rho_k(N+1)-\rho_k(N) \tag{1.20}$$

$$f_k^- = \rho_k(N)-\rho_k(N-1) \tag{1.21}$$

$$f_k^0 = [\rho_k(N+1)-\rho_k(N-1)]/2 \tag{1.22}$$

Here, $\rho_N(r)$, $\rho_{N+1}(r)$ and $\rho_{N-1}(r)$ are the electron densities of the N, N+1 and N-1 electron systems, respectively.

Yang and Mortier[74] introduced the condensed form of Fukui functions as:

$$f_k^+ = [q_k(N+1)-q_k(N)] \tag{1.23}$$

$$f_k^- = [q_k(N)-q_k(N-1)] \tag{1.24}$$

$$f_k^0 = [q_k(N+1) - q_k(N-1)]/2 \qquad (1.25)$$

Where q_k, the populations of atom k in the molecule.

The local softness $s(\vec{r})$ also provides the same information as the Fukui function with an additional information of molecular softness. The local softness is defined by Yang and Parr[75] as:

$$s(\vec{r}) = \left(\frac{\partial \rho(\vec{r})}{\partial \mu}\right)_{v(\vec{r})} \qquad (1.27)$$

so that $\int s(\vec{r})dr = S$ is satisfied. The local softness $s(\vec{r})$ then can be re-written in the following form,

$$s(\vec{r}) = \left(\frac{\partial \rho(\vec{r})}{\partial N}\right)_{v(\vec{r})} \left(\frac{\partial N}{\partial \mu}\right)_{v(\vec{r})} = f(\vec{r})S \qquad (1.28)$$

Thus, like Fukui functions, three different types of local softness can be expressed by the following equations.

$$s_k^+ = [\rho_k(N_0+1) - \rho_k(N_0)]S \quad \text{(for nucleophilic attack on the system)} \qquad (1.29)$$

$$s_k^- = [\rho_k(N_0) - \rho_k(N_0-1)]S \quad \text{(for electrophilic attack on the system)} \qquad (1.30)$$

$$s_k^0 = \frac{1}{2}[\rho_k(N_0+1) - \rho_k(N_0-1)]S \quad \text{(for radical attack on the system)} \qquad (1.31)$$

Roy *et al.* [76] introduced two different local reactivity descriptors, "relative electrophilicity" $\left(s_k^+/s_k^-\right)$ and "relative nucleophilicity" $\left(s_k^-/s_k^+\right)$ of any particular atom *k*, to locate the preferable site for nucleophilic and electrophilic attack on it, respectively. The individual values of s_k^+ and s_k^- are strongly influenced by the basis set or correlation effects. However, the ratio of s_k^+ and s_k^-, involving two differences of electron densities of the same system differing by one in the number of electrons, at constant nuclear framework , are expected to be less sensitive to the basis set and

correlation effects. These two newly proposed reactivity descriptors are shown to generate improved intramolecular reactivity trends than those obtained from condensed Fukui function indices.

1.3 Quantum mechanics/molecular mechanics methods

In quantum chemical studies of zeolites generally a small part of the framework is cut out and then dangling bonds of the cluster are saturated with hydrogen. The cluster models, however, do not reflect a specific zeolites framework and neglect the long-range electrostatic interactions. To include the effects of the zeolites framework, a periodic Hartree-Fock method may be ideal. However, this method is computationally expensive for most of the zeolites due to their relatively large unit cells. In order to overcome such limitation, hybrid quantum mechanics/molecular mechanics (QM/MM) techniques have been suggested at various levels.[77-79] ONIOM (our Own N-layer Integrated molecular Orbital molecular Mechanics) is a hybrid QM/MM method developed by Morokuma and co-workers[80-83]and this method has been implemented in Gaussian03 program. In this technique the region of the system where the chemical process takes place, for example bond breaking or bond formation, is treated with a high level quantum chemical method while the remaining part of the system is treated at a lower level such as molecular mechanics. The ONIOM scheme is more general in the sense that it can combine any number of molecular orbital methods as well as molecular mechanics methods. Using the terminology of Morokuma *et al.*, the full molecular geometry including all atoms is referred to as "real" geometry and it is treated using a "low"-level of theory. A subset of these atoms (referred to as the "model" geometry) are treated using both the "low"-

level and "high"-level of theory. A three layer model also introduces "intermediate" model geometry which treated with a "medium" level of theory.

In the two-layer ONIOM method, the total energy of the system is obtained from three independent calculations:

$$E^{ONIOM2} = E^{\text{high}}_{\text{model system}} + E^{\text{low}}_{\text{real system}} - E^{\text{low}}_{\text{model system}} \qquad (1.32)$$

The ONIOM method can be viewed as an extrapolation scheme. Starting from $E^{low}_{\text{model system}}$, the extrapolation to the high level calculation ($E^{high}_{\text{model system}} - E^{low}_{\text{model system}}$) and the extrapolation to the real system ($E^{low}_{real\ system} - E^{low}_{\text{model system}}$) are assumed to give an estimate for $E^{high}_{realsystem}$.

In case of the three-layered ONIOM methods, the ONIOM energy is defined according to following equation.

$$E^{ONIOM3} = E^{high}_{\text{model system}} + E^{medium}_{middle\ system} - E^{medium}_{\text{model system}} + E^{low}_{real\ system} - E^{low}_{middle\ system} \qquad (1.33)$$

The *real* system contains all the atoms and calculation is performed at MM level. The *model* system contains the part of the system that is treated at QM level. Both QM and MM calculations need to be carried out for the model system. ONIOM method has been found very successful in modeling zeolites and various other materials.

References

1. Dyer A., Zeolites. In *Encyclopedia of Inorganic Chemistry*, R. B. King, Ed. John Wiley and Sons: Chichester, **1994**, Vol. 8, pp 4363.

2. Sauer J., Zeolites: Applications of Computational Methods. In *Encyclopedia of Computational Chemistry*. P. Von Ragué-Schleyer, Ed. John Wiley and Sons: Chichester, **1998**, Vol. 5. pp 3248.

3. Corma A., *Chem. Rev.* **1995**, 95: 559.

4. Smart L., Moore E., Zeolites and related structure. *In Solid State Chemistry: An Introduction*. 2nd ed. Chapman & Hall. London **1995**, pp 238.

5. Wojciechowski B.W., Corma A., *Catalytic Cracking: Catalysts, Chemistry and Kinetics*, Dekker, New York, **1986**.

6. Maxwell I.E., Stork W.H.J., *Introduction to Zeolite Science and Practice*, Elsevier, Amsterdam, **1991**.

7. Olah G.A., Molnar A., *Hydrocarbon Chemistry*, John Wiley and Sons Inc., New York, **1995**.

8. Maxwell I.E., Stork W.H.J., Studies in surface science and catalysis, in: *Introduction to Zeolite Science and Practice*, vol. 137, second ed., **2001**, p. 747.

9. Smith J. V., *Chem. Rev.*, **1988**, 88:149.

10. Cronstedt A. F., Vetenskaps K., *Acad. Handl. Stockh.* **1956**, 17:120.

11. Olson R. H., Breck D. W., Sheppard R. A., Mumpton F. A., *Zeolites. In Industrial Minerals and Rocks*, S. J. Lefond Ed. Port City Press, Baltimore, **1983**, 2:1391.

12. Meier W. M., Olson D. M., *Atlas of Zeolite Structure Types*, 3rd Ed., Butterworth-Heinemann, London **1992**.

13. Baerlocher C., Meier W. M., Olson D. H., *Atlas of Zeolite framework Types;* Elsevier: Amsterdam, **2001**.

14. Taramasso M., Forlani O., Manara G., Notari, B, *U. K. Pat.* 2023562 **1979.**

15. Meyers B. L., Ely S. R., Kutz N. A., Kudak J. A., Van den Bossche E., *J. Catal.* **1985**, 91:352.

16. McNicol B. D., Pott G. T., *J. Catal.* **1972**, 25: 223.

17. Bhaumik A., Kumar R., *J. Chem. Soc. Chem. Commun.* **1995**, 349.

18. Kumar R., Ratnasamy P., *Catal. Lett.* 1993,**22**: 227.

19. Gabelica Z., Guth J. L., *Stud. Surf. Sci. Catal.* **1994,** 49**:** 421.

20. Taramaso M., Perego G., Notari B., *U. S. Pat.* 4410501 **1983.**

21. Thangaraj A., Kumar R., Mirajkar S. P., Ratnasamy P., *J. Catal.* **1991**, 130**:** 1.

22. Ramasawamy A. V., Sivasanker S., Ratnasamy P., *Catal. Lett.* **1993**, 22: 236.

23. Rakshe B., Ramasawamy V., Ramasawamy A. V., *J. Catal.* **1996**, 163: 501.

24. Ghobarkar H., Schäf O., Guth U., *Prog. Solid State Chem.* **1999**, 27: 29.

25. Olson R. H., Breck D. W., Sheppard R. A., Mumpton F. A., *Zeolites. In Industrial Minerals and Rocks:* Lefond. S. J. Ed.; Port City Press: Baltimore. **1983**, 2: 1391.

26. Corma A., *Chem. Rev.* **1995**, 95: 559.

27. Hölderich W., Hesse M., Näumann F., *Angew, Chem, Int. Ed. Engl.* **1988**, 27: 226.

28. Smart L., Moore E., *Zeolites and related structures. In Solid State Chemistry: An Introduction*; 2nd ed. Chapman & Hall: London, **1995**, pp 238.

29. Löwenstein, W. Am. Mineral. **1954**, 39: 92.

30. Tanabe K., Hölderich W. F., *Appl. Catal. A* **1999**, 181: 399.

31. KramerG. J., van Santen R. A., *J. Am. Chem. Soc.* **1995**, 117: 1766.

32. Gorte R. J., *Catal. Let.* **1999**, 62: 1.

33. Weisz P. B., Frilette V.J., *J Phys. Chem.* **1960**, 64: 382.

34. Weisz P. B., Frilette V. J., Maatman R. W., Mower E. B., *J. Catal.* **1962**, 1: 307.

35. Chen, N. Y.; Garwood, W. E.; Dwyer, F. G. *Shape selective Catalysis in*

Industrial Application, 2nd ed., revised and expanded, Marcel Dekker, New York, **1996**.

36. Csicsery S. M., J. *Catal.* **1971**, 23: 124.
37. Haag W. O., Lago R. M., Weisz P. B., *Faraday Discuss. Chem. Soc.* **1982**, 72: 317.
38. Bibby D. M., Milestone N. B., Aldrige L. P., *Nature* **1979**, 280: 664.
39. Notari B. *Adv. Catal.* **1996**, 41: 253.
40. Reddy J. S., Kumar R., Ratnaswamy P., *Appl. Catal.* **1990**, L1: 58.
41. Catlow C. R. A., *Modelling of Structure and Reactivity in Zeolites*, Academic press: London **1991**.
42. Moffat J. B., *Theoretical Aspects of Heterogenous Catalysis.* Van Nostrand Reinhold: New York **1990**.
43. Van Sanen R. A., Kramer G. J., *Chem. Rev.* **1995**, 95: 637.
44. Corma A., Garcia H., *Chem. Rev.* **2002**, 102: 3837.
45. Garcia H., Roth H. D., *Chem. Rev.* **2002**, 102: 3947.
46. Corma A., Garcia H., *Chem. Rev.* **2003**, 103: 4307.
47. Geerlings P., De Proft F., Langenaeker w., Chem. Rev. 2003, 103: 1793.
48. Wang L. L., Perera A., Cheng H. P., *Phys. Rev. B* **2003**, 6811: 5409.
49. Boese A. D., Chandra A., Martin J. M. L., Marx D., *J. Chem. Phys.* 2003, **119**: 5965.
50. Kobayashi C., Baldridge K., Onuchic J. N., *J. Chem. Phys.* **2003**, 119: 3550.
51. Penna G. L., Mitsutake A., Masuya M., Okamoto Y., *Chem. Phys. Lett.* **2003**, 380: 609.
52. Vink R. L. C., Barkema G. T., *Phys. Rev. B* **2003**, 6724: 5201.
53. Polak W., Patrykiejew A., *Phys. Rev. B* **2003**, 6711: 5402

54. Quintana J., Poire E. C., Dominguez H., Alejandre J., *Mo. Phys.* **2002**, 100: 2597.

55. Aussenac F., Laguerre M., Schmitter J. M., Dufourc E. J., *Langmuir* **2003**,19: 10468.

56. Rockenbauer A., Gaudel-Siri A., Siri D., Berchadsky Y., Moigne F. L., Olive G., Tordo P., *J. Phys. Chem.* **2003**, 107: 3851.

57. Hohenberg P., Kohn W., Phys. Rev. **1964**, 135B: 864

58 . Kohn W., Sham L. J., Phys. Rev. 1965, 140: A1133.

59. Süle P., Gritsenko O. V., Nagy A., Baerends E. J., *J. Chem. Phys.* 1995, 103: 10085.

60. Gritsenko O. V., Leeuwen R. V., Baerends E. J., *J. Chem. Phys.* 1996, 104: 8535.

61. Görling A., Ernzerhof A., *Phys. Rev. A* 1995, 51: 4501.

62. Harriman J. E., *Phys. Rev. A* 1986, 34: 29.

63 . Slater J. C., *The self-consistent Filed of Molecular and Solids in Quantum Theory of Molecular and Solids, Vol. 4*, McGraw-Hill: New York, **1974.**

64. Leeuwen R. V., Baerends E. J., *Phys. Rev. A* 1994, 49: 2421.

65. Becke A., *J. Chem. Phys.* **1992**, 96: 2155.

66 . Lee C., Yang W., Parr R. G., *Phys. Rev. B* **1988**, 37: 785.

67 . Perdew J. P., Wang Y., *Phys. Rev. B.* **1986**, 33: 8800.

68 . Perdew J. P., Wang Y., *Phys. Rev. B*, **1992**, 45: 13244.

69. Iczkowski R. P., Margrave J. L., *J. Am. Chem. Soc.* **1961**, 83: 3547.

70. Parr R. G., Pearson R. G., *J. Am. Chem. Soc.* **1983**, 105: 7512.

71. Koopmans T. A., *Physica* **1933**, 1: 104.

72. Parr R. G., Szentpály, L. V., Liu S., *J. Am. Chem. Soc.* **1999**, 121: 1922.

73. Parr R.G., Yang W., *J. Am. Chem. Soc.*, **1984**, 106: 4049

74 . Yang W., Mortier W., *J. Am. Chem. Soc.* **1986**, 108: 5708.

75. Yang W., Parr R. G., *Proc. Natl. Acad. Sci.* U.S.A. **1985**, 82: 6723.

76. Roy R. K., Krishnamurti S., Geerlings P., Pal S., *J. Phys. Chem. A* **1998**, 102: 3746.

77. Humbel S., Sieber S., Morokuma K., *J Chem Phys* **1996**, 105: 1959.

78. Svensson M., Humbel, S., Froese R. D. J., Matsubara T., Sieber S., Morokuma K., *J. Phys. Chem.* **1996**, 100: 19357.

79. Froese, R. D. J.; Morokuma, K. In Encyclopedia of Computational Chemistry, Vol. 2; Schleyer, P. v. R., Allinger, N. L., Kollman, P. A.,Clark, T., Schaefer III, H. F., Gasteiger, J., Schreiner, P. R., Eds.;Wiley: Chichester, **1998**; p 1244..

80. Dapprich S., Komaromi I., Byun K. S., Morokuma K., Frisch M. J., *J. Mol. Struct. (THEOCHEM)* **1999**, 461-462: 1.

81. Svensson M., Humbel S., Morokuma K., *J Chem Phys* **1996**, 105: 3654.

82. Karadakov P. B., Morokuma K., *Chem. Phys. Lett.* **2000**, 317: 589.

83. Vreven T., Morokuma K., *J. Comput. Chem.* **2000**, 21: 1419.

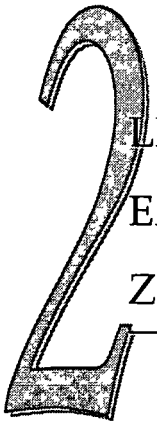

LEWIS ACIDITY OF ALKALI AND ALKALINE EARTH CATION EXCHANGED FAUJASITE ZEOLITES

Abstract

Lewis acidity of alkali and alkaline earth metal cation exchanged faujasite zeolites is investigated using density functional theory based global and local reactivity descriptors. The zeolite structure is represented by a 6T ring cluster model of faujasite which contain SII site of its supercage. The alkali cation exchanged zeolite cluster contains one aluminum atom whereas alkaline earth cation exchanged zeolite contains two aluminum atoms. Global reactivity descriptors, chemical hardness, chemical softness, electophilicity index of the optimized clusters and local reactivity descriptors, Fukui function and relative electrophilicity values of exchanged cations were calculated using PWC/DNP and VWN-BP/DNP methods to derive Lewis acidity sequence of the material. These reactivity descriptors show that Lewis acidity of alkali and alkaline earth metal cation exchanged faujasite zeolites decreases in the order: Na-FAU > K-FAU >Rb-FAU > Cs-FAU and Mg-FAU > Ca-FAU > Sr-FAU > Ba-FAU, respectively. These Lewis acidity sequences agree well with the available experimental as well as theoretical results.

2.1 Introduction

Cation exchanged faujasite zeolites are widely used as selective adsorbents for gas separation and purification as well as catalysts and supports for nanoparticles. The ion exchange capacity of faujasite zeolites leads to important industrial application for removal of ammonia and heavy metals from municipal, industrial and drinking water or in absorbing Cs and Sr from nuclear wastes.[1] Cation exchanged zeolites are also used in separation of p-xylene from C_8 aromatics,[2,3] separation of carbon dioxide from methane, nitrogen and oxygen from air.[4] Such processes are based on specific interactions of adsorbates with the electric field generated by extra-framework cations and neighbouring framework anions. These electric fields bring about polarization of the adsorbed molecule significantly altering the electron distribution and thus its reactivity. Both experimental and theoretical studies have been focused on the adsorption properties of monovalent and divalent cation exchanged X- and Y-zeolites with respect to different adsorbates such as methane, ethane, ethene, argon, nitrogen and water vapour.[5-8] In cation exchanged zeolites, the exchanged cations behave as Lewis acid sites and the framework oxygen atoms bearing partial negative changes act as Lewis base. The simultaneous presence of both acid and basic sites in these zeolites has been found to catalyze several organic reactions of industrial importance. Recently, it has been found that the alkali and alkaline earth exchanged faujasite zeolite promotes selective oxidation of hydrocarbon with molecular oxygen to corresponding oxygenates with high selectivity under mild thermal and photochemical activation.[9,10] Alkali and alkaline earth cations in zeolites do not show any redox properties and cannot dissociate either hydrocarbon or oxygen molecules. Thus, the activation of hydrocarbon and oxygen molecules in cation exchanged zeolites is different from conventional processes.

The Lewis acid strength of exchanged cations plays an important role in directing the guest molecules both for gas separation and their chemical activation. It has been shown by Pidko and van Santen[11] that in case of photo-oxidation process the main role of the cations is to prearrange the reactants in the zeolite cavity via adsorption so that they can be activated in the subsequent reaction steps. Obviously, depending on the Lewis acid strength of the exchanged cations and adsorption fashion of guest molecule within zeolite cavities, the property and reactivity of the adsorbed molecules will vary significantly. Hence, it is important to predict influence of different cations on structure as well as the activity of zeolites for catalytic reactions. The structure-property relationships of proton-exchanged zeolites have been extensively studied using various experimental and theoretical methods.[12,13] However, little attention has been paid to the Lewis acidity of alkali and alkaline earth cation exchanged zeolites.

Cohen De Lara and co-workers[14,15] had employed probe molecules such as N_2, H_2, CH_4 etc. to evaluate the strength of local electric fields of cation sites in zeolites. The acid-base properties of cation exchanged zeolites have been investigated by means of FT-IR and TPD-MS techniques using ammonia as a probe molecule.[16] Larsen and coworker[17] have studied a series of alkaline earth metal exchanged beta zeolites using CO as a probe molecule to investigate the effect of exchanged cation on electric field. Xie *et al.*[18] characterized the Lewis acid and Lewis basic sites of alkaline earth exchanged X zeolites by studying pyrrole chemisorption with FTIR spectroscopic technique and determined the Lewis acid and basic strength by calculating charges of cations and oxygen atoms, respectively, using the electronegativity equivalence method. The prediction of correct Lewis acidity trend of cation-exchanged zeolites has not been successful from positive charges of the cations. In this respect, the density functional based reactivity descriptors have been found to be quite useful.[19,20]

The goal of the present study is to elucidate the Lewis acid strength of different alkali and alkaline earth metal cation exchanged faujasite zeolites using density functional theory based reactivity descriptors, chemical hardness (η), chemical softness (S), chemical potential (μ), Fukui function (f_M^+ and f_M^-) and relative eletrophilicity (f_M^+/f_M^-).[21-23] The global reactivity descriptors, η, S and μ give the reactivity of a system as a whole whereas the local parameters, Fukui function and relative electrophilicity represent the reactivity of an atom in a molecule. Fukui functions f_M^+ and f_M^- values give the sites that are prone to nucleophilic and electrophilic attack, respectively. In most of the cases Fukui function values are found to be successful in explaining experimental reactivity sequences of chemical species.[24-26] However, in some systems the atom with high electrophilicity i.e having higher value of f_M^+ may also show high nucleophilicity i.e having higher value of f_M^-. Then their ratios 'relative electrophilicity', (f_M^+/f_M^-), and 'relative nucleophilicity', (f_M^-/f_M^+), express the reactivity of atoms in molecules in a better way.[27] Vos *et al.*[28,29] applied the DFT based local and global reactivity descriptors successfully to explain the mechanism of electrophilic aromatic substitution reaction involving zeolites. Hemelsoet *et al.*[30] studied the dependence of global reactivity descriptors on electronic structure methods as well as basis set for typical reactions in zeolite catalysis. Parr *et. al.*[31] proposed a new global reactivity parameter called electrophilicity index (ω) based on the chemical potential and chemical hardness of the system. Electrophilicity index measures the electrophilic power of molecular species. Domingo *et al.*[32] applied electrophilicity index to characterize quantitatively the electrophilic power of common diene/dienophile pairs used in Diels-Alder reactions. Padmanabhan *et al.*[33] also used electrophilicity index to explain toxicity and aromaticity of a series of chlorinated benzenes correctly. We have calculated these

global reactivity parameters for alkali and alkaline earth exchanged zeolites using a cluster model approach and determined their Lewis acid strength.

2.2 Computational details

The cluster model used in this study is generated from the crystalline structure of faujasite.[34] The framework of zeolite was modeled with a 6T (T=tetrahedral unit of zeolite) cluster containing the six-member ring (SII site) of the supercage of faujasite structure

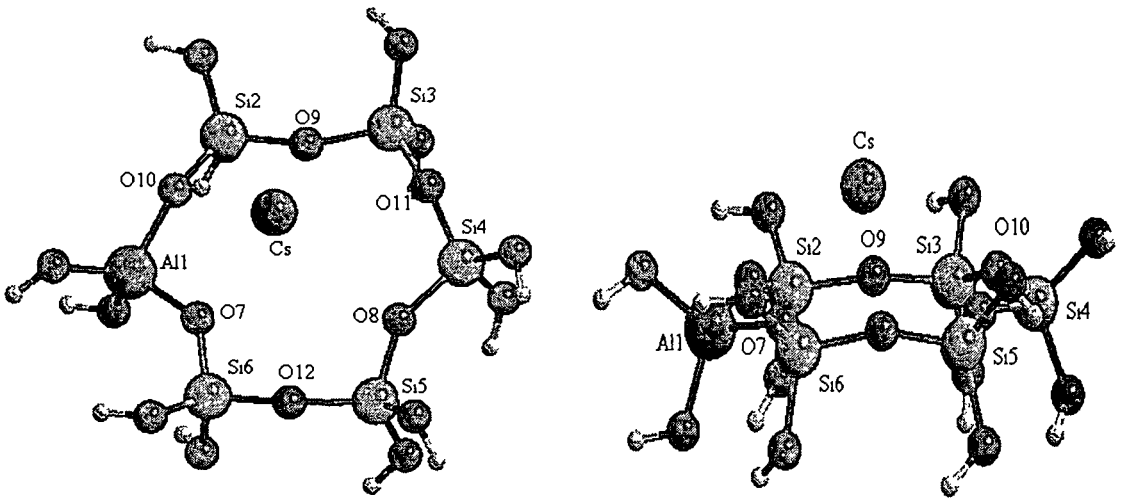

Figure 2.1: Top and side views of optimized 6T cluster of Cs-exchanged zeolite. Ring oxygen, silicon and aluminum atoms are numbered for easy reference in the discussion.

Lewis acidity of alkali (Na^+, K^+, Rb^+, Cs^+) and alkaline earth (Mg^{2+}, Ca^{2+}, Sr^{2+}, Ba^{2+}) cation exchanged faujasite zeolites are investigated by considering two types of 6T ring clusters by isomorphously substituting one Al atom for alkali (Figure 2.1) and two Al atoms for alkaline earth exchanged (Figure 2.2) cluster. The relative position of aluminum atoms in the cluster has been chosen in such a way that the cluster obeys

Löwenstein rule.[35] The free valences of the silicon and aluminum atoms of the cluster are saturated with O—H groups. During

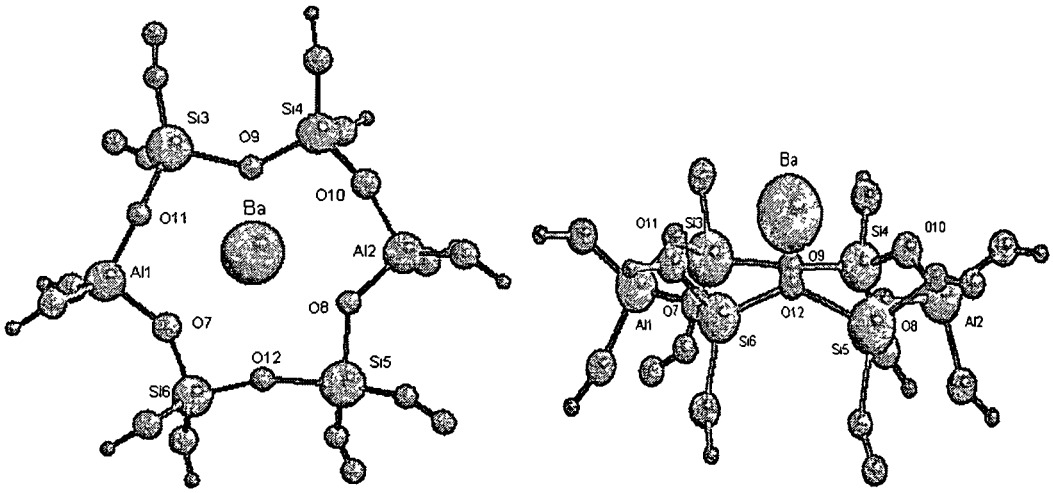

Figure 2.2: Top and side views of optimized 6T cluster of Ba-exchanged zeolite. Ring oxygen, silicon and aluminum atoms are numbered for easy reference in the discussion.

optimization of the clusters, first only the terminating O—H bonds were optimized keeping all other atoms fixed at their crystallographic positions. In subsequent calculations all the silicon, aluminum and terminating hydrogen atoms were kept fixed optimizing only oxygen atoms and exchanged cations of the cluster. Fixing of terminal hydrogen atoms avoids unrealistic hydrogen bonding in the system. Furthermore, the procedure of keeping T atoms fixed during optimization attempts to represent the real situation in the zeolite framework, where the motion of T atoms is restricted due to additional bonds present outside the ring. The full structure optimization of zeolite clusters leads to a structure which does not resemble the experimental geometry.[36] Hence, constrained optimization is commonly used in zeolite modeling.[37]

All calculations are performed using DMol3[38,39] program package. Alkali cation exchanged clusters have been optimized at local density approximation (LDA) with

Perdew-Wang (PWC) functional. Whereas, alkaline earth cation exchanged zeolite clusters have been optimized at LDA level with PWC functional and generalized gradient approximation (GGA) level with BP functional having local correlation replaced by Vosko-Wilk-Nusair (VWN) functional.[40,41] We used DNP basis set for all the atoms in our calculations. The "DNP" level basis set is of double numeric quality (i.e., approximately two atomic orbitals for each one occupied in the free atoms) augmented with polarization functions (i.e., functions with angular momentum one higher than that of the highest occupied orbital in the free atom). The integration grid referred to as FINE in the software program has been used for optimization of the clusters.

2.3 Results and Discussion

2.3.1 Optimized Structure

2.3.1.1 Alkali cation-exchanged clusters

Optimized structure of Cs^+ exchanged 6T ring cluster is shown in Figure 2.1 and selected geometric parameters of Na^+, K^+, Rb^+ and Cs^+ exchanged clusters are given in Table 2.1. The location of metal cation with respect to zeolite framework depends on the ionic radius of the cation. Different experimental and theoretical methods have been used to investigate the location of extraframework cations relative to zeolite framework and their interaction with guest molecules.[42] X-ray diffraction (XRD)[43] and neutron diffraction data have provided precise information regarding the location of extraframework cations. The deviation of the cation positions from the plane of six member rings can be evaluated from the values of O—X^+—O angles. As reported in Table 2.1, the cations move away from the centre of the six ring with the ionic radii (Li^+: 0.59 Å, Na^+: 0.99 Å, K^+: 1.35 Å, Rb^+: 1.52 and Cs^+:1.67 Å)[44]. The Cs^+ cation, due to its

Table 2.1: Variation of selected internal coordinates of optimized alkali cation exchanged 6T ring cluster of faujasite zeolites calculated at PWC/DNP set level.

Internal Co-ordinates	Exchanged cations			
	Na^+	K^+	Rb^+	Cs^+
$X^+—O_7$[a]	2.19	2.52	2.68	2.85
$X^+—O_8$[a]	2.65	2.88	2.90	3.62
$X^+—O_9$[a]	2.32	2.64	2.82	2.98
$X^+—O_{10}$[a]	2.96	3.12	3.18	3.40
$X^+—O_{11}$[a]	2.45	2.76	2.98	3.06
$X^+—O_{12}$[a]	3.27	3.42	3.42	3.62
<Al1—O>[a]	1.79	1.78	1.77	1.76
<Si2—O>[a]	1.67	1.66	1.66	1.66
<Si3—O>[a]	1.63	1.62	1.62	1.62
<Si4—O>[a]	1.66	1.66	1.66	1.66
<Si5—O>[a]	1.65	1.65	1.65	1.65
<Si6—O>[a]	1.64	1.64	1.64	1.64
$O_7—Al_1—O_{11}$[b]	92.8	95.1	95.4	96.0
$O_7—X^+—O_8$[b]	101.67	89.42	86.47	78.79
$O_9—X^+—O_{12}$[b]	152.26	127.76	121.04	110.76
$O_{11}—X^+—O_{10}$[b]	120.87	108.05	101.62	67.20

[a] values are in Å, [b] values are in degrees, < > represent average

larger size, naturally takes up a position significantly detracted from the plane of the six member ring. The simulated geometric parameters (both distances and angles) of cluster are in very good agreement with those collected from X-ray and neutron diffraction studies on periodic NaY[45], KY[46]and CsY faujasite structures (Table 2.1). Plant *et al.*[47] *performed quantum chemical studies on adsorption of carbon dioxide in alkali cation* exchanged Y zeolite and reported similar deviation of cation from the plane of six-

member ring. This preliminary step allowed us to validate the choice of the cluster size used in the calculations. The strength of interaction between the extraframework cation with framework oxygen atoms decreases in the series from Na^+ to Cs^+.[48] This trend correlates nicely with cation radii and corresponding internuclear distances, such as X^+—O as reported in Table 2.1. The interaction between cation and framework oxygen atoms leads to substantial deformation of zeolite structure around the cation. The interaction of a cation with framework oxygen atoms elongates Al—O and Si—O bond lengths (Table 2.1).

Elongation of Al—O and Si—O bond lengths is maximum for Na^+ and minimum for Cs^+ exchanged clusters. The O_7—Al —O_{11} bond angle decreases significantly from usual tetrahedral value and deformation of zeolites cluster is largest for Na^+ decreasing steadily to Cs^+ exchanged zeolites. Rösch and coworker[49] performed computational studies on the influence of alkali and alkaline earth cation on Brönsted acidity of cation exchanged faujasite zeolites, reported similar geometrical changes. It is also noticed from Table 2.1, with increasing ionic radii of the cations, the X^+—O distances increase and O—X^+—O bond angle decreases.

2.3.1.2 Alkaline earth cation exchanged clusters

The top and side views of optimized structure for Ba^{2+} exchanged 6T ring cluster of faujasite zeolite are shown in Figure 2.2. Some of the selected geometric parameters of the optimized clusters for all the alkaline earth exchanged zeolites, derived at PWC/DNP and VWN-BP/DNP levels are given in Table 2.2. Like alkali cation exchanged cluster, location of alkaline earth metal cation with respect to zeolite framework depends on ionic radius of the cation. It is seen from Table 2.2 that Mg^{2+} cation has three-fold coordination with framework oxygen atoms, O_7, O_8 and O_9, and stay at long distance from other

oxygen atoms (O_{10}, O_{11} and O_{12}). The Mg—O distances for O_7, O_8, O_9 atoms are almost same (2.05-2.09 Å). The Mg^{2+} ion is located near the centre of the 6T ring in agreement with the experimental XRD data for dehydrated MgNa—X zeolite.[50] In contrast to Mg^{2+}, larger cations, Ca^{2+}, Sr^{2+} and Ba^{2+} have six-fold coordination with framework oxygen atoms, O_7, O_8, O_9, O_{10}, O_{11} and O_{12}. The strength of interaction between the extraframework cation and framework oxygen atoms decreases in the series from Mg^{2+} to Ba^{2+}.[51] This sequence correlates quite nicely with the cation radii (Mg^{2+}: 0.65, Ca^{2+}: 0.99, Sr^{2+}: 1.13 and Ba^{2+}: 1.35 Å) and corresponding X^{2+}—O distances as reported in Table 2.2. Like alkali cations, it is noticed from Table 2.2 that with increasing ionic radii of the cations, the X^{2+}—O distances increase and O—X^{2+}—O angles decrease. Therefore, the exchanged cations move away from the plane of T atoms with the increase of their ionic radii. Similar to alkali cation, interaction between alkaline earth cation and framework oxygen atoms leads to deformation of zeolite structure around them. The interaction of a cation with framework oxygen atoms elongates Al—O and Si—O bond lengths and decreases O—Al—O bond angles.

2.3.2 **Lewis acidity of cation-exchanged zeolites**

The catalytic activity of cation exchanged zeolites depends upon the Lewis acidity of exchanged cations and Lewis basicity of framework oxygen atoms. To understand the Lewis acidity of alkali and alkaline earth cation exchanged faujasite zeolites, we have evaluated DFT based reactivity descriptors namely global hardness, global softness, electrophilicity, Fukui function and relative electrophilicity.

Table 2.2: Variation of selected internal coordinates of the optimized alkaline earth cation exchanged 6T ring cluster of faujasite zeolites calculated at PWC/DNP and BP-VWN/DNP levels.

Internal Co-ordinates	Exchanged cations							
	PWC/DNP				BP-VWN/DNP			
	Mg^{2+}	Ca^{2+}	Sr^{2+}	Ba^{2+}	Mg^{2+}	Ca^{2+}	Sr^{2+}	Ba^{2+}
$X^{2+}—O_7$[a]	2.058	2.248	2.380	2.556	2.054	2.278	2.427	2.610
$X^{2+}—O_8$[a]	2.074	2.258	2.386	2.563	2.069	2.286	2.437	2.619
$X^{2+}—O_9$[a]	2.103	2.282	2.457	2.659	2.097	2.325	2.515	2.731
$X^{2+}—O_{10}$[a]	2.592	2.479	2.591	2.724	2.623	2.535	2.655	2.809
$X^{2+}—O_{11}$[a]	2.540	2.475	2.579	2.716	2.559	2.512	2.632	2.786
$X^{2+}—O_{12}$[a]	3.131	3.025	2.981	3.059	3.166	3.098	3.096	3.179
<Al1—O>[a]	1.793	1.781	1.781	1.780	1.805	1.799	1.798	1.798
<Al2—O>[a]	1.781	1.769	1.767	1.768	1.797	1.789	1.788	1.789
<Si3—O>[a]	1.646	1.641	1.642	1.643	1.663	1.658	1.660	1.661
<Si4—O>[a]	1.657	1.652	1.653	1.654	1.672	1.668	1.670	1.671
<Si5—O>[a]	1.671	1.662	1.661	1.663	1.688	1.681	1.682	1.683
<Si6—O>[a]	1.661	1.653	1.652	1.653	1.677	1.671	1.671	1.672
$O_7—Al_1—O_{11}$[b]	88.58	90.21	92.47	93.79	88.98	90.36	92.32	93.63
$O_8—Al_2—O_{10}$[b]	92.48	93.65	96.28	97.59	93.08	94.07	96.20	97.61
$O_7—X^{2+}—O_8$[b]	107.33	104.05	98.48	90.19	107.09	100.50	93.79	86.07
$O_9—X^{2+}—O_{12}$[b]	176.71	161.25	145.56	130.94	174.44	152.27	137.97	125.03
$O_{11}—X^{2+}—O_{10}$[b]	117.24	120.15	116.58	110.68	117.40	119.91	115.16	108.48

[a] values are in Å, [b] values are in degrees, < > represent average

2.3.2.1 Lewis acidity of alkali cation-exchanged zeolites

2.3.2.1.1 Global reactivity descriptors

The global reactivity descriptors viz. chemical potential, chemical hardness, chemical softness and electrophilicity index of alkali cation exchanged faujasite zeolite clusters calculated using PWC/DNP level are presented in Table 2.3. Negative of chemical potential is equal to electronegativity. Hence, higher negative value of chemical potential implies higher Lewis acidity. Magnitude of negative value of chemical potential decreases from Na^+ exchanged cluster to Cs^+ exchanged cluster. Therefore, Lewis acidity of alkali cation exchanged zeolites decrease from Na^+ to Cs^+ exchanged derivative. The maximum hardness principle (MHP)[52] states that at constant external potential, the higher is the hardness the higher is the stability. Thus a higher value of hardness indicates a lower value of Lewis acidity. Conversely, lower is the softness value, higher is the stability and hence lower is the reactivity. It is seen from the Table 2.3 that chemical hardness values of model clusters derived at PWC/DNP level increase in the order: $Na^+ < K^+ < Rb^+ < Cs^+$. The global softness values of the clusters derived using PWC/DNP level decrease from Na^+ exchanged cluster down to Cs^+ exchanged cluster (Table 2.3). Hence, Lewis acidity of the exchanged cluster decreases in the order: $Na^+ > K^+ > Rb^+ > Cs^+$, which is in excellent agreement with experimental Lewis acidity trends.[53] Higher values of electrophilicity, (ω) measure the electrophilic power of molecular species, i.e. higher Lewis acidity. Na-exchanged zeolite cluster has the maximum electrophilicity value and hence higher is the Lewis acidity. The electrophilicity values calculated using PWC/DNP level decrease from Na- exchanged cluster to Cs-exchanged cluster (Table 2.3). The global reactivity descriptors namely chemical potential, chemical hardness, chemical

softness and electrophilicity values of the model clusters revealed that Lewis acidity of alkali metal exchanged faujasite zeolites decrease in the order: $Na^+ > K^+ > Rb^+ > Cs^+$.

Table 2.3: Calculated Chemical potential, μ, chemical hardness, η, chemical softness, S, and electrophilicity, ω, values of alkali cation exchanged 6T ring cluster of faujasite zeolites. These values are evaluated using PWC/DNP level.

Exchanged Cations	DFT Functional	Chemical potential (μ)	Chemical hardness (η)	Chemical softness (S)	Electrophilicity (ω)
Na^+		-4.277	2.244	0.223	4.078
K^+		-4.132	2.249	0.222	3.795
Rb^+		-4.107	2.252	0.221	3.745
Cs^+		-4.032	2.281	0.219	3.564

2.3.2.1.2 **Local reactivity descriptors**

Lewis acidity of a cation depends on its positive charge, ionic radius and polarizability. Experimentally, it has been found that the Lewis acidity of the alkali metal exchanged zeolite decreases in the order of $Na^+ > K^+ > Rb^+ > Cs^+$. Deka *et al.*[19] have studied Lewis acidity of alkali cation exchanged zeolites using density functional theory based local reactivity descriptors taking small zeolite clusters.

We have evaluated charge ($q_M{}^+$), Fukui function for nucleophilic and electrophilic attracts (f_M^+ and f_M^-) and relative electrophilicity, (f_M^+ / f_M^-). These values derived from MPA and HPA schemes using PWC/DNP level for exchanged alkali metals are summarized in Table 2.4. It is noticed from Table 2.4 that Mulliken and Hirshfeld

charges on the exchanged cation indicate no systematic trend of Lewis acidity of alkali metal exchanged zeolites.

Table 2.4: MPA and HPA derived charge, nucleophilic Fukui function, electrophilic Fukui function, relative electrophilicity of the cation in alkali cation exchanged 6T ring cluster of faujasite zeolites (see Figure 2.1). The values are evaluated using PWC/DNP level.

Exchanged Cations	DFT Functional	MPA derived parameters				HPA derived parameters			
		q_M	f_M^+	f_M^-	f_M^+/f_M^-	q_M	f_M^+	f_M^-	f_M^+/f_M^-
Na^+		0.674	0.245	0.019	12.895	0.533	0.095	0.013	7.308
K^+	PWC	0.747	0.191	0.019	10.053	0.513	0.093	0.018	5.167
Rb^+		0.709	0.178	0.022	8.091	0.541	0.093	0.021	4.429
Cs^+		0.744	0.142	0.029	4.897	0.567	0.081	0.027	3.000

The f_M^+ values of the exchanged cation calculated with MPA and HPA schemes using PWC/DNP level decrease in the order: $Na^+ > K^+ > Rb^+ > Cs^+$. Again, larger value of f_M^+/f_M^- of exchanged cations explains higher reactivity, hence, higher Lewis acidity. The reported f_M^+/f_M^- values of the cations derived from MPA and HPA at PWC /DNP level decreases in the order of $Na^+ > K^+ > Rb^+ > Cs^+$. Hence, the Lewis acidity of the alkali earth metal cation exchanged zeolite decreases in the order of $Na^+ > K^+ > Rb^+ > Cs^+$, which is in good agreement with the experimental acidity sequence.

2.3.2.2 Lewis acidity of alkaline earth cation exchanged zeolites

2.3.2.2.1 Global reactivity descriptors

The calculated global reactivity descriptors of alkaline earth cation exchanged zeolite clusters using PWC/DNP and VWN-BP/DNP levels are presented in Table 2.5. It is seen from Table 2.5 that the chemical hardness values of modeled clusters derived at PWC/DNP level increase in the order: $Mg^{2+} < Ca^{2+} < Sr^{2+} < Ba^{2+}$. The global softness values of the clusters derived using PWC/DNP level decrease from Mg^{2+} exchanged cluster down to Ba^{2+} exchanged cluster (Table 2.5). Hence, Lewis acidity of the exchanged cluster decreases in the order: $Mg^{2+} > Ca^{2+} > Sr^{2+} > Ba^{2+}$, which is in excellent agreement with experimental Lewis acidity trends.[53]

Table 2.5: Calculated Chemical potential, μ, chemical hardness, η, chemical softness, S, and electrophilicity, ω, values of alkaline earth cation exchanged 6T ring cluster of faujasite zeolites. These values are evaluated using PWC/DNP and VWN-BP/DNP levels.

Exchanged Cations	DFT Functional	Chemical potential (μ)	Chemical hardness (η)	Chemical softness (S)	Electrophilicity (ω)
Mg^{2+}	PWC/DNP	-3.970	2.009	0.249	3.923
Ca^{2+}		-3.734	2.147	0.233	3.247
Sr^{2+}		-3.725	2.155	0.232	3.219
Ba^{2+}		-3.604	2.157	0.232	3.011
Mg^{2+}	VWN-BP/DNP	-3.755	2.081	0.240	3.388
Ca^{2+}		-3.525	2.222	0.225	2.796
Sr^{2+}		-3.485	2.185	0.229	2.779
Ba^{2+}		-3.415	2.174	0.230	2.682

However, chemical hardness and global softness values calculated at VWN-BP/DNP level fail to predict the systematic acidity sequence. The electrophilicity index computed using PWC/DNP and VWN-BP/DNP levels are also given in Table 2.5. Mg-exchanged zeolite cluster has maximum electrophilicity value and hence is the most reactive one. The electrophilicity values decrease from Mg- exchanged cluster to Ba-exchanged cluster. Therefore, Lewis acidity of alkaline earth metal exchanged faujasite zeolites decreases in the order: $Mg^{2+} > Ca^{2+} > Sr^{2+} > Ba^{2+}$.

2.3.2.2.2 **Local reactivity descriptors**

We have evaluated $q_M{}^+, f_M^+$, f_M^-, and f_M^+ / f_M^- of the exchanged cations. These values derived from MPA and HPA schemes at PWC/DNP and VWN-BP/DNP levels for alkaline earth metals are summarized in Table 2.6. It is noticed from Table 2.6 that charges and Fukui function values of the exchanged cation evaluated using both MPA and HPA schemes at PWC/DNP and VWN-BP/DNP levels fail to predict the correct trend of acidity. The relative electrophilicity and relative nucleophilicity values have been found to be more reliable local reactivity descriptors compared to f_M^+ and f_M^-. The f_M^+ / f_M^- values of exchanged cations are presented in Table 2.6. The reported f_M^+ / f_M^- values of the cations derived from MPA and HPA at PWC /DNP level decreases in the order of $Mg^{2+} > Ca^{2+} > Sr^{2+} > Ba^{2+}$. Hence, the Lewis acidity of alkaline earth metal cation exchanged zeolite decreases in the order of $Mg^{2+} > Ca^{2+} > Sr^{2+} > Ba^{2+}$, which is in good agreement with the experimental acidity sequence. The relative eletrophilicity values derived from MPA and HPA schemes using DNP basis set and VWN-BP functional also agree well with the experimental Lewis acidity sequence.

Table 2.6: MPA and HPA derived charge, nucleophilic Fukui function, electrophilic Fukui function, and relative electrophilicity of the cation in alkaline earth cation exchanged 6T ring cluster of faujasite zeolites (see Figure 2.2). The values are evaluated using PWC/DNP and VWN-BP/DNP levels.

Exchanged Cations	DFT Functional	MPA derived parameters				HPA derived parameters			
		q_M	f_M^+	f_M^-	f_M^+/f_M^-	q_M	f_M^+	f_M^-	f_M^+/f_M^-
Mg^{2+}		1.166	0.487	0.007	69.571	0.689	0.240	0.008	30.000
Ca^{2+}	PWC/DNP	1.508	0.604	0.009	67.111	0.691	0.263	0.011	23.909
Sr^{2+}		1.321	0.605	0.013	46.538	0.736	0.359	0.016	22.436
Ba^{2+}		1.321	0.534	0.021	25.429	0.782	0.351	0.023	15.261
Mg^{2+}		1.236	0.475	0.008	59.375	0.715	0.241	0.008	30.125
Ca^{2+}	VWN-BP/DNP	1.574	0.573	0.010	57.300	0.734	0.279	0.011	25.364
Sr^{2+}		1.410	0.599	0.015	39.933	0.794	0.398	0.016	24.875
Ba^{2+}		1.422	0.564	0.023	24.522	0.847	0.421	0.024	17.542

2.4 Conclusions

DFT calculations on 6T ring cluster of alkali and alkaline earth cation-exchanged faujasite zeolite show a significant change in geometric parameters around the cations. The change in geometry is more pronounced for smaller cations. The global reactivity descriptors namely chemical potential and electrophilicity index values for the alkali cation exchanged zeolite clusters calculated using PWC/DNP and alkaline earth cation exchanged zeolite clusters evaluated using PWC/DNP and PW91/DNP levels decrease in the order: $Na^+ > K^+ > Rb^+ > Cs^+$ and $Mg^{2+} > Ca^{2+} > Sr^{2+} > Ba^{2+}$, respectively. Fukui function values of alkali and alkaline earth cation exchanged zeolites are found to be

weak reactivity parameters to obtain the experimental Lewis acidity sequences. The relative electrophilicity values of alkali and alkaline earth cations derived from HPA and MPA schemes using DNP basis set decrease in the order: $Na^+ > K^+ > Rb^+ > Cs^+$ and $Mg^{2+} > Ca^{2+} > Sr^{2+} > Ba^{2+}$, respectively. Thus, we conclude that electrophilicity index and relative electrophilicity are reliable parameters to predict acidity as well as reactivity of zeo-type materials.

References:

1. Moreno N., Querol X., Ayora C., Pereira C.F., Janssen M., *Environ. Sci.Technol.* **2001,** 35: 3526.

2. Broughton D.B., Neuzil R.W., Pharis J. M., Brearley C. S., *Chem. Eng. Prog.* **1970**, 6: 70.

3. Seko M., Miyake T., Inada V., *Ind. Eng. Chem. Prod. Res. Dev.* **1979**, 18: 263.

4. Gaffney T. R., *Curr. Opin. Solid State Mater. Sci.* **1996**, 1: 69.

5. Pidko E. A., Xu J., Mojet B. L., Lefferts L., Subbotina I. R., Kazansky V. B., van Santen R. A., *J. Phys. Chem. B* **2006**, 110: 22618.

6. Bezus A.G., Kiselev A.V., Sedlacek Z., Pham Quang D., *J. Chem. Soc., Faraday Trans. 1* **1971,** 167: 468.

7. Barrer R.M., Stuart F.R., *Proc. Roy. Soc.* **1959,** 464.

8. Dzhigit O.M., Kiselev A.V., Mikos K.N., Muttik G.G., Rahmanova T.A., *J. Chem. Soc. Faraday Trans.1* **1971**, 67: 458.

9. Blatter F., Frei H., *J. Am. Chem. Soc.* **1994**, 116: 1812.

10. Blatter F., Sun H., Vasenkov S., Frei H., *Catal. Today.* **1998**, 41: 297.

11. Pidko E. A., van Santen R. A., *J. Phys. Chem. B.* **2006**, 110: 2963.

12. Corma A., *Chem. Rev.* **1995**, 95: 559.

13. van Santen R. A., Kramer G. J., *J. Chem. Rev.* **1995**, 95: 637.

14. Cohen De Lara E., Nguyen Tan T., *J. Phys. Chem.* **1976**, 80: 1917.

15. Cohen De Lara E., Vincent-Geisse J., *J. Phys. Chem.* **1976**, 80:1922.

16. Gilles F., Blin J. L., Toufar H., Briend M., Su B. L., *Colloid and Surfaces A: Physiochem. Eng. Aspects* **2004**, 241: 245.

17. Xiang P.L., Grassian V. H., Larsen S. C., *J. Phys. Chem. B.* **1999**, 103: 5058.

18. Xie J., Huang M., Kaliaguine S., *Catal. Lett.* **1994**, 29: 281.

19. Deka R.C., Roy R. K., Hirao K., *Chem. Phys. Lett.* **2004**, 389: 186.

20. Deka R.C., Roy R. K., Hirao K., *Chem. Phys. Lett.* **2000**, 332: 576.

21. Geerlings P., De Proft F., Langenaeker W., *Chem. Rev.* **2003**, 103: 1793.

22. Pal S., Chandrakumar K. R. S., *J. Am. Chem. Soc.* **2000**, 122: 4145.

23. Chattaraj P. K., Sarkar U., Roy D. R., *Chem. Rev.* **2006**, 106: 2065.

24. Langenaeker W., De Decker M., Geerlings P., *J. Mol. Struct. (THEOCHEM).* **1990**, 207: 115.

25. Melin J., Aparicio F., Subramanian V., Galvan M., Chattaraj P. K., *J. Phys. Chem. A.* **2004**, 108: 2487.

26. Ayers P. W., Parr R. G., *J. Am. Chem. Soc.* 2000, 122: 2010.

27. Roy R. K., Krishnamurti S., Geerlings P., Pal S., *J. Phys. Chem. A.* **1998**, 102: 3746.

28. Vos A. M., Nulens K. H. L., De Proft F., Schoonheydt R. A., Geerling P., *J. Phys. Chem. B* **2002**, 106: 2026.

29. Vos A. M., Schoonheydt R. A., De Proft F., Geerling P., *J. Phys. Chem. B.* **2002**, 107: 2001.

30. Hemelsoet K., Lesthaeghe D., Van Speybroeck V., Waroquier M., *J. Phys. Chem. C* **2007**, 111: 3028.

31. Parr R. G., Szentpaly L. V., Liu S., *J. Am. Chem. Soc.* **1999**, 121: 1922.

32. Domingo L. R., Aurell J. M., Perez P., Contreras R., *Tetrahedron.* **2002**, 58: 4417.

33. Padmanabhan J., Parthasarathi R., Subramanian V., Chattaraj P. K., *J. Phys. Chem. A.* **2005**, 109: 11043.

34.Uytterhoeven L., Dompas D.,Mortier W.J., *J. Chem. Soc., Faraday Trans.***1992**, 88: 2753.

35. Loewenstein W., *Am. Mineral.* **1954**, 39: 92.

36. Sauer J., Pacchioni G., Bagus P. S., *Cluster Models for Surface and Bulk Phenomena,* Parmigiani (Herausg.) eds., Plenum Press, New York, **1992**, pp. 533.

37. Pidko E. A., Xu J., Mojet B. L., Lefferts L., Subbotina I. R., Kazansky V. B., van Santen R. A., *J. Phys. Chem. B* **2006**, 110: 22618.

38. Delley B. J., *J. Chem. Phys.***1990**, 92: 508.

39. Software from Accelrys Inc., www.accelrys.com.

40. Perdew J. P., Wang Y., *Phys. Rev. B* **1992**, 46: 6671.

41. White J. A., Bird D. M., *Phys. Rev. B* **1994**, 50: 4954.

42. Grey C. P., Poshni F. I., Gualtieri A. F., Norby P., Henson J. C., Corbin D. R., *J. Am. Chem. Soc.* **1997**, 119: 1981.

43. Olson D H *Zeolites* **1995**, 15: 439.

44. C.R.C. Handbook of Chemistry and Physics, 83rd edn., CRC Press, Boca Raton, FL, 2002.

45. Fitch A.N., Jobic H., Renouprez A., *J. Phys. Chem. B* **1986,** 90: 1311.

46. Kirschhock C.E.A., Hunger B., Martens J., Jacobs P.A., *J. Phys. Chem. B* **2000**, 104: 439.

47. Plant D. F., Maurin G., Deroche I., Gaberova L., Llewellyn P. L., *Chem. Phys. Lett.* 2006, 426: 387.

48. Vayssilov G. N., Staufer M., Belling T., Neyman K. M., Knozinger H., Rösch N., *J. Phys. Chem. B* **1999,** 103: 7920.

49. Vassilov G. N., Rösch N., *J. Phys. Chem. B* **2001**, 105: 4277.

50. Anderson A. A., Shepelev Y. F., Smolin Y. I., **1990**, 10: 32.

51. Vayssilov G. N., Staufer M., Belling T., Neyman K. M., Knozinger H., Rösch N., *J. Phys. Chem. B.* **1999**, 103: 7920.

52. Pearson R. G., *J. Chem. Educ.* 1987, 64: 561

53. Barthomeuf D., *Catal. Rev.* **1996**, 38: 521.

3 BRÖNSTED ACIDITY OF ALKALI AND ALAKLINE EARTH CATION EXCHANGED FAUJASITE ZEOLITES

Abstract

Density functional theory based reactivity descriptors are used to investigate the effect of alkali and alkaline earth cations on Brönsted acidity of bridging OH group of faujasite zeolites. Faujasite is modelled by cutting the 6T ring of its supercage which contains the SII cationic position as active site. The alkali cation exchanged cluster contains two tetrahedral aluminum atoms whereas alkaline earth cation exchanged cluster contains three Al atoms. Thus single negative charge developed in a model cluster is compensated by proton. The global reactivity descriptors chemical potential, chemical hardness, chemical softness and electrophilicity of the clusters and local reactivity descriptors charge, Fukui function and relative electrophilicity values of acidic proton are calculated to derive Brönsted acidity. DFT based reactivity descriptors show that Brönsted acidity of alkali exchanged zeolites decreases in the order: H-Li-FAU> H-Na-FAU> H-K-FAU> H-Rb-FAU> H-Cs-FAU while that of alkaline earth exchanged faujasite decreases in the order of H-Mg-FAU> H-CaFAU> H-Sr-FAU> H-Ba-FAU. This Brönsted acidity sequence of faujasite agrees well with available experimental results.

3.1 Introduction

Thorough understanding of mechanism of zeolites and other solid acid catalysed reactions are necessary to design more effective heterogeneous catalysts.[1] Unfortunately, we do not yet have even a simple measure for quantifying the acidity of Brönsted acid sites in zeolites. Various measures have been proposed, including the O—H bond length, intensities of O—H stretching frequency[2], deprotonation energy (proton affinity), heats of adsorption of ammonia, pyridine and other small base probe molecules measured by microcalorimetry and themperature programmed desorption[3], and energy jump between neighboring oxygen atoms measured by variable temperature ^{1}H NMR.[4] Brönsted acidic sites of zeolites have major industrial importance as catalyst in the host of commercially important processes, due to large number of chemical reactions that are initiated or promoted by proton transfer. The catalytic activity of protonated zeolite depends strongly on acid strength and number of bridging protons.[5] Acidic zeolites are extensively used in industrial processes such as cracking, isomerization and alkylation of hydrocarbons. The mechanisms by which these reactions proceed involve proton transfer and formation of carbenium ions as reaction intermediates. In alkylation reactions, zeolites offer numerous advantages as compared to the traditional Friedel-Crafts catalysts; e.g., they allow streochemical control over the reaction, and they are more environmental friendly. The strength of Brönsted acid site depends on a number of factors including Si—O—Al bond angles, number of next-nearest neighbour Al atoms and the presence of extraframework cations in the proximity of Brönsted acidic sites.[6,7] Therefore, understanding the effects of metal cations on the structure and acidity of active sites of H-M-zelites (M=exchanged cation) is a crucial step toward rationalization of their chemical and catalytic properties. Previous experimental and theoretical studies have provided valuable insights in distinguishing different types of bridging OH groups in the mixed forms of zeolites with

two kinds of charge compensating cations (proton and metal cations).[8-13] Datka *et al.*[8] identified four different types of bridging OH groups in H-Na-Y zeolites by performing both experimental and MNDO quantum chemical studies. Hunger *et al.*[9] showed two adsorption states of ammonia in H-Na—Y zeolite differing the adsorption energies of about 20 $kJmol^{-1}$. Gonzales *et al.*[10] modelled various extra-framework cations in the vicinity of bridging OH groups and found an increase in Brönsted acidity in the order: $H^+ < Li^+ < Al(OH)_2^+ < K^+ < Na^+ < AlO^+ < Ca(OH)^+$ for cation exchanged H-ZSM-5 zeolite by calculating proton affinity values. Vayssilov and Rösch[12] reported the effect of some alkali and alkaline earth metal cations on Brönsted acidity by calculating deprotonation energy of the bridging OH group. They also found that Brönsted acidity of the mixed forms of zolites increases upon cation exchange and the order of acidity for alkali exchanged zeolites was observed as : $Li^+ < K^+ < Na^+$. On the other hand, the polarizing ability as well as the Lewis acidity of bare Na^+ ion is higher as compared to that of K^+ due to the higher charge-to-radius ratio. Thus, one expects a more effective polarization of the bridging OH group by the Na^+ ion, which in turn, leads to higher Brønsted acidity of H-Na-Y than H-K-Y zeolite. Barbosa and van Santen[13] studied the effect of Zinc cations on Brönsted acidity of the bridging protons in one or two of the coupled 4T rings of zeolite structure. They found an increase of Brönsted acidity of bridging OH group only when a Zn-OH cation is located at the same 4T ring with OH group. Coughlan and Keane[14] generated Brönsted acidic sites by reducing a range of copper Y zeolites that were proved with infrared spectroscopy. The nature of the alkali metal cations (Li^+, Na^+, K^+, Rb^+ and Cs^+) had been found to influence both the acid strength and location of Brönsted sites. They reported a decrease of Brönsted acid strength in the order of CuLi-Y> CuNaY> CuKY> CuRbNaY> CuCsNaY. In another experimental paper, Bai and

Sachtler[15] observed that the acid strength of protons in Pd/H-M-Y zeolite is lowered in the sequence of Pd/H-Li-Y > Pd/H-Na-Y > Pd/H-K-Y.

The goal of this chapter is to investigate the effect of alkali and alkaline earth metal cations on Brönsted acidity of mixed forms of faujasite zeolites using density functional based reactivity descriptors. In recent years, a number of chemical concepts have been developed based on Density Functional Theory. Indeed, concepts such as electronic chemical potential, μ, global chemical hardness, η, chemical softness, S, and electrophilicity, ω, have proved successful in rationalization of chemical processes.[16-18] These reactivity descriptors are used in describing chemical reactivity of a molecule as a whole. On the other hand, local reactivity descriptors like Fukui function, local softness[19,20] etc., have attracted considerable interests to describe the relative reactivity and site selectivity in chemical reactions. Here, we have demonstrated the potential of these reactivity parameters in determining Brönsted acidity of zeolites.

3.2 Computational details

To investigate the geometry and electronic properties of zeolites with high accuracy it is necessary to select most appropriate theoretical methods as well as the best models to represent the structure of zeolites. Nevertheless, cluster approach is very popular to model active sites of zeolites. The effect of alkali (Li^+, Na^+, K^+, Rb^+, Cs^+) and alkaline (Mg^{2+}, Ca^{2+}, Sr^{2+}, Ba^{2+}) cations on Brönsted acidity of faujasite zeolite is investigated with 6T ring clusters. In alkali cation exchanged clusters two tetrahedral silicon atoms are isomorphously substituted by two aluminum atoms whereas in alkaline earth cation exchanged zeolite cluster three silicon atoms are substituted by three aluminum atoms so as to have two types of charge compensating cations in each cluster. The relative position of aluminum atoms in the cluster has been chosen in such as way that the cluster obeys

the Löwenstein rule[21]. Alkali and alkaline earth cation exchanged faujasite zeolite clusters are shown in Figure 3.1 and Figure 3.2, respectively. In both types of clusters, free valences of silicon and aluminum atoms are saturated with hydrogen atoms. In alkali metal cation exchanged zeolite clusters, location of two aluminium atoms are taken as para to each other. At first, only Si-H, Al-H and O-H bonds and the position of exchanged cations were optimized keeping the position of other atoms fixed at their crystallographic position.[22] In subsequent calculations, the obtained positions of the terminating hydrogen atoms were held fixed and all other atoms were optimized.

All the calculations were performed with DMol3[23,24] program using local density approximation (LDA) with Perdew-Wang (PWC) functional and generalized gradient approximation (GGA) with PW91[25,26] functional. The DNP basis set which comparable to 6-31G** Gaussian orbital basis [27,28] were used in our calculations. Local reactivity parameters are derived using both MPA and HPA schemes.

3.3 Results and Discussion

3.3.1 Optimized Structure

3.3.1.1 Alkali cation-exchanged clusters

Top and side views of the optimized 6T ring cluster used to model Brönsted acidity of alkali cation-exchanged zeolites is shown in Figure 3.1. The selected geometrical parameters evaluated at PWC/DNP and PW91/DNP levels for all alkali exchanged zeolites are summarized in Table 3.1. As discussed in the previous chapter, location of alkali metal cations with respect to zeolite framework strongly depends on the ionic radii of cations.

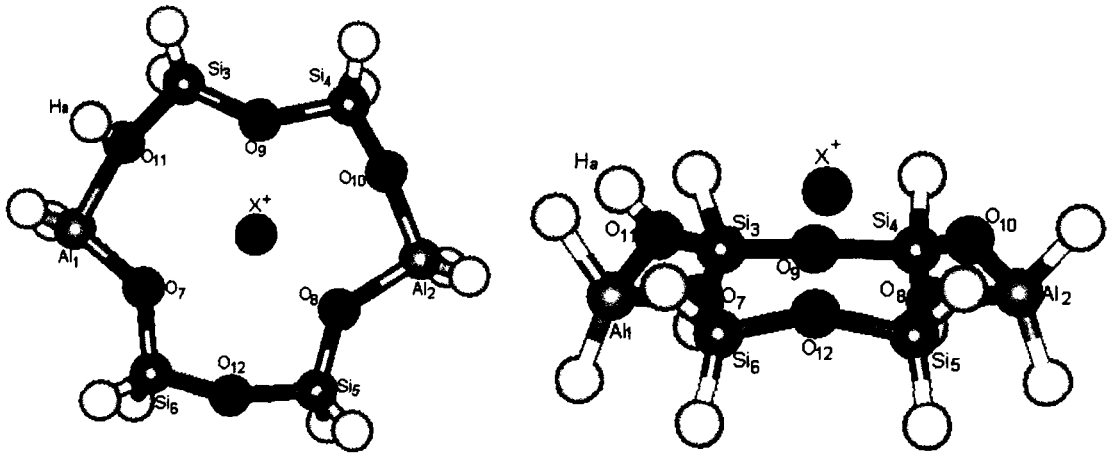

Figure 3.1: Ball and Stick model cluster of 6T ring faujasite zeolite. The oxygen and bridging hydrogen atoms are labeled for easy reference in the discussion. Where X^+ = Li^+, Na^+, K^+, Rb^+, Cs^+.

Cation-oxygen bond distances are found to increase with the increase of cation radii (Table 3.1). Alkali-cations are basically interacted with the oxygen centre of Si—O—Al bridges. The framework oxygen centers are directed towards metal cations except the oxygen atom of the bridging O—H group. The smaller cation, Li^+ is located very near to the plane of T atoms and with increasing radius, the cations move away from the plane of T atoms. The smaller alkali metal cations such as Li^+ and Na^+ have two-fold coordination with the framework oxygen atoms, O_7 and O_8 and stay at longer distance from other oxygen atoms. On the other hand, larger cations such as K^+, Rb^+ and Cs^+ have three fold coordinations with O_7, O_8 and O_{10} atoms. The shortest Li—O_8 distance is 1.88 Å whereas the longest Li—O_{11} distance is 3.25 Å. In all the cases the metal, M—O_8 distance is minimum and M—O_{11} is maximum.

Table 3.1: Variation of selected internal coordinates of optimized 6T ring cluster of alkali cation exchanged faujasite zeolites calculated at PWC/DNP and PW91/DNP levels.

Internal Co-ordinates	Exchanged cations									
	PWC/DNP					PW91/DNP				
	Li^+	Na^+	K^+	Rb^+	Cs^+	Li^+	Na^+	K^+	Rb^+	Cs^+
$X^+—O_7$[a]	2.097	2.341	2.662	2.816	3.058	2.105	2.372	2.782	2.992	3.297
$X^+—O_8$[a]	1.879	2.140	2.462	2.586	2.757	1.893	2.186	2.540	2.678	2.868
$X^+—O_9$[a]	2.301	2.328	2.705	2.843	3.038	2.303	2.392	2.883	3.042	3.283
$X^+—O_{10}$[a]	2.816	2.649	2.901	2.986	3.121	2.870	2.772	3.044	3.156	3.285
$X^+—O_{11}$[a]	3.153	3.042	3.192	3.305	3.482	3.182	3.099	3.336	3.553	3.784
$X^+—O_{12}$[a]	2.998	3.080	3.143	3.259	3.402	3.046	3.136	3.272	3.380	3.570
Al1—O11[a]	1.909	1.927	1.934	1.930	1.929	1.933	1.952	1.949	1.948	1.950
Al1—O7[a]	1.785	1.756	1.740	1.740	1.736	1.802	1.773	1.575	1.757	1.753
<Al2—O>[a]	1.818	1.806	1.801	1.801	1.799	1.839	1.825	1.821	1.818	1.817
<Si3—O>[a]	1.654	1.646	1.645	1.645	1.644	1.666	1.660	1.658	1.657	1.655
<Si4—O>[a]	1.649	1.642	1.638	1.636	1.635	1.663	1.655	1.682	1.649	1.648
<Si5—O>[a]	1.644	1.634	1.633	1.634	1.633	1.656	1.649	1.647	1.647	1.647
<Si6—O>[a]	1.643	1.635	1.631	1.631	1.630	1.655	1.648	1.645	1.644	1.642
$O_7—Al_1—O_{11}$[b]	98.3	97.3	97.9	98.2	98.580	98.5	97.8	98.6	99.020	99.4
$O_8—Al_2—O_{10}$[b]	97.9	97.2	99.3	99.5	100.5	98.5	98.4	100.2	100.7	101.6
$O_7—X^+—O_8$[b]	118.7	108.9	93.9	87.5	80.1	118.3	105.8	88.9	81.7	73.7
$O_9—X^+—O_{12}$[b]	172.3	158.3	129.9	121.4	111.7	172.3	151.5	122.4	113.5	103.6
$O_{11}—X^+—O_{10}$[b]	112.5	116.6	105.9	101.7	95.9	112.6	114.7	101.9	96.2	90.1

[a] values are in Å, [b] values are in degrees, < > represent average

3.3.1.2 Alkaline earth-exchanged clusters

Selected geometric parameters of optimized structures, evaluated by DFT calculation at PWC/DNP and PW91/DNP levels are reported in Table 3.2. It is seen from Table 3.2 that the Mg^{2+} cation has three-fold coordination with framework oxygen atoms, O_7, O_8, O_9 and stay far apart from the other framework oxygen atoms. But the cations Ca^{2+}, Sr^{2+} and Ba^{2+} have five-fold coordination with framework oxygen atoms, O_7, O_8, O_9, O_{11}, O_{12} and stay at long distance from oxygen atom (O_{10}) of the bridging O—H group. In the model cluster of alkaline-earth metal cation exchanged zeolite, all oxygen atoms are connected with at least one aluminum atom. The strong interaction between cation and framework oxygen atoms elongate Al—O and Si—O bond lengths and compress O—Al—O and O—Si—O bond angles. These elongations of Al—O and Si—O bond lengths are larger for the smaller

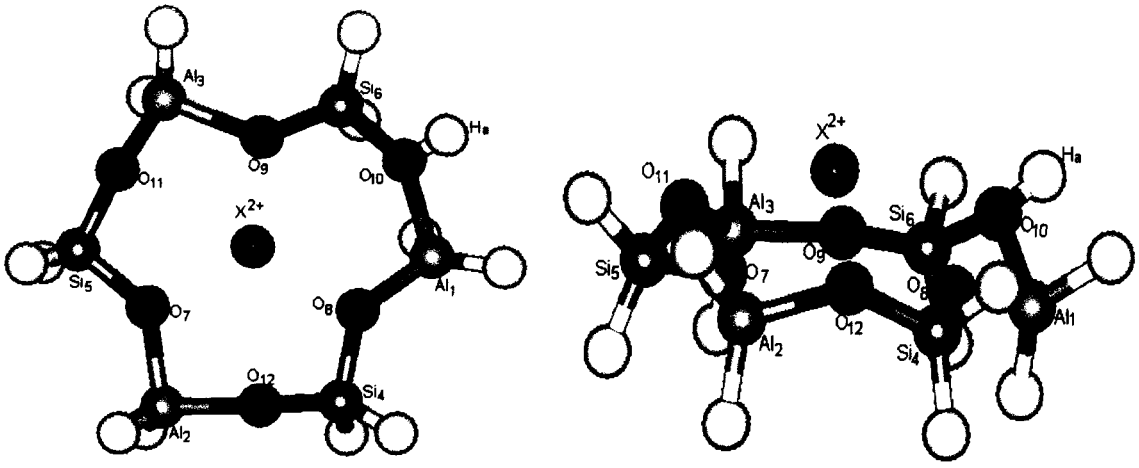

Figure 3.2: Ball and Stick model cluster of 6T ring cluster of faujasite zeolite. The oxygen and bridging hydrogen atoms are labeled for reference in the discussion. Where $X^{2+} = Mg^{2+}$, Ca^{2+}, Sr^{2+}, Ba^{2+}.

Table 3.2: Variation of selected internal coordinates of optimized 6T ring cluster of alkaline earth cation exchanged faujasite zeolites calculated at PWC/DNP and PW91/DNP levels.

Internal Co-ordinates	Exchanged cations							
	PWC/DNP				BP-VWN/DNP			
	Mg^{2+}	Ca^{2+}	Sr^{2+}	Ba^{2+}	Mg^{2+}	Ca^{2+}	Sr^{2+}	Ba^{2+}
$X^{2+}—O_7$ [a]	1.932	2.156	2.304	2.468	1.936	2.147	2.295	2.458
$X^{2+}—O_8$ [a]	2.031	2.328	2.496	2.685	2.041	2.335	2.504	2.691
$X^{2+}—O_9$ [a]	2.042	2.333	2.501	2.689	2.055	2.342	2.514	2.703
$X^{2+}—O_{10}$ [a]	3.322	3.351	3.364	3.438	3.317	3.335	3.361	3.435
$X^{2+}—O_{11}$ [a]	3.020	2.778	2.880	3.012	3.003	2.782	2.879	3.023
$X^{2+}—O_{12}$ [a]	2.849	2.687	2.816	2.981	2.818	2.692	2.806	2.963
$Al_1—O_{10}$ [a]	1.958	1.979	1.991	2.000	1.964	1.990	2.001	2.010
$Al_1—O_8$ [a]	1.823	1.779	1.775	1.771	1.817	1.775	1.770	1.766
$<Si_4—O>$ [a]	1.673	1.662	1.659	1.658	1.661	1.650	1.647	1.642
$<Si_5—O>$ [a]	1.660	1.648	1.649	1.651	1.648	1.638	1.639	1.640
$<Si_6—O>$ [a]	1.699	1.691	1.692	1.673	1.686	1.680	1.680	1.681
$<Al_2—O>$ [a]	1.846	1.823	1.823	1.835	1.844	1.824	1.823	1.825
$<Al_3—O>$ [a]	1.896	1.863	1.858	1.853	1.896	1.862	1.856	1.851
$O_8—Al_1—O_{10}$ [b]	100.2	99.4	98.9	99.2	100.2	99.2	98.9	99.1
$O_7—Al_2—O_{12}$ [b]	95.5	93.8	95.5	96.7	95.1	93.9	95.4	96.5
$O_9—Al_3—O_{11}$ [b]	97.1	93.7	95.2	96.5	96.8	94.1	95.4	96.9
$O_7—X^{2+}—O_8$ [b]	126.1	115.9	105.4	95.1	126.5	116.1	105.8	95.5
$O_9—X^{2+}—O_{12}$ [b]	171.2	151.4	136.9	124.3	170.9	151.1	136.8	124.1
$O_{11}—X^{2+}—O_{10}$ [b]	115.4	114.1	111.2	106.7	115.2	113.9	110.8	106.2

[a] values are in Å, [b] values are in degrees, < > represent average

cations as they are very near to the plane of the T atoms. Like alkali cation, location of alkaline-earth cations relative to zeolite framework also depends on the ionic radii of the cations. The cation to oxygen bond distance increases with increase in ionic radii of the cations.

3.4 Brönsted acidity

The strength of Brönsted acidity and thus catalytic activity of zeolites depend on various extraframework cations present in the zeolite cluster. It is believed that rises in Brönsted acidity is attributable to the withdrawal of electron density from framework oxygen atoms caused by the increase of positive charge on Al atoms due to the presence of a polyvalent cation in proximity to Brönsted site. We performed a systematic study to know the effect of different alkali and alkaline earth cations on Brönsted acidity of mixed forms of faujasite. DFT based global and local reactivity descriptors have been evaluated for this purpose.

3.4.1 Brönsted acidity of alkali cation-exchanged zeolites

3.4.1.1 Global reactivity descriptors

The calculated values of global reactivity descriptors chemical potential, chemical hardness, chemical softness and electrophilicity index of alkali cation exchanged zeolite clusters evaluated using PWC/DNP and PW91/DNP levels are presented in Table 3.3. It is seen from the table that for alkali cation exchanged zeolites, chemical hardness values decrease in the order: H-Li-FAU> H-Na-FAU> H-K-FAU> H-Rb-FAU> H-Cs-FAU. Hence, Brönsted acidity of alkali cation exchanged zeolites decrease from Li^+ to Cs^+. It is noticed from Table 3.3, that the electrophilicity index values calculated at PWC/DNP and

PW91/DNP levels also decrease from Li-exchanged to Cs-exchanged zeolites. Therefore, Brönsted acidity of alkali exchanged faujasite zeolites decrease from H-Li-FAU to H-Cs-FAU.

Table 3.3: Calculated Chemical potential, chemical hardness, chemical softness, and electrophilicity, values of optimized 6T ring cluster of alkali cation exchanged faujasite zeolite. These values are evaluated using PWC/DNP and PW91/DNP levels.

Exchanged Cations	DFT Functional	Chemical potential (μ)	Chemical hardness (η)	Chemical softness (S)	Electrophilicity (ω)
Li^+		-3.961	1.540	0.325	5.055
Na^+		-3.894	1.546	0.323	4.891
K^+	PWC/DNP	-3.793	1.551	0.322	4.638
Rb^+		-3.781	1.569	0.319	4.556
Cs^+		-3.753	1.596	0.313	4.415
Li^+		-3.886	1.680	0.298	4.400
Na^+		-3.791	1.693	0.295	4.244
K^+	PW91/DNP	-3.677	1.704	0.293	3.967
Rb^+		-3.652	1.727	0.290	3.861
Cs^+		-3.608	1.764	0.283	3.690

3.4.1.2 Local reactivity descriptors

3.4.1.2.1 Charge, (q_H^+)

Mulliken and Hirshfeld charges of the bridging proton of alkali cation exchanged Faujasite zeolites calculated using PWC/DNP and PW91/DNP levels are summarized in Table 3.4. It is seen that Mulliken charges of the bridging proton evaluated using PWC/DNP and PW91/DNP levels vary irregularly.

Table 3.4: MPA and HPA derived charges, nucleophilic Fukui function, electrophilic Fukui function, and relative electrophilicity of proton in alkali cation exchanged 6T ring cluster of faujasite zeolite. The values are evaluated using PWC/DNP and PW91/DNP levels.

Exchanged Cations	DFT Functional	MPA derived parameters				HPA derived parameters			
		q_M	f_M^+	f_M^-	f_M^+ / f_M^-	q_M	f_M^+	f_M^-	f_M^+ / f_M^-
Li^+		0.359	0.335	0.009	37.222	0.222	0.154	0.005	30.800
Na^+		0.364	0.328	0.009	36.444	0.219	0.158	0.006	26.333
K^+	PWC/DNP	0.363	0.322	0.010	32.200	0.209	0.154	0.006	25.667
Rb^+		0.363	0.319	0.010	31.900	0.207	0.153	0.006	25.500
Cs^+		0.364	0.305	0.010	30.500	0.204	0.148	0.006	24.667
Li^+		0.332	0.299	0.009	33.222	0.214	0.154	0.006	25.667
Na^+		0.336	0.292	0.010	32.444	0.209	0.149	0.006	24.833
K^+	PW91/DNP	0.341	0.257	0.010	25.700	0.202	0.131	0.006	21.833
Rb+		0.342	0.247	0.010	24.700	0.200	0.126	0.006	21.000
Cs+		0.343	0.236	0.010	23.600	0.199	0.124	0.006	20.667

These values are found almost constant irrespective of the exchanged cations. However, the Hirshfeld changes of the proton calculated using PWC/DNP and PW91/DNP levels decrease in the order: H-Li-FAU> H-Na-FAU> H-K-FAU> H-Rb-FAU> H-Cs-FAU. These results also indicate that q_H values are sensitive to basis set and the population analysis used. Hence, there is a need for more reliable reactivity parameters to describe Brönsted acidity correctly.

3.4.1.2.2 Fukui function,(f_H^+)

Fukui function values (f_H^+ and f_H^-) of bridging proton of alkali cation exchanged zeolites derived from MPA and HPA schemes using PWC/DNP and PW91/DNP levels are listed in Table 3.4. It is seen from Table 3.4 that f_H^+ values of the bridging proton calculated with MPA and HPA schemes at PWC/DNP and PW91/DNP levels decrease from Li^+ to Cs^+-exchanged faujasite zeolites. Therefore, from f_H^+ values of bridging protons, we can report that Brönsted acidity of alkali cation exchanged faujasite zeolite decreases in the order: H-Li-FAU> H-Na-FAU> H-K-FAU> H-Rb-FAU> H-Cs-FAU. Santos *et al.*[29] reported basicity of zeolites using Fukui function values. Unfortunately, they could not reproduce correct basicity of zeolite using f^-. This has lead to use of better reactivity descriptors, relative electrophilicity and relative nucleophilicity to study acidity and basicity, respectively of zeolites.

3.4.1.2.3 Relative electrophilicity, (f_H^+ / f_H^-)

The relative electrophilicity, (f_H^+ / f_H^-) values of bridging proton of alkali metal-cation exchanged faujasite zeolite derived from MPA and HPA schemes at PWC/DNP and PW91/DNP levels are reported in Table 3.4. It is noticed from the Table 3.4 that f_H^+ / f_H^- values of bridging proton derived with MPA and HPA schemes at PWC/DNP and PW91/DNP levels decrease in the order: H-Li-FAU> H-Na-FAU> H-K-FAU> H-Rb-FAU> H-Cs-FAU. Therefore, Brönsted acidity of alkali-exchanged faujasite zeolites decreases in the order: H-Li-FAU> H-Na-FAU> H-K-FAU> H-Rb-FAU> H-Cs-FAU. This sequence is in perfect agreement with experimental and previous theoretical results on some of these clusters.

3.4.2 Brönsted acidity of alkaline earth cation-exchanged zeolites

3.4.2.1 Global reactivity descriptors

The calculated global reactivity descriptors of alkaline earth cation exchanged zeolites are presented in Table 3.5. The electrophilicity index and chemical potential values of the optimized clusters evaluated at PWC/DNP and PW91/DNP levels revealed that the Brönsted acidity of Mg-exchanged zeolite is maximum and that of Ba-exchanged zeolite minimum. However, global hardness and global softness values failed to reproduce the correct acidity trend.

Table 3.5: Calculated Chemical potential, μ, chemical hardness, η, chemical softness, S, and electrophilicity, ω, values of alkaline earth exchanged 6T ring cluster of faujasite zeolite. These values are evaluated using PWC/DNP and PW91/DNP methods.

Exchanged Cations	DFT Functional	Chemical potential (μ)	Chemical hardness (η)	Chemical softness(S)	Electrophilicity (ω)
Mg^{2+}		-3.959	1.895	0.264	4.135
Ca^{2+}		-3.903	1.851	0.271	4.115
Sr^{2+}	PWC/DNP	-3.865	1.816	0.275	4.113
Ba^{2+}		-3.776	1.752	0.285	4.069
Mg^{2+}		-4.286	1.778	0.281	5.166
Ca^{2+}		-4.265	1.773	0.282	5.129
Sr^{2+}	PW91/DNP	-4.230	1.767	0.283	5.063
Ba^{2+}		-4.151	1.762	0.284	4.889

3.4.2.2 Local reactivity descriptors

3.4.2.2.1 Charge, (q_H^+):

The Mulliken and Hirshfeld charges of bridging proton (H_a) of alkaline-earth metal exchanged faujasite zeolite evaluated using PWC/DNP and PW91/DNP methods are listed in Table 3.6. Table 3.6 revealed that Mulliken charges on bridging protons are almost constant. Thus the variation of Brönsted acidity of alkaline-earth cation exchanged zeolites from Mg^{2+} to Ba^{2+} cannot be explained using Mulliken charges. The Hirshfeld charges of the proton decrease from Mg^{2+} ion exchanged zeolites to Ba^{2+} ion exchanged zeolites. Therefore, from Hirshfeld charges on proton, we can report that Brönsted acidity alkaline-earth exchanged zeolites increases in the order: $Mg^{2+} > Ca^{2+} > Sr^{2+} > Ba^{2+}$. This order of Brönsted acidity of alkaline-earth cation exchanged zeolites correlate well with experimental acidity.

3.4.2.2.2 Fukui function,(f_H^+)

Fukui function values (f_H^+ and f_H^-) of bridging proton (H_a) derived from MPA and HPA schemes are reported in Table 3.6. It is observed from Table 3.6 that Fukui function values (for nucleophilic attack) of bridging protons calculated with PWC/DNP level decrease from Mg^{2+} to Ba^{2+}-exchanged zeolites barring a slight increase of this value for Ca^{2+} from that of Mg^{2+}. Thus higher Brönsted acidity is found for Ca^{2+} exchanged zeolite and least Brönsted acidity for Ba^{2+}-exchanged zeolite. However, f_H^+ values of the bridging protons calculated using HPA and MPA schemes at PW91/DNP level decrease from Mg^{2+} to Ba^{2+} - exchanged faujasite zeolites. Therefore, Brönsted acidity of alkaline-

earth cation exchanged faujasite zeolites decreases in the order: Mg^{2+} > Ca^{2+} > Sr^{2+} > Ba^{2+} in agreement with experimental results.[30]

3.4.2.2.3 Relative electrophilicity, (f_H^+ / f_H^-)

Relative electrophilicity, (f_H^+ / f_H^-) values of the bridging protons (H_a) of alkaline earth cation exchanged zeolites derived from HPA and MPA schemes are reported in Table 3.6. The f_H^+ / f_H^- values calculated using HPA and MPA schemes show a much improved result of Brönsted acidity.

Table 3.6: MPA and HPA derived charges, nucleophilic Fukui function, electrophilic Fukui function, and relative electrophilicity of proton in alkaline earth cation exchanged 6T ring cluster of faujasite zeolite. The values are evaluated using PWC/DNP and PW91/DNP levels.

Exchanged Cations	Basis set	MPA derived parameters				HPA derived parameters			
		q_H^+	f_H^+	f_H^-	f_H^+ / f_H^-	q_H^+	f_H^+	f_H^-	f_H^+ / f_H^-
Mg^{2+}		0.307	0.268	0.012	22.333	0.2061	0.132	0.007	18.857
Ca^{2+}	PWC/DNP	0..312	0.277	0.013	21.308	0.2015	0.128	0.008	16.000
Sr^{2+}		0.314	0.139	0.014	9.929	0. 1985	0.063	0.009	7.000
Ba^{2+}		0.315	0.141	0.015	9.400	0.1959	0.062	0.009	6.889
Mg^{2+}		0.314	0.285	0.011	25.909	0.2062	0.135	0.007	19.286
Ca^{2+}	PW91/DNP	0.322	0.161	0.012	13.417	0.2012	0.072	0.008	9.000
Sr^{2+}		0.326	0.062	0.013	4.769	0.1983	0.028	0.008	3.500
Ba^{2+}		0.328	0.048	0.013	3.692	0.1961	0.023	0.009	2.556

The relative electrophilicity values of the bridging proton decreases from Mg^{2+} to Ba^{2+}-exchanged zeolites. Therefore, we can conclude that relative electrophilicity is a better reactivity descriptor to reproduce experimental Brönsted acidity sequence.

3.5 Conclusions

In this study, for the first time, we used DFT based reactivity descriptors to study the Brönsted acidity of mixed form of zeolites containing two types of charge compensating cations (alkali or alkaline earth cation and proton). Positive charge of the bridging proton (q_H^+) of alkali and alkaline earth cation exchanged zeolites are found to be a weak reactivity parameter to explain their Brönsted acidity. Chemical potential, electrophilicity index values show that in the mixed form of zeolites, Brönsted acidity is affected by the presence of extra-framework cations. The f_H^+ and f_H^+/f_H^- values of the bridging protons of alkali and alkaline earth cation exchanged zeolites derived from HPA and MPA schemes are found to be reliable parameters in determining Brönsted acidity.

References

1. Gorte R.J., Catal. Lett. **1999**, 62: 1.

2. Kazansky V. B., Serykh A. I., Semmer-Herledan V., Fraissard J.. Phys.Chem. Chem. Phys. 2003, 5: 966.

3. Biaglow A.I., Gorte R.J., Kokotailo G.T., White D., J. Catal. **1994**, 148:779.

4. Sierka M., Sauer J., J. Phys. Chem. B **2001**,105: 1603.

5. Simpler A., Bell R. G., Foster M. D., Gray A. E., Lewis D. W. Anderson M. W., *J. Phys. Chem. B* **2004,** 108: 7152.

6. Carvajal R., Chu P. –J., Lunsford J. H., *J. Catal.* **1990**, 125: 123.

7. Brunner E., Ernst H., Freude D., Frohlich T., Hunger M. Pfeifer H., *J. Catal.* **1991**, 127: 34.

8. Datka J., Broclawik E., Gill, B., *J. Phys. Chem.* **1994**, 98: 5622.

9. Hunger B., Miessner H., Szombathely M., Geidel E., *J. Chem. Soc., Faraday Trans.* **1996**, 92: 499.

10. Gonzales N. O., Chakrabory A. K., Bell A. T., *Catal. Lett.* **1998**, 50: 135.

11. Huang W. F., Hung D. C., Huang C. C., Tseng P. K., *Catal. Lett.* **1999**, 59: 213.

12. Vayssilov G. N., Rosch N., *J. Phys. Chem. B* **2001**, 105: 4277.

13. Barbosa L. A. M. M., van Santen R. A., *Catal. Lett.* **1999**, 63:97.

14. Coughlan B., Keane M. A., *Catal. Lett.* **1990**, 5:113.

15. Bai, X., Sachtler W.M.H., *Catal. Lett.* **1990**, 4: 319.

16. Pearson, R.G. *Chemical Hardness: Applications from Molecules to solid*, Wiley-VCH Verlag GMBH, Weinheim, **1997**.

17. De Proft F., Geerlings P., *Chem. Rev.* **2001**, 101:1451.

18. Chattaraj P. K., Roy D. R., *Chem. Rev.* **2007**, 107:PR46-PR-74.

19. Parr R. G.,Yang W., *J. Am. Chem. Soc.* **1984,** 106:4049.

20. Cuan A., Galva´n M., Chattaraj, P. K., *J. Chem. Sci.* **2005**, 117:541.

21. Loewenstein W., *Am. Mineral* **1954**, 39:92.

22. D. H. Olson, *Zeolites.* **1995,** 15: 439.

23. Delley B., *J. Chem. Phys.* **1990,** 92:508.

24. Software from Accelrys Inc., www.accelrys.com.

25. Perdew J. P., Wang Y., *Phys. Rev. B* **1992,** 46:6671.

26. White J. A., Bird D. M., *Phys. Rev. B* **1994**, 50:4954.

27. Gordon M. S., *Chem. Phys. Lett.* **1980,** 76: 163.

28. Hehre W. J., Ditchfield R., Pople J. A., *J. Chem. Phys.* **1972,** 56: 2257.

29. Santos J. C., Contreras R., *J. Chem. Phys.* **2002,** 116:4311.

30. Xu J., Mojet B. L., van Ommen J. G., Lefferts L., *Phys. Chem. Chem. Phys.* **2003**, 5: 4407.

4 BRÖNSTED ACIDITY OF ISOMORPHOUSLY SUBSTITUTED ZSM-5 ZEOLITE

Abstract

The Brönsted acidity of a series of isomorphously substituted ZSM-5 zeolite has been studied using density functional theory (DFT) based global and local reactivity indices. The global reactivity descriptors such as chemical potential, (μ) chemical hardness, (η) chemical softness, (S) and electrophilicity index, (ω) of the clusters and local reactivity descriptors namely charge, Fukui function (f^+) and relative electrophilicity (f^+/f^-) of acidic hydrogen atoms of Al, Ga and B substituted zeolite show that the acidity of these isomorphously substituted zeolites decreases in the order [Al]-ZSM-5 > [Ga]-ZSM-5 >> [B]-ZSM-5. This finding is in good agreement with the experimental results.

4.1 Introduction

The industrial organic reactions have undergone important changes by the invention of new type of solid acid catalysts namely zeolites. The main characteristics of these solid acids in comparison with liquid acids are that they operate in a very different medium and their bonding characteristics are unique. In the last three decades, isomorphous substitution of Si in the zeolitic framework by other tetrahedrally-coordinated elements such as Ti(IV)[1], Fe(III)[2-4], Ga(III)[5-7] and B(III)[8], has provided new materials showing specific catalytic properties related to the coordination state of the heteroatom. With only exception of Al(III), which has an ionic radius very close to that of Si(IV), the remaining heteroatoms can be inserted inside the zeolitic framework only in trace amounts (up to few wt%)[9]. The unique structure, channels, cages, and thermal stability of zeolites have an important consequence in their catalytic performance. Zeolites, as catalyst have number of commercial applications in petroleum refining, petrochemicals and more recently fine chemical production.[10] When a trivalent metal substitutes a Si atom, zeolite framework develops a negative charge which can be balanced by a bridging Si(OH)M(III) protons (M = B, Al, Fe, Ga), thus producing a microporous solids with Brönsted acidity. Incorporation of hetero atoms in to the zeolite framework can change the acidity and pore structure of zeolites. The new materials thus produced show different catalytic properties with altered activity, selectivity and stability, offering the potential to design zeolites for new applications.[11-14] Many efforts have been devoted to the synthesis, characterization and application of isomorphously substituted zeolites with elements in their framework other than Si and Al, such as B, Ga, and Fe.[15] Indeed, MFI polymorphs are used in several industrial processes. For example, Fe-ZSM-5 is an active catalyst for the production of methanol by the direct oxidation of methane and for the oxidation of benzene to phenol.[16] Ga-ZSM-5 shows high selectivity in the aromatization of alkanes[17]. B-ZSM-5 has been shown to be an active catalyst for the conversion of

methoxy butane to methanol and isobutene and it is also used in xylene isomerization as well as ethylbenzene conversion[7]. However, despite the considerable volume of information obtained, and the important catalytic role played by such isomorphously substituted zeolites, many facets of their behavior are poorly understood. For example, regarding the acidic properties, it is found that the intrinsic strength of the sites depends not only on the nature of atoms in the next neighbor coordination sphere but also on the crystalline structure of the zeolite. The intrinsic acid strength of these catalysts has been found to be very important for their activity. There has been an upsurge of interest in recent years in understanding the catalytic activity of zeolites. [18-20] Most of these studies highlight the creation of Brönsted acid sites owing to the substitution of silicon by aluminum in the tetrahedral units of the zeolite framework. Both theory and experiments have contributed significantly to understand the catalytic activity and acidity.[21,22]

Chu and Chang[23] used IR spectroscopy and temperature-programmed desorption (TPD) of NH_3 to study the acidity of several isomorphously substituted ZSM-5 zeolites and observed an increase of acidity in the order: Si—(OH) < B—(OH)—Si << Fe—(OH)—Si < Ga—(OH)—Si < Al—(OH)—Si. Stave and Nicholas[24] performed density functional calculations on dimer clusters and made a correlation of calculated vibrational frequency with the acidity of zeolite clusters. Chatterjee *et. al*[25,26] calculated proton affinity of acidic hydrogen atoms using local density functional (LDA) calculations. Their results also agree well with experimental data. While, the influence of zeolite composition and structure on acid strength has been studied by several theoretical methods,[27-30] only a very few of these studies have used DFT based reactivity parameters. Geerlings and co-workers[31] investigated the relative acidity of dimer cluster of isomorphously substituted zeolites using the condensed local softness, (s_H^+), as reactivity index, and they found that the Brönsted acidity increases in the order H_3Si—O(H) —GaH_3 < H_3Si—O(H) —BH_3 < H_3Si—O(H) —AlH_3. This acidity

sequence does not match with the experimental acidity. The less accurate description of acidity by local softness can be due to the choice of basis set, size of the cluster or the population analysis. The small cluster models could not explain the reason for low acidity of highly electronegative B-substituted species. However, Deka *et. al.* used, Hartree-Fock methods on dimer and trimer clusters of zeolites to mimic B, Al and Ga substituted zeolites.[32,33] The relative acidity of these materials derived from the local softness values showed a good agreement with the experimental results. In this study, we have investigated strength of Brönsted acidity of B, Ga, and Al substituted ZSM-5 in a 11 T cluster model using some DFT based global and local reactivity descriptors. We use the global reactivity parameters such as chemical potential, (μ) chemical hardness, (η) chemical softness, (S) and electrophilicity index, (ω) and local reactivity descriptors, namely, Fukui function, (f^+) for nucleophilic attack on the system, (f^-) for electrophilic attack on the system and their ratio (f^+/f^-) as measure of reactivity in order to investigate the acidity of the bridging O—H groups.

4.2 Computational details

The active sites of zeolite are modeled with an 11T cluster cut out from crystalline structure of orthorhombic ZSM-5. The model cluster investigated in this study is composed of $(X)_3SiOT(X)_2$—OH—$Si(X)_3$ structure with $X=OSiH_3$ and T=B, Ga and Al. The orthorhombic structure of ZSM-5 contains 12 distinct crystallographic tetrahedral sites. Theoretical studies indicated that T12 is the favourable site for aluminum substitution, but small energy differences among various isomers show a distribution of aluminum atom over a number of substitution sites.[34] In this chapter, we have considered T12 site for location of Al atom, since Si(12)—O(24)—Si(12) bridge lies in the intersection of straight and zigzag

channels, allowing the significant interaction between bridging hydroxyl group and adsorbed molecules and thus being considered as the catalytically active site. During optimization of the clusters, first only the terminating Si—H bonds were optimized keeping all other atoms fixed at their crystallographic positions.[35] The obtained positions of terminating hydrogen atoms in all subsequent calculations were kept fixed, while rest of the atoms were allowed to relax freely during optimization. The terminal hydrogen atoms were kept fixed to avoid the unrealistic hydrogen bonding. The full structure optimization of zeolite clusters leads to a structure which may not resemble the experimental geometry.[36] We performed density functional theory calculations with the program DMol3 using DNP basis set and PWC and BLYP functional.[37] The global reactivity descriptors, such as chemical potential, (μ) chemical hardness, (η) and electrophilicity inex, (ω) have been calculated. The local reactivity descriptors are evaluated using both Hirshfeld population analysis (HPA)[38] and Mulliken population analysis (MPA)[39] schemes.

4.3 Results and discussion

4.3.1 Structure

The optimized 11T cluster used to model Brönsted acidity of isomorphously substituted zeolites is shown in Figure 4.1 and selected structural parameters of the clusters evaluated a PWC/DNP and BLYP/DNP levels are given in Table 4.1. The O—H bond length of the central bridge has been used as a measure of acidity of zeolites. When the model cluster is optimized, we notice no regular trend of change in O—H bond lengths (Table 4.1). The O—H bond distances in the model cluster (Table 4.1) show a shorter value for B-substituted clusters compared to that of Al and Ga- substituted clusters. However, the O—H bond distances evaluated in Al and Ga- substituted clusters are found to be almost same. Thus O—H bond length can explain the low acidity of B-substituted ZSM-5 zeolite although

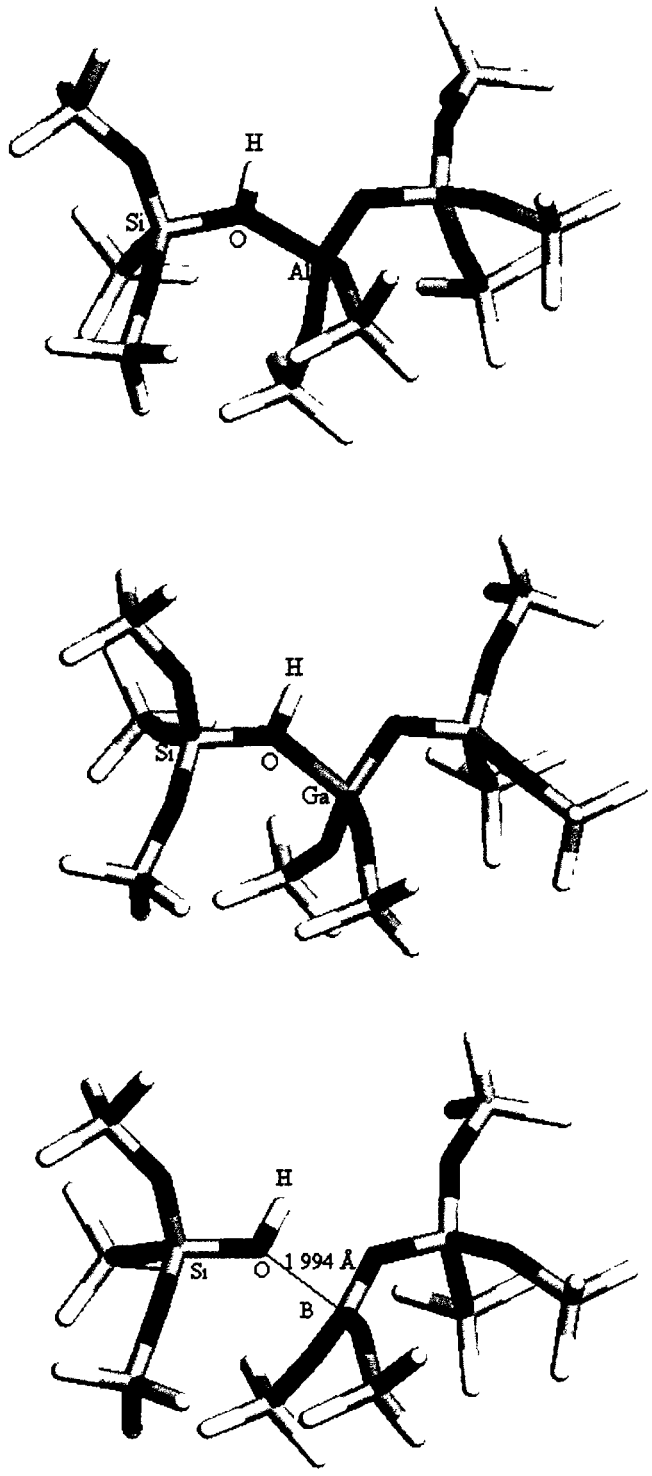

Figure 4.1: Optimized geometry of Al, Ga and B substituted ZSM-5 zeolite. Both Al and Ga have tetrahedral co-ordination whereas B has a trigonal co-ordination.

Table 4.1: Selected optimized geometric parameters of the central Si—O(H_b) —T (T=Al, Ga, B) of the ZSM-5 of cluster model at PWC/DNP and BLYP/DNP levels of calculation.

Cluster	DFT Functional	O—H_b bond in length(Å)	Si—O(H_b) bond in length(Å)	T—O(H_b) bond in length(Å)	Si—O(H_b)—T bond angle in (degree)
[Al]-ZSM-5		0.983	1.664	1.852	138.7
[Ga]-ZSM-5	PWC	0.985	1.654	1.944	138.9
[B]-ZSM-5		0.979	1.635	1.994	145.3
[Al]-ZSM-5		0.978	1.697	1.898	138.2
[Ga]-ZSM-5	BLYP	0.978	1.684	2.007	137.9
[B]-ZSM-5		0.971	1.644	2.253	142.8

it has high electronegativity. Since B is more electronegative among these elements, B should attract more electrons from the bridging oxygen atom and O—H bond in B-[ZSM-5] should have been longer and also should have higher acidity. The shorter O—H bond length in B-[ZSM-5] could be understood from T—O_b bond distances. The T—O_b bond distance in Ga-[ZSM-5] is larger than that in Al-[ZSM-5]. This is due to larger size of Ga atom compared to Al atom. The Si—O_b and T—O_b bond distances are in close agreement with other theoretical values. However, calculations show that T—O_b bond is much longer for the smaller atom B in B-[ZSM-5] indicating a tendency of B atom to have a trigonal coordination instead of a tetrahedral coordination when it is isomorphouly substituted in zeolites. Due to longer B—O_b distance in B-[ZSM-5], there is less attraction between the electrons of bridging oxygen and B atoms and therefore, the O—H bond length in B-[ZSM-5] is less than

that of Al and Ga- substituted species. The Si—O_b bond distance is found to be larger in B-[ZSM-5] than Al-ZSM-5 and Ga-ZSM-5 zeolites. The substituent atoms appear to cause significant changes in the zeolite geometry.

4.3.2 Brönsted Acidity

The catalytic activity of zeolites is primarily determined by Brönsted acidity sites present on the surfaces of zeolite channels and cavities. The relative acidity of these hydroxyl groups is influenced by differences in electronegativities of the associated T atoms and the local geometry. For the series of zeolite structures studied in this work, the acidity of bridging hydroxyl groups are derived by calculating chemical potential, (μ), chemical hardness, (η), chemical softness (S), electrophilicity index, (ω), charge, (q_H) Fukui function for nucleophilic, (f_H^+), Fukui function for electrophilic attract (f_H^-) and relative electrophilicity, (f_H^+ / f_H^-).

4.3.2.1 Global reactivity descriptors

The global reactivity descriptors evaluated using PWC/DNP and BLYP/DNP levels are presented in Table 4.2. The electrophilicity index is considered as a measure of electrophilic power of a system. Larger of the electrophilic power of a chemical system, higher is its acidity. It can be seen from the Table 4.2 that the electrophilicity index calculated with PWC/DNP and

Table 4.2: Calculated Chemical potential, μ, chemical hardness, η, chemical softness, S, and electrophilicity, ω, values of isomorphously substituted cluster model. These values are evaluated using PWC/DNP and BLYP/DNP level.

Exchanged Cations	DFT Functional	Chemical potential (μ)	Chemical hardness (η)	Chemical softness (S)	Electrophilicity (ω)
[Al]-ZSM-5		-4.313	2.335	0.214	3.983
[Ga]-ZSM-5	PWC	-4.299	2.344	0.213	3.951
[B]-ZSM-5		-4.203	2.714	0.184	3.254
[Al]-ZSM-5		-3.870	2.270	0.220	3.299
[Ga]-ZSM-5	BLYP	-3.869	2.319	0.216	3.228
[B]-ZSM-5		-3.806	2.664	0.188	2.719

BLYP/DNP levels decreases in the order: [Al]-ZSM-5 > [Ga]-ZSM-5 > [B]-ZSM-5. Therefore, the Brönsted acidity decreases from [Al]-ZSM-5 to [B]-ZSM-5 via [Ga]-ZSM-5. The chemical softness and chemical hardness values calculated using PWC/DNP and BLYP/DNP levels (Table 4.2) also correlate well with Brönsted acidity. Higher negative value of chemical potential of a zeolite cluster reveals the higher Brönsted acidity. The negative chemical potential value is maximum for [Al]-ZSM-5 zeolite and minimum for [B]-ZSM-5 zeolite as listed in Table 4.2. Hence, Brönsted acidity is higher for [Al]-ZSM-5 and lowers for [B]-ZSM-5. The global reactivity parameters calculated for the zeolite clusters indicate that Brönsted acidity decreases in the order: [Al]-ZSM-5> [Ga]-ZSM-5> [B]-ZSM-5, which is in excellent agreement with the experimental Bronsted acidity trend.

4.3.2.2 **Charge**

Charges on acidic hydrogen atoms are the most direct measure of acidity.[40] Molecules that exhibit hydroxyl groups with high positive charges on hydrogen atom have high Brönsted acidity. The charge on the bridging hydrogen atoms calculated by MPA and HPA schemes using PWC/DNP and BLYP/DNP levels for the zeolite clusters are given in the Table 4.3. It is seen from Table 4.3 that the HPA derived charge of acidic proton decrease from Al-[ZSM-5] to B-[ZSM-5] via Ga-[ZSM-5] indicating an acidity order of [Al]-ZSM-5> [Ga]-ZSM-5> [B]-ZSM-5. However, the charges on the bridging protons calculated using MPA scheme does not obey the experimental Brönsted acidity sequences. The charges are less significant to predict the acidity and basicity of zeolites correctly. It is also clear that charges on hydrogen atoms of hydroxyl groups are sensitive to basis set. Hence, there is a need for more reliable reactivity parameters to describe Brönsted acidity of isomorphously substituted zeolites.

4.3.2.3 Fukui function

DFT based local reactivity descriptor, like Fukui function has been used successfully to study the acidity and basicity of zeolites. We calculated the condensed Fukui function values (f_H^+ and f_H^-) of acidic hydrogen atom of each of the cluster from HPA and MPA schemes using PWC/DNP and BLYP/DNP levels and they are presented in Table 4.3. It is seen from Table 4.3 that Fukui function, f_H^+ (for nucleophilic attack) values of the bridging proton calculated with MPA and HPA schemes at PWC/DNP level decrease from [Al]-ZSM-5 to [B]-ZSM-5 zeolites.

Table 4.3: The MPA and HPA derived Fukui function for nucleophilic and electrophilic attacks and relative electrophilicity of bridging H-atom of isomorphously substituted zeolite cluster.

Exchanged Cations	DFT functional	MPA derived parameters				HPA derived parameters			
		q_H^+	f_H^+	f_H^-	f_H^+/f_H^-	q_H^+	f_H^+	f_H^-	f_H^+/f_H^-
[Al]-ZSM-5		0.373	0.120	0.014	8.571	0.208	0.047	0.008	5.875
[Ga]-ZSM-5	PWC	0.381	0.111	0.016	5.938	0.193	0.043	0.009	4.778
[B]-ZSM-5		0.349	0.073	0.017	4.294	0.173	0.027	0.009	3.000
[Al]-ZSM-5		0.326	0.100	0.014	7.143	0.1977	0.038	0.008	4.750
[Ga]-ZSM-5	BLYP	0.326	0.099	0.015	6.600	0.1867	0.036	0.009	4.000
[B]-ZSM-5		0.298	0.046	0.011	4.182	0.1658	0.018	0.007	2.571

Similar results were obtained from f_H^+ values calculated using BLYP functional for acidic hydrogen atom in isomorphously substituted zeolites. Hence, in general, the Brönsted acidity of isomorphously substituted zeolites derived from f_H^+ values decrease in the order: [Al]-ZSM-5> [Ga]-ZSM-5> [B]-ZSM-5, which in very good agreement with the experimental results.

4.3.2.5 Relative electrophilicity, (f_H^+/f_H^-)

The relative electrophilicity values calculated for the model clusters using Mulliken population analysis and Hirshfeld population analysis at PWC/DNP and BLYP/DNP levels are presented in Table 4.3. It is noticed from the Table 4.3, that the acidity trend derived from relative electrophilicity does not change with the functionals. Hence, relative

electrophilicity can be used as a reliable parameter to predict the acidity (or basicity) of zeolites.

4.4 Conclusions

In this study, we have used DFT based global reactivity parameters namely, chemical potential, chemical hardness, chemical softness and electrophilicity of the zeolite clusters and local reactivity descriptors, such as charge, Fukui function and relative electrophilicity of the bridging hydrogen atom to study the Brönsted acidity of isomorphously substituted ZSM-5 using 11T cluster. The Fukui function derived from HPA and MPA schemes provides experimental Brönsted sequence. The correct acidity trend is also obtained with the charge of the bridging proton derived from HPA scheme. However, the MPA scheme derived charge provides incorrect result. Relative electrophilicity values derived from MPA and HPA schemes have given the experimental acidity sequence as [Al]-ZSM-5> [Ga]-ZSM-5> [B]-ZSM-5. Hence, the relative electrophilicity values are found to be more reliable reactivity parameter to predict the experimental Brönsted acidity sequence of isomorphously substituted ZSM-5.

References

1. Taramasso M., Perego G. Notari B., US Pat. no. 4410501,**1983**.

2. Szostak R., Thomas T. L., *J. Catal.*, **1986**, 100: 555.

3. Ratnasamy P., Kumar R., Catal. Lett., **1993**, 22: 227.

4. Bordiga S., Buzzoni R., Geobaldo F., Lamberti C., Giamello E., Zecchina A., Leofanti G., Petrini G., Tozzola G., Vlaic G., J.Catal., **1996**, 158: 486.

5. Simmons D. K., Szostak R., Agrawal P. K. Thomas T. L., J.Catal., **1987**, 106: 287.

6. Axon S. A., Huddersman K., Klinowski J., Chem. Phys. Lett., **1990**, 172: 398.

7. Otero Areán O., Turnes Palomino G., Geobaldo F., Zecchina A., J. Phys. Chem., **1996**, 100: 6678.

8. Coudurier G., Auroux A., Vedrine J. C., Farlee R. D., Abrams L., Shannon R. D., J. Catal., **1987**, 108: 1.

9. Bordiga S., Bonino F., Damin A., Lamberti C., Phys. Chem. Chem. Phys. **2007**, 9: 4854.

10. Venuto, P.B., *Mircroporous Mat.* **1994**, **2**: 297.

11. Sauer J., *Chem. Rev.* **1989**, 89: 199.

12. Langenaeker W., Coussement N., De Proft F., Geerlings P., *J. Phys. Chem.***1994**, 98: 3010.

13. Dong M., Wang J., Sun Y., *Micropor. Mesopor. Mater.* **2001**, 43: 237.

14. Coudurier G., Vedrine J. C., *Pure Appl. Chem.* **1986**, 58: 1389.

15. Barrer R. M., *Hydrothermal Chemistry of Zeolites*; Academic Press: New York, 1982.

16. Durrant V. A., Walker D. A., Gussou S. N., Lyons J. E., US Patent 5 918 249, **1972**.

17. Gnep N. S., Biyemet J. D., Guisnet M. D., *J. Mol. Catal.* **1988**, 45: 281.

18. Corma, A., García, H., *Cat. Today* **1997**, 38: 257.

19. Kramer, G.J., van Santen, R.A., *J. Am. Chem. Soc.* **1993**, 115: 2887.

20. Kramer, G.J., van Santen, R.A., *Chem. Rev.* 1995, 95: 637.

21. Sauer J., Ugliengo P., Garrone E., Saunders V. R., *Chem. Rev.* **1994,** 94: 2095.

22. Vetrivel R., Catlow C. R. A., In modeling of structure and reactivity of zeolites. (ed) C. R. A. Catlow (London: Academic Press) **1992**, pp. 217.

23. Chu C. T. W., Chang C. D., *J. Phys. Chem.* **1985**, 89: 1569.

24. Stave M. S., Nicholas J. B., *J. Phys. Chem.* **1993**, 97: 9630.

25. Chatterjee A., Chandra A. K., *J. Mol. Catal.* **1997**, 51: 119.

26. Chatterjee A., Iwasaki T., Ebina T., Miyamoto A., *Micropor. Mesopor. Mater.* **1998**, 21: 421.

27. Goursot A., Vasilyev V., Arbuznikov A., *J. Phys. Chem.* **1997**, 101: 6420.

28. Langenaeker W., De Decker M., Geerlings P., *J. Mol. Struct. (THEOCHEM)* **1990**, 207: 115.

29. Schroeder K. –P., Sauer J., Leslie M., Catlow C. R. A., Thomas J. M., *Chem. Phys. Lett.* **1993**, 188: 320.

30. Schroeder K. –P., Sauer J., Leslie M., Catlow C. R. A., *Zeolites* **1992**, 12: 20.

31. Langenaeker W., Coussement N., De Proft F., Geerlings P., *J. Phys. Chem.* **1994**, 98: 3010.

32. Deka R. C., Vetrivel R., Pal S., *J. Phys. Chem. A* **1999**, 103: 5978.

33. Deka R.C., Roy R.K., Hirao K., *Chem. Phys. Lett.* **2000**, 332: 576.

34. Lonsinger S., Chakraborty A. K., Theodorou D. N., Bell A. T., *Catal. Lett.* **1991**, 11: 209.

35. E. A. Pidko, J. Xu, B. L. Mojet, L. Lefferts, I. R. Subbotina, V. B. Kazansky, and R. A. van Santen, *J. Phys. Chem. B.* 110 **2006**, pp. 22618–22627.

36. J. Sauer, G. Pacchioni and P. S. Bagus, *Cluster Models for Surface and Bulk Phenomena,* Parmigiani (Herausg.) eds., Plenum Press, New York, 1992, pp. 533.

37. Becke A., *J. Chem, Phys.* **1988**, 88: 2547.

38. Hirshfeld F. L., *Theoret. Chim. Acta.* **1977**, 44: 129.

39. Mulliken R. S., *J. Chem. Phys.* 23 (1955), pp. 1833–1840.

40. O'Malley P. J., Dwyer J., *J. Phys. Chem.* **1988**, 92: 3005.

5 STRUCTURE, LOCATION AND REACTIVITY OF TITANIUM, ZIRCONIUM AND TIN SUBSTITUTED MFI ZEOLITE

Abstract

The structure and preferential location of Ti, Zr and Sn atoms in titanium, zirconium and tin substituted MFI zeolite are investigated using 10T cluster model. The substitution energy of Ti, Zr and Sn atoms revealed that they are not equally distributed in all the 12 crystallographically distinct tetrahedral sites of MFI framework. The preferential location of them are found in four of the twelve distinct tetrahedral sites, namely T10, T8 and T4 with decreasing order of preference. The calculated location of Ti, Zr and Sn atoms in MFI framework and their geometric parameters agree well with some of the experimental and theoretical results. Density functional study suggests that Lewis acidity of isomorphously substituted Ti, Zr and Sn zeolites increases in the order: Sn < Zr <Ti.

5.1 Introduction

Isomorphous substitution of Si^{4+} by other tetrahedral metal ions namely, Ti^{4+}, Zr^{4+} and Sn^{4+} in MFI, MEL and BEA structures has led to the production of a new class of selective oxidation catalyst.[1-4] It has been a well-established fact that the reactivity of zeolites can be finely tuned by incorporation of various atoms such as B, Al, Ti, Zr, Fe etc. These atoms substituted in the zeolites framework act as active Brönsted and Lewis acid sites depending upon their valence states. Nature of acid sites created due to isomorphous substitution plays a crucial role in understanding some important oxidation and reduction reactions.[5,6,7]

Ti containing zeolite TS-1 has exhibited excellent catalytic activities for oxidation of various organic reactions such as olefin epoxidation, conversion of ammonia to hydroxylamine, secondary amine to dialkylhydroxylamine, secondary alcohols to ketones and phenol hydroxylation in presence of hydrogen peroxide under mild conditions.[8] It is believed that the determining factors explaining the unique behavior of TS-1 are the presence of isolated tetrahedrally coordinated Ti sites and the hydrophobic character of this material that allows hydrocarbons to diffuse and adsorb on the zeolites when water is present in the system.

The successful catalytic results obtained with Ti zeolites led to the synthesis of zeolites containing other transition metals in the framework positions. Such attempts have been made to incorporate Zr- and Sn- in the zeolites. Tin and zirconium have been incorporated tetrahedrally into the framework of zeolite BEA. Mal and Ramaswamy,[9,10] for the first time synthesized Al-free-Sn BEA. They also predicted that Sn atom in BEA is tetrahedrally coordinated. Isomorphous substitution of framework Si ions by Zr ions in AlPO-5, MFI and MEL possess Brönsted and Lewis acidity[11]. Zr substituted AlPO-5 was found to be active in the isomerization of *m*-xylene[12] and Zr-ZSM-5 was found to be active

for the hydroxylation of benzene to phenol.[13] Occelli *et al.*[14] synthesized isomorphously substituted Zr-MCM-41 and characterized the acidity by microcalorimetry experiments. However, geometry, coordination and distribution of Zr in the framework have not been established. XRD, FTIR, DR UV-Vis and ^{29}Si MAS NMR spectroscopic techniques elucidates the presence of zirconium in the MFI framework. Isomorphous substitution of Si^{4+} by Zr^{4+} ions was inferred based on increase of the unit cell volume and presence of a band at 963 $cm^{-1}$from IR studies probably due to Si—O—Zr linkages, but not conclusively proven. Microporous materials such as ZSM-11, ZSM-12, and AlPO-11 have also been explored for incorporation of Zr^{4+} ions, but no definite proof for incorporation of Zr^{4+} into framework Si^{4+} positions was presented.[15,16] Ramaswamy and coworkers[17] synthesized crystalline and microporous Al-free zirconium silicates with MFI structure by hydrothermal process. Synthesis of zirconium containing mesoporous silica (Zr-MS/Zr-HMS) has also been reported using hexadecylamine surfactant at room temperature.[18,19]

The catalytic activity of Sn- and Zr- substituted zeolites are different from those of Ti containing zeolites. For example Sn-beta zeolite is able to perform chemoselective Baeyer-Villiger oxidation of ketones and aldehydes[20], whereas Ti or Zr-beta is not. On the other hand Ti-, Sn- and Zr-beta are all active catalysts for the Meerweing-Ponndorf-Verley reduction of cyclohexanone with 2-butanol, but their catalytic activities are different. Corma *et al.* proposed a new mechanism of the Baeyer-Villiger oxidation reaction, in which the carbonyl group of the ketone is initially activated, and then followed by a reaction with the non activated H_2O_2, in contrast to what occurs in Ti-BEA zeolites. It is also mentioned that Sn-BEA acts as a better catalyst than Ti-BEA for the Meerwein-Ponndorf-Verley reduction of aldehydes and Oppenauer's oxidation of alcohols.

When Si or Al atoms of zeolite framework are substituted by heteroatoms, a question arises regarding the exact location of crystallographic site where the substitution has occurred. Detailed knowledge of the T sites is needed for a complete understanding of the system, as the location of the heteroatom will affect its catalytic activity[21]. There have been many studies that tried to address this issue. None of these studies are absolutely conclusive. The main reasons for these are non-availability of experimental techniques, which can differentiate the population of Si, Al, Ti etc. in zeolites. A large number of spectroscopic, theoretical, and crystallographic studies of TS-1 and its analogues have been performed to solve the problems of Ti location. The physical characterizations of TS-1 have been carried out using X-ray diffraction (XRD), extended X-ray absorption fine structure (EXAFS), X-ray absorption near edge structure (XANES), X-ray photoelectron spectroscopy (XPS), vibrational spectroscopies (IR and Raman), MAS NMR and UV-VIS spectroscopies. [22-28] These results suggested that Ti is isomorphously substituted in MFI framework rather than being either grafted on to the framework or ion-exchanged into the channels. While the evidence for tetrahedral nature and isomorphous substitution of Ti is satisfactory, the specific sitting of titanium within the framework is under discussion.

A few literatures are available which deals with location, coordination, and geometry of Zr^{4+} and Sn^{4+} in mesoporous materials.[29] In this work, we presented a systematic theoretical investigation of substitution of Si by Ti, Zr and Sn at all the 12 crystallographic positions of MFI with a constraint geometry optimization method.

5.2 **Computational Details**

It is necessary to take larger clusters to perform quantum chemical calculation to investigate the structure and properties of zeolites. We have taken 10T clusters for each of the 12 T sites

of MFI zeolite. The model clusters used in our studies were cut out from the crystalline structure of MFI. The dangling bonds of the clusters are terminated with hydrogen atoms. In each of the cluster the central silicon atom is isomorphously substituted by Ti, Zr or Sn atoms to calculate the substitution energies of Ti, Zr and Sn, respectively for silicon in MFI framework. All the 12 crystallographically distinct T sites in the MFI structure are shown in Figure 5.1. Similar to our earlier work, during optimization of the clusters, first only terminating hydrogen atoms were optimized keeping all other atoms fixed at their crystallographic positions. The obtained positions of boundary hydrogen atoms in all subsequent calculations were kept fixed, while other atoms of the clusters are allowed to relax freely. [30] All density functional calculations were performed using DMol3[31] program package. The geometry optimization has been done at generalized gradient approximation (GGA)[32] with BLYP[33] functionals. DMol3 supports several nonlocal exchange and correlation functionals. The most popular Becke exchange functional (B88) is used in conjunction with Lee-Yang-Parr correlation functional (BLYP). We used DNP basis set for optimization of all the zeolite clusters.[34,35] The integration grid referred to as FINE in the software program has been used for optimization. Substitution energies have been evaluated to derive the preferential location of M (M=Ti, Zr and Sn) atoms in MFI framework. The substitution energy is calculated by considering the following virtual reaction:

$Si(OSiH_3)_4 + M(OH)_4 \rightarrow M(OSiH_3)_4 + Si(OH)_4$

Thus substitution energy is

$$\Delta E_{sub} = E^{opt}[M(OSiH_3)_4] + E^{opt}[Si(OH)_4] - \{ E^{opt}[Si(OSiH_3)_4] + E^{opt}[M(OH)_4]\} \quad (5.1)$$

$$\Delta E_{sub} = E^{opt}[M(OSiH_3)_4] - E^{opt}[Si(OSiH_3)_4] + E^{opt}[Si(OH)_4] - E^{opt}[M(OH)_4] \quad (5.2)$$

$$\Delta E_{sub} = E^{opt}[M(OSiH_3)_4] - E^{opt}[Si(OSiH_3)_4] + \text{constant} \quad (5.3)$$

Where last two terms of equation 5.2 are constant for a particular metal.

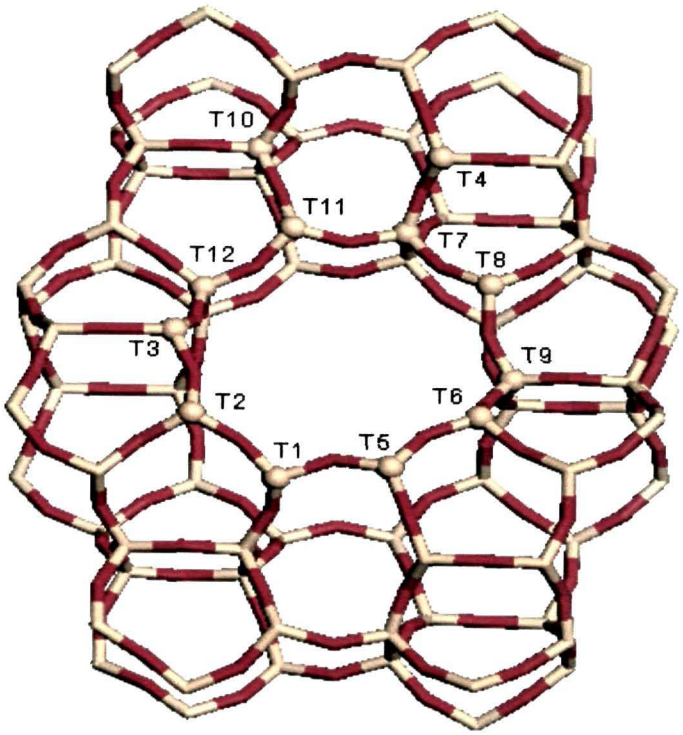

Figure 5.1: Stick representation of orthorhombic structure of MFI zeolite. The positions of all the twelve crystallographically distinct T sites are shown by ball representation.

5.3 Results and Discussion

5.3.1 Optimized geometry of purely siliceous zeolites

The orthorhombic structure of MFI zeolite contains 12 crystallographically distinct T sites and they are represented by T1, T2,.....,T12. It has two intersecting channels, straight and zigzag. Sites T1-T3, T5-T9, T11 and T12 are located at the walls of straight channel, whereas all the T sites, including T4 and T10, construct the part of the zigzag channel. The optimized structure of the model 10T cluster is shown in Figure 5.2. The average bond distances and bond angles for each of the 12 T sites of purely siliceous lattice as well as Ti, Zr and Sn substituted clusters evaluated with BLYP/DNP level are given in Table 5.1. It is

seen from Table 5.1 that the average Si—O distances of central SiO_4 moiety of all the clusters are around 1.614-1.621Å. These values are in good agreement with experimental Si—O bond lengths (1.58 – 1.61 Å).

The average Si—O—Si angles of all the twelve clusters, calculated using BLYP/DNP levels are reported in Table 5.2. It is observed from Table 5.2 that average Si—O—Si angles fall into the interval of (148-157°). These angles are in consistent with the experimentally determined values (150.5°-162.8°). The small variation of Si—O—Si angles with experimental values observed may be due to geometrical constrained used during optimization.

5.3.2 Optimized geometry of Ti substituted zeolites

In order to study the geometry of Ti substituted MFI zeolite, the central Si atom of all the 10T clusters are substituted by Ti. The average geometric parameters of Ti-containing 10T clusters obtained from DFT calculations at BLYP/DNP level are summarized in Table 5.1. A significant change in geometry around the central TiO_4 region is observed. There is a remarkable increase in T—O bond lengths upon Ti insertion into the framework of MFI zeolite in comparison to Si —O distances. The calculated Ti—O bond lengths are found to be 1.78-1.80 Å. These values are in well agreement with some of the available experimental and theoretical results. The experimental EXAFS data provide the Ti—O distances of 1.81±0.01 Å. Fois *et al.* reported Ti—O bond length of 1.821 Å from Car-Parrinello *ab initio* molecular dynamics calculation. Damin *et al.*[36] reported a Ti—O bond length of 1.790-1.802 Å from periodic Hartree-Fock calculation on Ti-chabazite zeolite. Zicovich-Wilson and coworkers[37] obtained a similar result for Ti— O distances (1.780-1.790 Å). Elongation of T—O bond distances upon Ti incorporation in MFI causes a local expansion and,

consequently, a deformation of the MFI framework, resulting in significant changes of the T—O—Si angles

Table 5.1: Average T-O bond distances (Å) and T—O—Si angles (degree) of all T sites of purely siliceous and Ti, Zr and Sn-incorporated MFI structure calculated using BLYP/DNP level.

Location of T Sites	T—O				T—O—Si			
	Siliceous	Ti	Zr	Sn	Siliceous	Ti	Zr	Sn
T1	1.621	1.799	1.946	1.924	148.0	139.7	135.0	129.7
T2	1.617	1.796	1.940	1.920	155.1	144.9	140.1	133.8
T3	1.614	1.783	1.939	1.916	152.9	144.8	144.4	136.9
T4	1.621	1.793	1.942	1.931	155.2	150.1	143.7	134.9
T5	1.620	1.800	1.946	1.924	147.4	139.3	134.5	134.5
T6	1.618	1.800	1.933	1.924	149.8	143.0	139.5	132.3
T7	1.617	1.799	1.937	1.927	149.3	136.9	130.4	127.6
T8	1.619	1.799	1.943	1.925	157.4	149.8	146.4	135.9
T9	1.623	1.797	1.938	1.929	144.9	137.9	133.5	127.4
T10	1.627	1.808	1.955	1.926	145.5	138.2	134.3	133.3
T11	1.621	1.801	1.946	1.931	151.5	143.1	138.5	135.5
T12	1.620	1.798	1.939	1.920	148.4	140.2	135.9	129.2

compared to corresponding angles in the siliceous structure. The calculated individual Ti—O—Si bond angles are smaller in comparison with Si—O—Si bond angles. The Ti—O—Si angles of the 10T clusters evaluated at BLYP/DNP level are listed in Table 5.1. It

is notice from Table 5.1 that average Ti—O—Si bond angles are within the range of 136-150°. The calculated Ti—O—Si values contradict the results of previous quantum chemical cluster calculations. de Man and Sauer[38] performed Hartree-Fock calculations on $Ti[OSi(OH)_3]_4$ cluster of TS-1 and found that the Ti—O—Si angles are hardly changed upon substitution of silicon with titanium. Atoguchi and Yao[39] studied the Ti-containing MFI zeolite applying hybrid QM/MM modeling with the ONIOM method and obtained smaller Ti—O—Si angles (116-132 °). As Ti—O bond lengths are larger than Si—O bond lengths; the size of TiO_4 moiety is larger than SiO_4. The Ti—O—Si angles decrease so as to fit TiO_4 moiety in the constrained zeolite framework by compensating the enlargement of Ti—O bond lengths. The terminal Si—O bonds lengths and O—Ti—O bond angles are hardly affected due to incorporation of Ti atom in the MFI framework.

5.3.3 Optimized geometry of Zr substituted zeolites

In order to study the geometry of Zr substituted MFI zeolite, the central Si atom of all the 10T clusters are substituted with Zr. The optimized geometric parameters of Zr-containing 10T clusters obtained from DFT calculations using BLYP/DNP level are presented in Table 5.1. The optimized 10T cluster of Zr substituted zeolite is shown in Figure 5.2. A significant geometrical change around the central TO_4 region was observed on substitution of Si with Zr. The Zr—O bond lengths increase upon Zr insertion into the framework of MFI zeolite in comparison to Si—O distances. The BLYP/DNP level calculation provides Zr—O bond lengths around 1.933-1.955 Å. These results are good agreement with the experimental observation. Ramaswami *et al.* [40] reported Zr—O distance of 1.94 Å from EXAFS data. Like TS-1, elongation of T—O bond distances upon Zr incorporation in MFI causes a local expansion and, consequently, a deformation of the MFI

framework, resulting in significant changes of the Zr—O—Si angles compared to corresponding angles in the siliceous structure.

Figure 5.2: Optimized T10 site of purely siliceous, titanium, zirconium and tin substituted 10T cluster of MFI zeolite. The dangling bonds are saturated by hydrogen atoms

The calculated individual Zr—O—Si bond angles are smaller in comparison to Si—O—Si bond angles. The average Zr—O—Si bond angles (133-146°) obtained using BLYP/DNP levels are listed in Table 5.1.

5.3.4 Optimized geometry of Sn substituted zeolites

The optimized structural parameters of Sn substituted MFI framework for all the twelve T sites evaluated at BLYP/DNP level are summarized in Table 5.1. It is seen from Table 5.1 that average Sn—O bond distances of the twelve T sites vary from 1.916 to 1.931Å. Our observation is good agreement with some of the experimental and theoretical results. Bare *et al.*[41], with the help of EXAFS techniques, showed that the Sn—O bond length is 1.906 for Sn-BEA zeolite. Pal *et al.*[42] reported the Sn—O bond distances around 1.912 ± 0.002 Å from periodic density functional theory study on Sn-Beta zeolite. As expected, after substitution of Sn in the MFI framework Sn—O bond length increases and subsequently Sn—O—Si bond angle decreases. The Sn—O—Si bond angles of all the clusters calculated using BLYP/DNP level are reported in Table 5.3. This shows that incorporation of Sn atom in MFI increases the average Sn—O bond length by about 0.3Å with respect to Si—O bond lengths, and decreases Sn—O— Si bond angles by about 20° relative to Si—O—Si bond angles. Compared to Ti—O bond distances, the Sn—O distances are larger. This is due to the larger atomic size of Sn with respect to Ti.

From the data of Table 5.1, it can be noticed that the average Sn—O, Zr—O and Ti—O bond distances are very similar for all the twelve T sites, whereas the corresponding bond angles have a large variations. It is also observed that on substitution of Si atom with Ti, Zr or Sn, the average T—O bond lengths increase in the order of Si—O < Ti—O < Sn—O < Zr—O and average T—O—Si bond angles decrease in the order: Si— O— Si > Ti— O— Si > Zr—O—Si > Sn—O—Si. The T—O—Si bond angles calculated at BLYP/DNP level varies in the range of 137—150°, 130—146° and 127—137° on substitution of Si with Ti, Zr and Sn, respectively.

5.3.5 Substitution energy and stability

Both theoretical and experimental studies confirmed the isomorphous substitution of Si by Ti, Zr and Sn in zeolites. However, the preferential siting of Ti, Zr and Sn in zeolite framework is still a debate. In this study, preferential location of Ti Zr and Sn in MFI is investigated from thermodynamic energy consideration.

If the distribution of Ti in MFI structure is determined by thermodynamic stability of the final adsorbate-free zeolite framework, then the substitution energy will be an appropriate criterion for preferential siting of Ti. The substitution energy measures the energy gained by virtual substitution reaction when a Si center is replaced by Ti at a given T site. To identify the preferential location of Ti in TS-1, substitution energies of all 12T sites of MFI framework are calculated using BLYP/DNP level and they are summarized in Table 5.2. It is seen from Table 5.2 that the substitution energies of all 12T sites vary within a range 35-80 kJ/mole. These results demonstrate that the process of titanium incorporation in MFI is endothermic and energetically less favourable. Thus Ti-MFI is shown to be thermodynamically less stable than the Si-MFI. On the basis of substitution energy values calculated at BLYP/DNP level revealed that T10, T8 and T4 are thermodynamically preferential sites for Ti in MFI structure. However, different experimental studies suggest different preferential positions of Ti in zeolite TS-1. Our results are in partial agreement with some of the experimental and theoretical studies reported earlier. Lamberti *et al.*[43] from their powder neutron diffraction studies reported the non-random distribution of Ti centers in TS-1. They advocated the preferential location of titanium at T6, T7 and T11 and weak evidence at T10 sites. In a similar study, Hijar *et al.*[44] detected the favorable sites of titanium at T3, T7, T8, T10 and T12. Henry *et al.*[45] carried out neutron and X-ray diffraction studies and reported that titanium is preferentially sited at T8, T10 and T3 while the silicon vacancies

resides mainly on T1 and T5. In a very recent paper, Deka *et al.*[46] predicted that the preferential location of Ti in MFI is T12 followed by T5, T7 and T8 from QM/MM calculation. The local structure of Al atoms in Zr-ZSM5 and H-ZSM5 has been probed using ^{27}Al NMR-MAS. But ^{29}Si NMR study does not provide conclusive evidence for Zr framework incorporation because chemical shifts arising from framework Si—O—Al cannot

Table 5.2: Calculated substitution energies of Ti, Zr and Sn for Si in MFI framework using BLYP/DNP level.

	Substitution Energy(kJ/mol)		
T- Sites	Ti	Zr	Sn
T1	59.5	151.7	166.2
T2	56.2	149.7	170.6
T3	80.6	179.2	205.1
T4	44.0	123.5	151.4
T5	58.7	149.4	157.0
T6	68.5	176.1	187.5
T7	61.6	159.8	164.3
T8	39.5	115.6	147.9
T9	62.5	167.1	167.3
T10	35.8	108.4	127.1
T11	45.9	130.7	149.7
T12	61.4	151.5	157.5

be distinguished from those for Si—O—Zr structures in H-ZSM5.[47] The substitution energies of Zr for Si in all the twelve T sites of MFI calculated at BLYP/DNP level are summarized in Table 5.3. It is seen from Table 5.3 that substitution energies for zirconium in MFI structure is also endothermic. The calculated substitution energies of zirconium are in the ranges of 108.4-179.2 kJ/mole. This indicates that the incorporation of Zr in MFI is thermodynamically less favourable than Ti. The substitution energy values Zr in MFI calculated using BLYP/DNP level revealed that preferential location of Zr in MFI is in the increasing order of T4 <T8 < T10. Thus we can propose that the zirconium distribution in MFI framework is indeed non-random.

Regarding the investigation on the location of Sn in MFI, we have calculated the substitution energies of Sn in all the twelve T sites of MFI. The substitution energy values evaluated at BLYP/DNP level are reported in Table 5.2. Similar to Ti and Zr, the substitution energies of Sn in MFI is endothermic (127.1-205.1 kJ/mole). That is substitution of Si by Sn is less favourable. The substitution energy of Sn for Si in MFI framework increases in the order of T4 < T8 < T10, hence preferential location of Sn in MFI increases in the order of T4 < T8 <T10. Considering the substitution energy values, we can conclude that preferential locations of Ti, Zr and Sn in MFI framework are T10, T8 and T4 sites. Among Ti, Zr and Sn, we found that substitution of Sn in MFI is least favourable and Ti is more favourable.

5.3.6 Lewis acidity of Ti, Zr and Sn substituted zeolites

To understand the mechanism of Ti, Zr and Sn substituted MFI catalyzed reaction, it is essential to know the reactivity of these zeolites. DFT based local reactivity descriptor, relative electrophilicity values of Ti, Zr and Sn at their most favourable site in MFI framework are calculated for this purpose. In the earlier chapters, we successfully explained the reactivity of cation exchanged and isomorphously substituted zeolites with the help this

reactivity descriptor. The relative electrophilicity values of titanium, zirconium and tin at their most preferable sites calculated at BLYP/DNP level are presented in Table 5.3. It is noticed from Table 5.3 that the reactivity of titanium, zirconium and tin substituted MFI zeolites increases in the order: Sn-MFI < Zr-MFI < Ti-MFI.

Table 5.3: The HPA derived nucleophilic Fukui function, electrophilic Fukui function, and relative electrophilicity of Ti, Zr and Sn atoms in 10T cluster of MFI. The values are evaluated using BLYP/DNP level.

T atoms	f_M^+	f_M^-	f_M^+ / f_M^-
Ti	0.194	0.023	8.434
Zr	0.252	0.038	7.200
Sn	0.225	0.040	5.625

Similar sequence reactivity is also reported by Corma *et al.*[48] by calculating the LUMO energy of Ti, Zr and Sn substituted BEA zeolites.

5.4 Conclusion:

We have presented density functional theory calculation to investigate the structure, reactivity and non-random distribution of titanium, zirconium and tin in MFI zeolite. On the basis of cluster calculation, it is observed that incorporation of Ti, Zr and Sn atoms into the tetrahedral site of MFI framework involves important geometrical changes. The T—O bond length increases and T—O—Si bond angle decreases on incorporation of Ti, Zr and Sn so as

to accommodate the TO_4 moieties. As per the geometric parameters are concerned, the values obtained at BLYP/DNP level are well within the experimental range.

The calculated substitution energies of Ti, Zr and Sn for Si in MFI framework at different T sites suggest that location of Ti, Zr and Sn atoms in MFI framework is energetically favorable for sites T10, T8 and T4. DFT based reactivity descriptor suggests that reactivity of Ti, Zr and Sn substituted zeolites increase in the order: Sn-MFI < Zr-MFI < Ti-MFI.

References

1. Taramasso M., Perego G., Bellusi G., US Patent 4, 410, 501, **1983**.

2. Bellusi G., Carati A., Clerici M. G., Esposito A., Millini R., Bounomo F., Belg. Patent 1, 001, 038, **1989**.

3. Mal N. K., Ramaswami V., Ganapathy S., Ramaswami A. V., *Chem. Commun.* **1994**, 1933.

4. Mal N. K., Ramaswami V., Ganapathy S., Ramaswami A. V., *Appl. Catal. A* 1995, 125: 233.

5. Jansen J. C., Creyghton E. J., Njo S. L., van Koningsveld H., van Bekkum H., *Catal Today* **1997**, 38: 205.

6. Corma A., Camblor H. M., Esteve P., Martinez A., Perez-pariente J., *J. Catal.* **1994**, 145: 151.

7. Valerio G., Goursot A., Vetrivel R., Malkina O., Malkina V., Salahub D, R., *J. Am. Chem. Soc.* **1998**, 120: 11426.

8. Reddy J. S., Sivasanker S., *Catal. Lett.* **1991**, 11: 241.

9. Mal N. K., Ramaswami A. V., *Chem. Commun.* **1997**, 425.

10. Renz M., Blasco T., Corma A., Jensen R., Nemeth L. T., *Chem. Eur. J.* **2002**, 8: 4708.

11 . Dongare M. K.., Singh P., Moghe P., Ratnasamy P., *Zeolites* **1991**,11: 690

12 . Dongare M. K., Sabde D. P., Shaikh R. A., Kamble K. R., Hegde S. G., *Catal. Today* **1999**, 49: 267.

13 . Tanabe K.., Yamaguchi T., *Catal. Today* **1994**, 20: 185.

14. Occelli M. L., Biz S., Aurox A., *Appl. Catal. A: General* **1999**, 183: 231.

15. Ji S., Li H. –l., Liao S. –j., Wang L.-f., *Fenzi Cuihua* **2001**, 15: 273.

16. Wang Z.-M., Yan Z. F., *Preprints-American Chemical Society, Division of Petroleum Chemistry* **2001**, 46: 292.

17. Rakshe B., Ramaswamy V., Hegde S. G., Vetrivel R., Ramaswamy A.V., *Catal. Lett.* **1997**, 45: 41.

18. Tuel A., Gontier S., Teissier R. *J., Chem. Soc., Chem. Commun.* **1996**, 651.

19. Gontier S., Tue A., *Appl. Catal. A: General* **1996**, 143: 125.

20. Corma A., Nemeth L. T., Renz M., Valencia S., *Nature* **2001**, 412: 423.

21. Bare S. R., Kelly S. D., Sinkler W., Low J. J., Modica F. S., Valencia S., Corma A., Nemeth L. T., *J. Am. Chem. Soc.* **2005**, 127: 12924.

22. Ricchiardi G., Damin A., Bordiga S., Lamberti C., Spano G., Rivetti F., Zecchina A. *J Am Chem Soc* **2001**, 123: 11409.

23. Bordiga S., Coluccia S., Lamberti C., Marchese L., Zecchina A., Boscherini F., Buffa F., Genoni F., Leofanti G., Petrini G., Vlaic G., *J Phys Chem* **1994**, 98: 4125.

24. Zecchina A., Bordiga S., Lamberti C., Ricchiardi G., Scaranto D., Petrini G., Leofanti G., Mantegazza M., *Catal Today* **1996**, 32: 97.

25. Tozzola G., Mantegrazza M.A., Ranghino G., Petrini G., Bordiga S., Recchiardi G., Lamberti C., Zulian R., Zecchina A., *J Catal* **1998**, 179: 64.

26. Blasco T., Camblor M.A., Corma A., Perez-Pariente J., *J Am Chem Soc* **1993**, 115: 11806.

27. Bordiga S., Boscherini F., Coluccia S., Genoni F., Lamberti C., Leofanti G., Marchese L., Petrini G., Vlaic G., Zecchina A., *Catal. Lett.* **1994**, 26: 195.

28. Reddy J.S., Sivasanker S., Ratnasamy P., *J. Mol. Catal.* **1991**, 69: 383.

29. Jian-Ming Lü, Ranjit K. T., Rungrojchaipan P., Kevan L., *J. Phys. Chem. B* **2005**, 109: 9284.

30. Pidko E. A., Xu J., Mojet B. L., Lefferts L., Subbotina I. R., Kazansky V. B., van Santen R. A., *J. Phys. Chem. B.* **2006**, 110: 22618.

31. DMol3, Materials Studio 2.0, Accelrys Inc., San Diego, CA, USA.

32. White J.A., Bird D.M., *Phys Rev B* **1994**, 50: 4954.

33. Becke A. D., *J. Chem. Phys.* **1993**, 98: 5648.

34. Gordon M. S., *Chem. Phys. Lett* **1980,** 76: 163.

35. Hehre W. J., Ditchfield R., Pople J. A., *J. Chem. Phys.* **1972**, 56: 2257.

36. Damin A., Bordiga S., Zecchina A., Doll K., Lamberti C., *J. Chem. Phys.* **2003**, 118: 10183.

37. Zicovich-Wilson C. M., Dovesi R., Corma A., *J Phys Chem B* **1999**, 103: 988.

38. de Man A. J. M., Sauer J., *J. Phys. Chem.* **1996**, 100: 5025.

39. Atoguchi T., Yao S., *J. Mol. Catal. A* **2003**, 191: 281.

40. Ramaswamy V., Tripathi B., Srinivas D., Ramaswamy A. V., Cattaneo R., Prins R., *J. Catal.* **2001**, 200: 250.

41. Bare S. R., Kelly S. D., Sinkler W., Low J. J., Modica F. S., Valencia S., Corma A., Nemeth L. T., *J. Am. Chem. Soc.* **2005**, 127: 12924.

42. Shetty S., Pal S., Kanhere D. G., Goursot A., *Chem. Eur. J.* **2006**, 12: 518.

43. Lamberti C., Bordiga S., Zecchina A., Artioli G., Marra G. L., Spano G., *J. Am. Chem. Soc.* **2001**, 123: 2204.

44. Hijar C. A., Jacubinas R. M., Eckert J., Henson N.J., Hay P.J., Ott K.C., *J. Phys. Chem. B* **2000**, 104: 12157.

45. Henry P. F., Weller M. T., Wilson C. C., *J. Phys. Chem. B* **2001**, 105: 7452.

46. Deka R. C., Nasluzov V. A., Ivanova Shor E. A., Shor A. M., Vayssilov G. N., Rösch N., *J. Phys. Chem. B* **1995**, 109: 24304.

47. Lacheen H. S., Iglesia E., *Chem. Mater.* **2007**, 19: 1877.

48. Boronat M., Corma A., Renz M., Viruela P. M., *Chem. Eur. J.* **2006**, 12: 7067.

6 ADSORPTION OF SMALL MOLECULES ON TI-ZEOLITES: AN EMBEDDED CLUSTER APPROACH

Abstract

The structure and energetic of Ti substituted MFI zeolite and its adsorption behaviour with small molecules *viz.* water, hydrogen peroxide, methanol and ammonia, are studied using 5T and 16T model clusters. Full geometry optimization has been carried out for 5T cluster with B3LYP/6-31G (d,p), LANL2DZ level and 16T cluster using ONIOM (Our-own-N-layered Integrated molecular Orbital + molecular Mechanics) approach, as implemented in Gaussian03 code at ONIOM2 (B3LYP/6-31G (d,p), LANL2DZ: RHF/3-21G, 3-21G(d)) level. Adsorption of small molecules on Ti(IV) site of TS-1 shows that ammonia molecule is more effective in distorting the local environment around Ti(IV) site in comparison to other molecules.

6.1 Introduction

Isomorphous substitution of Si^{4+} by Ti^{4+} in synthetic zeolites gives rise to an interesting family of very active and selective catalysts. Titanium silicalite (TS-1)[1] catalyst is one of the most important innovations in heterogeneous catalysis over the last decades. Ti-containing siliceous nanoporous and mesoporous materials have been found to exhibit excellent performance in low-temperature oxidation reactions in the presence of aqueous solutions of H_2O_2.[2] Such reactions include phenol hydroxylation[2], olefin epoxidation[2-6], alkane oxidation,[2,7,8] oxidation of ammonia to hydroxylamine,[2,4,9] cyclohexanone ammoximation,[2,9-11] ammoximation of *ortho* and *para*-hydroxyacetophenones,[11] conversion of secondary amines to dialkylhydroxylamines[2,10] and conversion of secondary alcohols to ketones.[2] Several experimental[2-17] and theoretical studies[18-25] reveal that the substitution of Si by Ti is isomorphous in well-prepared samples. It is also believed that the distribution of Ti over the available framework sites is partially disordered. High coordination ability of Ti (IV) sites associated with the hydrophobicity of silicalite structure, spatial selectivity and random distribution of Ti (IV) sites are responsible for the remarkable and unusual catalytic activity of TS-1. Since, there is a low concentration of Ti atoms present in TS-1; the catalytically active Ti centers are believed to be site isolated from each other. This site isolation is thought to give rise to its unique catalytic activity and selectivity. Mesoporous Ti-silicates are also used as effective pollution control catalyst, especially for the photocatalytical removal of NO and other nitrogen oxides as well as in the reduction of carbon dioxide with water into valuable chemicals. In decomposition of NO, TS-1 led to the formation of N_2 and O_2 with a high activity, while TiO_2 resulted in the formation of N_2O and O_2.[26] In the reaction of CO_2 and H_2O, the use of TS-1 led to the formation of methane and methanol, while TiO_2 yielded only methane.[27-29] The shape selectivity due to the well defined MFI pores makes the appropriate use of the terms 'mineral enzyme' or 'zeozyme' to

TS-1.[30] Again, the tetrahedral Ti (IV) ions are supposed to have a relatively high propensity to expand their coordination sphere (up to six) by adsorbing molecules, as for instance the reactants in the catalytic process.[31] It was assumed that the expansion of coordination takes place with partial hydrolysis of the Ti–O–Si bonds and this increases the accessibility of the Ti centre for additional ligands. This argument was supported by IR and ^{17}O NMR spectroscopic measurements[32]. For these reasons, it has led to the primary importance in determination of geometry, electronic structure and adsorption properties of Ti (IV) center in TS-1. Extensive studies were carried out with respect to the catalytic activity and general structure[33-35] of TS-1, including powder diffraction experiments (using both X-rays and neutrons),[13,36] IR and Raman,[37-39] UV-Vis,[40,16] EXAFS[41,42] and XANES[43,44] spectroscopies, micro calorimetric measurements[43,44] and computer modeling.[45-47] The first structural study on TS-1 was made by Lamberti *et al.*[48] using synchrotron X-ray diffraction data. At room temperature, high quality data were collected on a series of dehydrated TS-1 samples, $Ti_xSi_{1-x}O_2$, with x values ranging from 0 to 0.022. From this work, it was concluded that titanium was either homogeneously distributed throughout the framework or slightly partitioned on different sites in different samples. de Man and Sauer[18] made Hartree-Fock calculations on $Ti(OSi(OH)_3)_4$, as a model cluster for Ti site in TS-1 and obtained a Ti–O distance of 1.790 Å. They also interpreted the major vibrational features due to $Ti(OSi)_4$ moiety in TS-1. Ti–O bond distance of 1.810 Å was reported by Sinclair *et al.*[49] on a $Ti(OSiH_3)_4$ cluster using BP functional. In the same work, they adopted $Ti(OSiH_3)_4/nH_2O$ (n=1,2) clusters to study adsorption of water molecules at Ti site. For this calculation, coordinates of Si atom were kept fixed during optimization of $Ti(OSiH_3)_4$ cluster. They obtained binding energy values of +12.0 kJ mol^{-1} and +29.0 kJ mol^{-1}, respectively for monohydrated and bihydrated complexes. Munakata *et al.*[22] obtained binding energies of +41.0, +31.0 and +52.0 kJ mol^{-1} for water, hydrogen peroxide and ammonia adsorption, respectively on $Ti(OSi(OH)_3)_4$. Ricchiardi *et*

al.[21] studied Ti-chabazite (Ti/Si=1/11) and TS-1 (Ti/Si=1/95) and their interaction with water by means of a hybrid periodic/embedded QM/MM cluster approach. Choosing a model cluster of $Ti(OSi(OH)_3)_4$ for TS-1, they obtained Ti–O distance of 1.770–1.780 Å for the three different T-sites studied. They also reported the BSSE corrected binding energies +23, +28 and +31 kJ mol^{-1} for monohydrated complex at three T-sites, T_5, T_7, T_8, to be, respectively. Damin *et al.*[25] observed a remarkable increment of binding energies (BSSE corrected) for water adsorption, by moving from 2.1 kJ mol^{-1} for the unconstrained $Ti(OSiH_3)_4$ cluster to 16.9 kJ mol^{-1} for the $TiSi_{17}O_{26}H_{20}$ cluster of MFI framework. Similar results were obtained for ammonia molecule, where the binding energy (BSSE corrected) increased from 17.4 to 35.4 kJ mol^{-1}. Zhanpeisov and Anpo[50] studied adsorption of water, methanol and ammonia on 5T cluster of Ti-silicalites, either H- or OH- terminated at B3LYP/6-31G* level and found that absorption energy for the three molecules is in the order of $CH_3OH < H_2O < NH_3$.

In the present work, we will study the structure and energetic of the adsorption of H_2O, H_2O_2, NH_3, and CH_3OH molecules at Ti sites of 5T and 16T model clusters of MFI framework.

6.2 Computational Details

6.2.1 Models

In this study, we have chosen 5T and 16T clusters to model TS-1 zeolite, where T represents tetrahedral sites. The model clusters are cut out from the crystallographic structure of MFI. The 5T cluster $Ti(OSiH_3)_4$ (Figure 6.1(a)) is considered as the smallest unit required to represent the Ti(IV) active site of TS-1. The dangling bonds of the model clusters are terminated by H atoms. The long distance effect of framework structure of MFI cannot be totally neglected if more accurate results are required. Thus, 16T cluster, illustrated in Figure

6.2(a) has been modelled, which contain four six member rings, including eleven more tetrahedral atoms at the base next to the Ti atom.

6.2.2 Method

According to the two-layer ONIOM method, energy calculation can be simplified by treating the active region with a high-level quantum mechanical (*ab initio* or density functional) approach, and environment with a less expensive HF level, semiempirical and molecular mechanics force fields methods. The total energy of the whole system can be expressed as given by Morokuma and co-workers,

$$E_{ONIOM2} = E_{High}^{Model} + (E_{Low}^{Real} - E_{Low}^{Model}), \quad (1)$$

where the superscripts 'Real' and 'Model' mean the whole system and the active region, respectively. Subscripts 'High' and 'Low' mean the high- and low-level of calculations used in the ONIOM method.

In our work, the active region is treated by density functional theory with the hybrid functional B3LYP. The remaining extended framework is treated by Hartree-Fock method. 3-21G basis set for H, N, O, C, Si and 3-21G* basis set for Ti are used in the Hartree-Fock calculations. In the B3LYP calculations, 6-31+G(d,p) basis set for H, N, O, C, Si and LANL2DZ basis set for Ti are used. All calculations have been performed in Gaussian 03 program[51] without imposing any geometrical constraints.

6.2.3 Binding energy and basis set superposition error (BSSE) calculation

In order to obtain more accurate binding energies, basis set superposition error (BSSE) corrections have been incorporated by following the *a posteriori* counterpoise method proposed by Lendvay and Mayer[52]. According to this method, the binding energy

BE, the BSSE and BE^c (BSSE corrected BE) of the AB complex formed from A (zeolite cluster) and B (H_2O, H_2O_2, CH_3OH and NH_3) moieties, are:

$$BE = E_a(A) + E_b(B) - E_{ab}(AB), \quad (2)$$

$$BE^c = E_a(A) + E_b(B) - [E_a(A^{def}) - E_{ab}(A^{def}) + E_b(B^{def}) - E_{ab}(B^{def})] - E_{ab}(AB) \quad (3)$$

$$BSSE = BE - BE^c = [E_a(A^{def}) - E_{ab}(A^{def}) + E_b(B^{def}) - E_{ab}(B^{def})] \quad (4)$$

where (i) a and b are the basis sets of A and B respectively; (ii) $E_{ab}(AB)$ is the energy of AB complex and $E_a(A), E_b(B)$ are the energies of the two isolated systems at their equilibrium geometries and with their own basis sets. (iii) $E_{ab}(A^{def})$ and $E_{ab}(B^{def})$ are, respectively, the energy of A at the actual geometry in the complex plus basis functions only of B (at the actual geometry in the complex) and *vice versa*; (iv) $E_a(A^{def})$ and $E_b(B^{def})$ are the energies of A and B at the actual geometry in the complex with their own basis sets.

6.3 Results and discussion

Figure 6.1(a) and Figure 6.2(a) show the fully optimized 5T and 16T model clusters, respectively of MFI structure. Each of the probe molecules (H_2O, H_2O_2, NH_3, and CH_3OH) has been fully optimized at B3LYP/6-31+G(d,p) level prior to studying their adsorption behaviour with TS-1 clusters. Optimized structures of the adsorption complexes are shown in Figure 6.1(b-e) and Figure 6.2(b-e). All the atoms of the adsorbates and active part of the zeolite cluster have been treated with B3LYP functional using LANL2DZ basis for Ti and 6-31+G(d,p) basis for all other atoms. The structural parameters of optimized 5T and 16T clusters and their adsorption complexes are listed in Table 6.1 and Table 6.2, respectively.

Table 6.1: Structural parameters of the 5T cluster model and its adsorption complex with H_2O, H_2O_2, CH_3OH, NH_3 molecules.

Models	Ti-L (L= OH_2, OH, NH_3) (Å)	<Ti-O> (Å)	<Ti-Si> (Å)	O-Ti-O (deg)		<Ti-O-Si> (deg)
				α	β	
5T	—	1.796	3.459	109.5	109.4	179.5
5T_H_2O	2.436	1.818	3.378	115.7	101.2	150.5
5T_H_2O_2	2.471	1.825	3.356	115.6	102.3	150.7
5T_CH_3OH	2.415	1.825	3.368	115.9	100.8	150.5
5T_NH_3	2.343	1.824	3.418	117.0	99.0	156.2

Table 6.2: Structural parameters of 16T model cluster and its adsorption complexes with H_2O, H_2O_2, CH_3OH and NH_3 molecules.

Models	Ti-L (L= OH_2, OH, NH_3) (Å)	<Ti-O> (Å)	<Ti-Si> (Å)	O-Ti-O (deg)		<Ti-O-Si> (deg)
				α	β	
16T	—	1.797	3.371	109.5	108.4	155.5
16T_H_2O	2.429	1.818	3.378	115.5	100.2	156.7
16T_H_2O_2	2.487	1.814	3.380	114.6	104.3	159.7
16T_CH_3OH	2.391	1.821	3.381	116.9	100.8	157.5
16T_NH_3	2.360	1.829	3.389	118.0	98.0	157.5

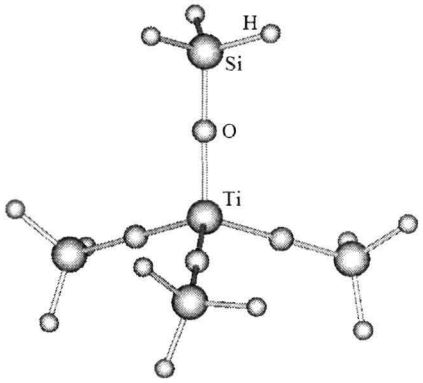

(a) 5T

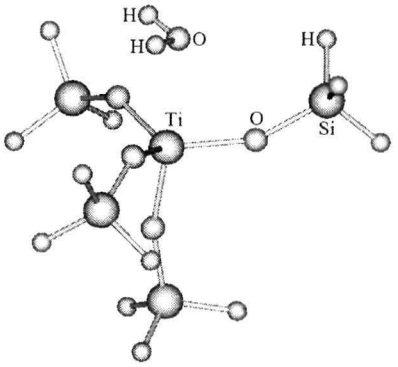

(b) H_2O/5T complex

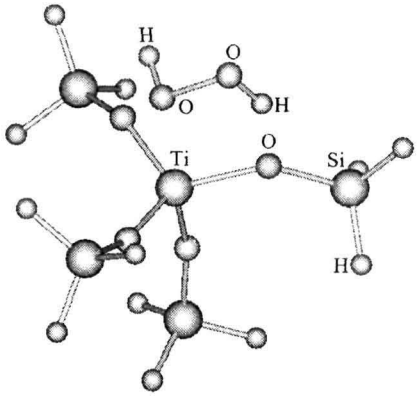

(c) H_2O_2/5T complex

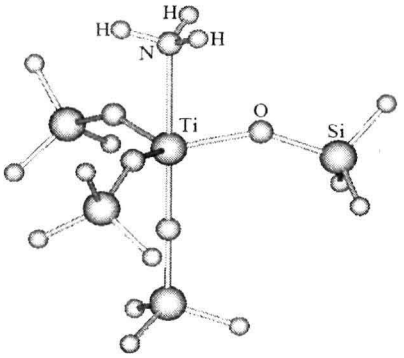

(d) NH_3/5T complex

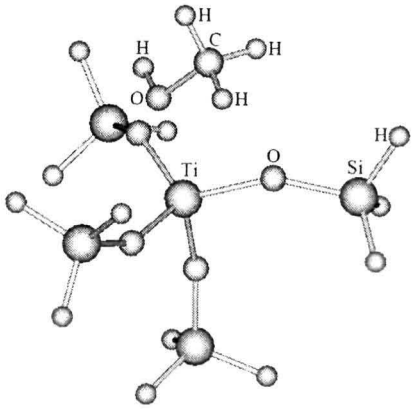

(e) CH_3OH/5T complex

Figure 6.1: Structures of bare and H_2O, H_2O_2, NH_3, CH_3OH adsorption complexes of 5T cluster.

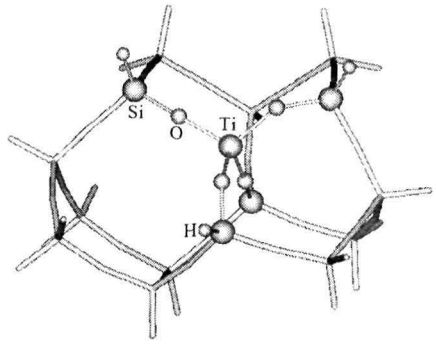

(a) 16T

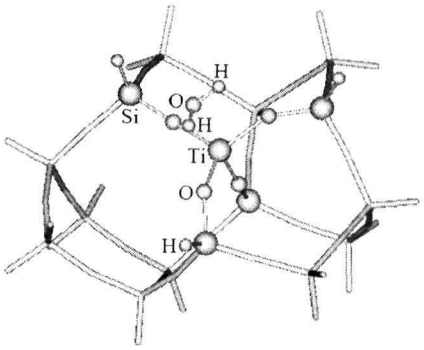

(b) H_2O/16T complex

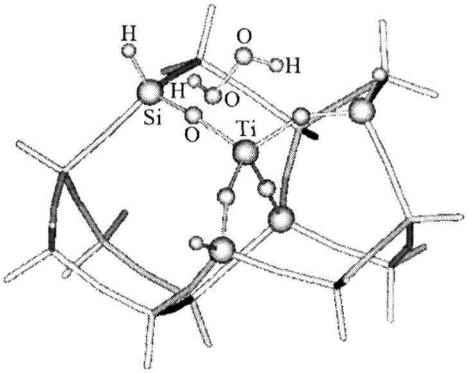

(c) H_2O_2/16T complex

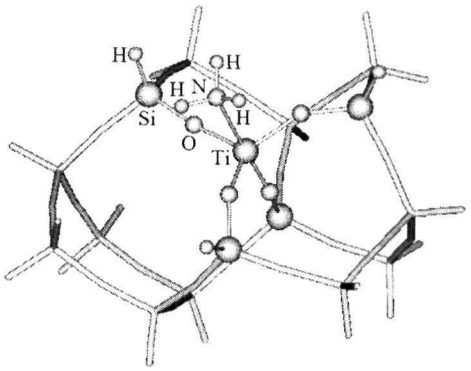

(d) NH_3/16T complex

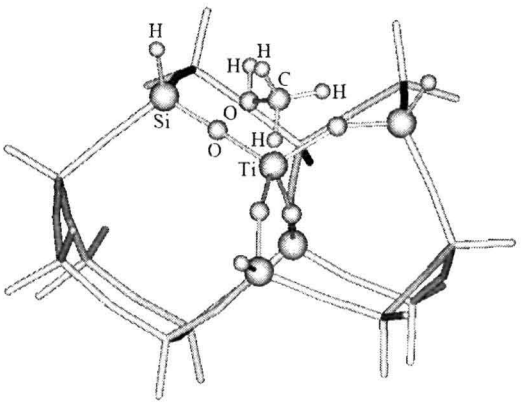

(e) CH_3OH/16T complex

Figure 6.2: Structures of bare and H_2O, H_2O_2, NH_3, CH_3OH adsorption complexes of 16T cluster.

6.3.1 Bare 5T and 16T clusters

Incorporation of Ti atom in the zeolite cluster strongly perturbs the geometrical features of the local structure. It has been observed that the average value of Ti—O bond length in 5T

as well as 16T clusters are 1.796 Å (Table 1) and 1.801 Å (Table 6.2), respectively, which is in good agreement with the theoretical [25,50] and experimental [16,53-55] results. Calculated values of Ti—Si distances give a satisfactory agreement with the experimental values of 3.26—3.38±0.02 Å[16,56]. From Table 6.1, it is seen that all the O—Ti—O angles for 5T clusters are nearly equal to 109.5° *i.e.* the optimize 5T model cluster retains a structure close to perfect T_d symmetry. High flexibility of Ti—O—Si angle and complete absence of framework constraints lead to an average value of 178.9°, a large deviation from the two couples of Ti—O—Si angles at 143±5° and at 162±5° as measured by EXAFS[16]. Zicovich-Wilson *et al.*[57] studied Ti-chabazite (Si/Ti = 1:1) using periodic approach and obtained Ti—O distances, Ti—O—Si angles and Ti—Si distances in the 1.78-1.79 Å, 150-157° and 3.28-3.34 Å ranges, respectively. Our results are almost similar to these values except a slightly higher value for Ti—O—Si angle. However, values of Ti—O—Si angles in larger 16T model clusters (Table 6.2) agree well with the experimental results.[16] From the above discussion, it is clear that less satisfactory results are obtained with respect to Ti—O—Si angles and Ti—Si distances with the 5T model cluster, giving definitely too long Ti—Si distances which may be due to Ti—O—Si≈180° (Table 6.1). Fully optimized 5T cluster model does not take into account the presence of third and higher order shell effects, which cannot be adequate to reliably describe the observed phenomena, in particular, the energetic feature of Ti(IV) centers in Ti-containing silica.

6.3.2 Adsorption of H_2O, H_2O_2, CH_3OH and NH_3 molecules on 5T and 16T clusters

The interaction of probe molecules with Ti(IV) centers in TS-1 has been widely used to prove the isomorphous insertion of titanium in the framework.[42] Distortion of local geometry around Ti induced by adsorption of probe molecules (L= H_2O, H_2O_2, CH_3OH and NH_3), gives relevant information regarding the active sites of the catalysts. Adsorption of

probe molecules causes distortion of the T_d symmetry toward bipyramidal symmetry of the bare clusters.[25,58] As a result of this, the four oxygen atom and the six O—Ti—O angles of the TiO_4 unit are no more equivalent upon adsorption. For this reason we have divided the four oxygen atoms into three equatorials and one apical (O_{eq} and O_{ap}, respectively, in Figure 6.3). We label the three O_{eq}—Ti— O_{eq} angles with α and the three O_{eq}—Ti— O_{ap} with β. Distortion of 5T and 16T clusters, due to the adsorption of probe molecules, are monitored from the modification of Ti—O bond length and O—Ti—O bond angles as reported in Table 6.1 and Table 6.2, respectively. Adsorption also modifies the Ti—O—Si angles as well as the Ti—Si distances as observed in the literature.[56] H_2O adsorption involves modification in the zeolite structure around Ti(IV) site. H_2O molecule locates opposite to one of the oxygen atom of TiO_4, whereas, Ti and other three oxygen atoms are nearly coplanar.

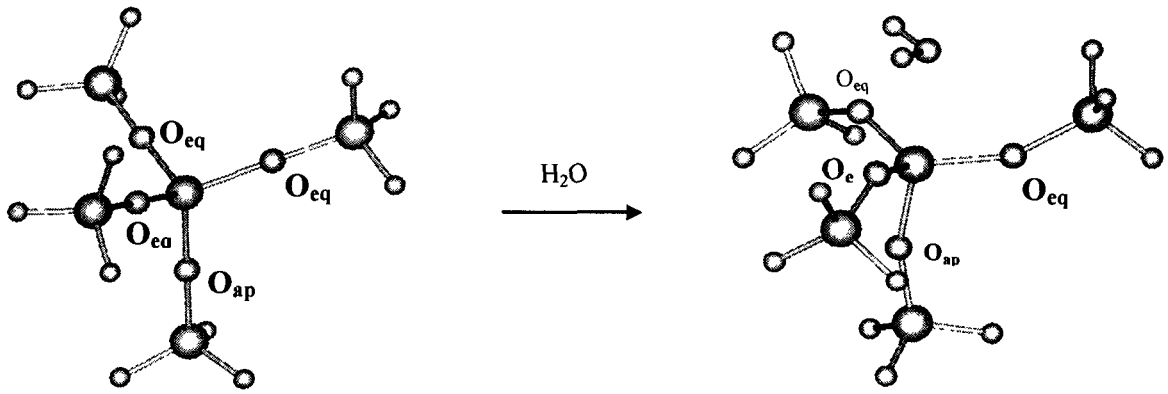

T5

H_2O adsorbed T5 model

Figure 6.3: Schematic representation of H_2O adsorption in 5T model cluster.

The interaction of H_2O with TS-1 is mainly electrostatic, involves lone pair electron of oxygen atoms and electron deficient Ti atom. Average Ti—O bond lengths in 5T_H_2O and 16T_H2O adducts are 1.819 and 1.818 Å, respectively. This is in well agreement with

the value of 1.79 Å obtained from XRD experiments[59] and of 1.80-1.81±0.01 Å from EXAFS experiments.[55,60] Our calculated Ti—Si distances and α, β angles of 5T and 16T clusters are close to the results reported by Bordiga *et al.*[56] Ti—O—Si angles in 5T cluster are slightly less but those for 16T cluster are in perfect agreement with Bordiga *et al.*[56]. Ti—L [O of H_2O] distances in 5T and 16T clusters are found to be 2.436 Å and 2.429 Å, respectively, which agrees well with the values reported in the literature (2.43 Å for 5T and 2.41 Å for 16T).[25]

Ti—O bond lengths in 5T and 16T clusters increase to 1.828 Å and 1.827 Å, respectively, as a result of NH_3 adsorption. These values are in good agreement with earlier results.[56] This leads to the fact that upon expansion of the coordination sphere caused by NH_3 adsorption, Ti(IV) slightly moves outward from four-fold to five-fold and six-fold coordinate positions with subsequent increase of the Ti—O bond distances. Our results for Ti—Si distances and α, β and Ti—O—Si angles in 5T and 16T clusters are close to those obtained by Bordiga *et al.*[56]. Ti—L [N of NH_3] distances in 5T and 16T clusters are found to be in the range of 2.343-2.360 Å, which is close to the values obtained by Damin *et al.* (2.33 Å for 5T)[25], (2.35 for both 5T and 16T)[56] and 2.343 Å by Zhanpeisov and Anpo[50]. Unfortunately, lack of higher shell analysis of the EXAFS data has not permitted the localization of the adsorbed molecules, so the experimental Ti—OH_2 and Ti—NH_3 distances are still missing and hence a computational approach is mandatory.

The Ti—L [O of H_2O_2] distances are found to be 2.471 and 2.487 Å due to adsorption of hydrogen peroxide in 5T and 16T clusters, respectively. This result is in the line of experimental data on ligand adsorption at Ti site in TS-1 as well as with theoretical calculations.[61,62] Our calculated values of Ti—O bond lengths, Ti—O—Si and O—Ti—O angles are in agreement with the available experimental and theoretical results.[61,62]

For 5T_CH_3OH and 16T_CH_3OH complexes, Ti—L [O of CH_3OH] bond distances are 2.415 and 2.391 Å, respectively, which is higher than the value of 2.304 Å as observed earlier.[50] From the above discussion it is observed that among all the probe molecules, NH_3 is found to be slightly more effective in the distortion of T_d geometry of TS-1 zeolite structure around Ti centre.

6.3.3 Binding energies

The calculated binding energies of small probe molecules with 5T and 16T clusters are reported in Table 6.3. Remarkable binding energy differences are observed in moving from 5T cluster to 16T clusters. The BSSE corrected binding energy of H_2O with 5T cluster is found to be 5.75 kJ mol^{-1}, which is higher than that of the observation reported by Bogidiga *et.al.*[25,56]. Our calculated binding energy value of H_2O with 16T cluster is 12.30 kJ mol^{-1}, which is slightly lower than the value of Bordiga *et al.*[25,56] Zhanpeisov and Anpo reported the binding energy value of 10.4 kJ mol^{-1} for H_2O with Ti-zeolite[50], which is close to our calculated results. BSSE corrected binding energies of H_2O_2 with 5T as well as 16T clusters are 10.65 kJ mol^{-1} and 13.05 kJ mol^{-1}, respectively. These values are close to the values of 11.4 kJ mol^{-1} (RHF) and 14.6 kJ mol^{-1} (B3LYP) in the recent work of Bordiga *et al.*[63] From our calculation, binding energy of H_2O with T5 as well as 16T cluster has been found to be higher than the binding energy of H_2O_2. Munakata *et al.*[22] reported the binding energies for water, hydrogen peroxide and ammonia adsorption on $Ti(OSi(OH)_2$, calculated with BP functional of to be +41.0, +31.0 and +52.0 kJ mol^{-1}, respectively. They found that the adsorption energy of water with Ti-silicate is higher than that with H_2O_2. Our results are contradictory to this report. The calculated BSSE corrected binding energy of NH_3 with 5T cluster is 18.2 kJ mol^{-1}, which is in agreement with literature values.[25,56] NH_3 binding energy with 16T cluster is found to be 28.3 $kJmol^{-1}$, which is slightly less than the other theoretical

results.[25,56] The BSSE corrected binding energies of methanol calculated with 5T and 16T clusters are 3.40 and 10.78 kJ mol^{-1}, respectively.

TABLE 6.3: Binding energies of 5T and 16T cluster models and their adsorption complex with H_2O, H_2O_2, CH_3OH and NH_3.

Models	BE (kJ mol^{-1})		Models	BE (kJ mol^{-1})	
	BSSE uncorrected BE	BSSE corrected BE[†]		BSSE uncorrected BE	BSSE corrected BE[‡]
5T_H_2O	17.06	5.74	16T_H_2O	25.05	12.30
5T_H_2O_2	23.44	10.65	16T_H_2O_2	26.88	13.05
5T_CH_3OH	14.61	3.40	16T_CH_3OH	22.57	10.78
5T_NH_3	3.33	18.26	16T_NH_3	41.59	28.27

These Values of binding energies are less than the value reported by Zhanpeisov *et al.*[50] Methanol adsorption leads to the formation of hydrogen bonded complex with zeolite clusters. However, the adsorption energy calculated for methanol, either in a conventional way or with a correction to the BSSE is lower than those of water. This may be due to the formation of physisorption complex. From this comparison, NH_3 is found to have higher binding energy than the corresponding values of H_2O, H_2O_2 and CH_3OH. Higher binding energy of NH_3 with TS-1 cluster is due to the higher basicity of NH_3 molecule.

6.4 Conclusions

The results presented in this work clearly show that the role played by the zeolite framework constrains in enhancing the activity of Ti(IV) centers toward the adsorption of

[†] Boys–Bernardi counterpoise correction scheme, (a) S. F. Boys, F. Bernardi, Mol. Phys. **19**, 553 (1970), (b) M. Urban, P. Hobza, Theor. Chim. Acta **36**, 215 (1975), (c) I. Mayer, P. R. Surjan, Chem. Phys. Lett. **191**, 4 (1992).

[‡] *a posteriori* counterpoise method proposed by Lendvay and Mayer, G. Lendvay and I. Mayer, Chem. Phys. Lett. **297**, 365 (1998).

probe molecules. Regarding the optimized structures is concerned, larger cluster (16T) provide more correct results than the smaller clusters (5T). The Ti—O distances in the bare clusters are smaller than adsorbed complexes. Our results show that the Ti—O, Ti—Si distances and Ti—O—Si angles in both types of clusters are in very good agreement with the experimental results. The results confirm that ammonia distort the local environment of Ti(IV) to a greater extent than the other molecules.

References

1. Taramasso M., Perego G., Notari B., U. S. Patent **1983**, 4, 410501
2. Notari B., *Adv Catal.* **1996,** 41: 253 and references therein
3. Clerici M.G., Bellussi G., Romano U., *J. Catal.* **1991** 129: 159.
4. Mantegazza M. A., Leofanti G., Petrini G., Padovan M., Zecchina A., Bordiga S., *Stud. Surf. Sci. Catal.* **1994,** 82: 541.
5. Lane B. S., Burgess K., *Chem. Rev.* **2003**, 103: 2457.
6. Clerici M. G., Ingallina P., *J. Catal.* **1993**, 140: 71.
7. Clerici M.G., *Appl. Catal.* **1991,** 68: 249.
8. Clerici M. G., *Top. Catal.* **2001**,15: 257.
9. Mantegazza M. A., Petrini G., Spano' G., Bagatin R., Rivetti F., *J Mol Catal A: Chem* **1999,** 146: 223
10. Roffia P., Tonti S., Cesana A., Mantegazza M.A., Padovan M., U S Patent **1990,** 4, 918194.
11. Lebars J., Dakka J., Sheldon R. A., *Appl. Catal. A* **1996**,136: 69.
12. Vayssilov G. N., *Catal. Rev. – Sci. Eng.* **1997**, 39:209 and references therein
13. Milliani R., Previde Massara E., Perego G., Bellussi G., *J. Catal.* **1992**, 137: 497.
14. Lamberti C., Bordiga S., Arduino D., Zecchina A., Geobaldo F., Spanó G., Petrini G., Carati A., Villain F., Vlaic G., *J. Phys. Chem. B* **1998**, 102: 6382.
15. Lamberti C., Bordiga S., Zecchina A., Fitch A. N., Artioli G., Petrini G., Salvalaggio M., Marra G. L., *J. Catal.* 1999, 183: 222.
16. Gleeson D., Sankar G., Catlow C. R. A., Thomas J. M., Spanò G., Bordiga S., Zecchina A., Lamberti C., Phys. Chem. Chem. Phys. **2000**, 2: 4812.
17. Antcliff K. L., Murphy D. M., Griffiths E., Giamello E., *Phys. Chem. Chem. Phys.* 2003, 5: 4306.

18. de Man A. J. M., Sauer J., *J. Phys. Chem.* **1996**, 100: 5025.

19. Yudanov I. V., Gisdakis P., Divalentin C., Rösch N., *Eur. J. Inorg. Chem.* **1999**, 1999: 2135.

20. Njo S. L., van Koningsveld H., van de Graaf B., *J. Phys. Chem. B* **1997**, 101: 10065.

21. Ricchiaridi G., de Man A., Sauer J., *Phys. Chem. Chem. Phys.* 2000, 2: 2195.

22. Munakata H., Oumi Y., Miyamoto A., *J. Phys. Chem. B* **2001**, 105: 3493.

23. Vayssilov G. N., van Santen R. A., *J. Catal.* **1998**, 175: 170.

24. Atoguchi T., Yao S., *J. Mol. Calal. A* **2003**, 191: 281.

25. Damin A., Bordiga S., Zecchina A., Lamberti C., *J. Chem. Phys.* **2002**, 117: 226.

26. Ichihashi Y., Yamashita H., Anpo M., Abstrct 11th Int. Zeolite Conf., Seoul, pp. **1996**, 129.

27. Anpo M., Chiba K., *J. Mol. Catal.* 1992, 74: 207.

28. Anpo M., Yamashita H., Ichihashi Y., Ehara S., *J. Electroanal. Chem.* **1995**, 396: 21.

29. Yamashita H., Ichihashi Y., Harada M., Stewart G., Fox M. A., *J. Catal.* **1996**, 158: 97.

30. Sheldon R. A., *Stud. Surf. Sci. Catal.* **1997**, 110: 151.

31. Barker C. M., Gleeson D., Kaltsoyannis N., Catlow C. R. A., Sankar G., Thomas J. M., Phys. Chem. Chem. Phys. **2002**, 4: 1228.

32. Bellussi G., Carati A., Clerici M. G., Maddinelli G., Millini R., J. Catal. **1992**, 133 :220.

33. Van der Pol A. J. H. P., Van Hooff J. H. C., *Appl. Catal. A* 1992, 92: 113.

34. Thangaraj A., Kumar R., Mirajkar S.P., Ratnaswamy P. *J. Catal.* 1991, 130: 1.

35. Zecchina A., Spoto G., Bordiga S., Ferrero A., Petrini G., Leofanti G., Padovan M., *Stud. Surf. Sci. Catal.* **1991**,69: 251.

36. Marra G. L., Artioli G., Fitch A. N., Milanesio M., Lamberty C., Micropor. Mesopor. Mater. **1999**, 183: 222.

37. Tozzola G., Mantegazza M. A., Ranghino G., Petrini G., Bordiga S., Ricchiardi G., Lamberty C., Zulian R., Zecchina A., *J. Catal.* **1998**, 179: 64.

38. Boccuti M. R., Rao K. M., Zecchina A., Leofanti G., Petrini G., Stud. Surf. Sci. Catal. **1989**, 48: 133.

39. Zecchina A., Spoto G., Bordiga S., Podovan M., Leofanti G., *Stud. Surf. Sci. Catal.* **1991**, 65: 671.

40. On D. T., Noc L. L., Bonneviot L., *Chem. Commun.* **1996**, 299.

41. Bolis V., Bordiga S., Lamberty C., Zecchina A., Petrini G., Rivetti F., Spanó G., *Langmuir* **1999**, 155:753.

42. Bolis V., Bordiga S., Lamberty C., Zecchina A., Petrini G., Rivetti F., Spanó G., *Micopor. Mesopor. Mater.* **1999**, 30: 67.

43. Bordiga S., Geobaldo F., Lamberty C., Zecchina A., Boscherini F., Genoni F., Leofanti G., Petrini G., Podovan M., Geremia S., Vlaic G., *Nucl. Instrum. Methods. B* **1995**, 97: 23.

44. Zecchina A., Bordiga S., Lamberty C., Ricchiardi G., Scarano D., Petrini G., Leofanti G., Mantegazza M., *Catal. Today.* **1996**, 32: 97.

45. Chaudari K., Srinivas D., Ratnasamy P., *J. Catal.* **2001**, 203: 25.

46. Server R. R, Root T. W., *J. Phys. Chem.* **2003**, 107: 4080.

47. Server R. R, Root T. W., *J. Phys. Chem.* **2003**, 107: 4090.

48. Lamberty C., Bordiga S., Zecchina A., Carati A., Fitch A. N., Artioli G., Petrini G., Salvalaggio M., Marra G. L., *J. Catal.* **1999**, 182: 222.

49. Sinclair P. E., Catlow C. R. A., *J. Phys. Chem. B* **1999**, 103: 1084.

50. Zhanpeisov N. U., Anpo M., *J. Am. Chem. Soc.* **2004**, 126: 9439.

51. Frisch M. J., Trucks G. W., Schlegel H. B., Scuseria G. E., Robb M. A., Cheeseman J. R., Montgomery J. A., Vreven T., Kudin K. N., Burant J. C., Millam J. M., Iyengar S. S.,

Tomasi J., Barone V., Mennucci B., Cossi M., Scalmani G., Rega N., Petersson G. A., Nakatsuji H., Hada M., Ehara M., Toyota K., Fukuda R., Hasegawa J., Ishida M., Nakajima T., Honda Y., Kitao O., Nakai H., Klene M., Li X., Knox J. E., Hratchian H. P., Cross J. B., Adamo C., Jaramillo J., Gomperts R., Stratmann R. E., Yazyev O., Austin A. J., Cammi R., Pomelli C., Ochterski J. W., Ayala P. Y., Morokuma K., Voth G. A., Salvador P., Dannenberg J. J., Zakrzewski V. G., Dapprich S., Daniels A. D., Strain M. C., Farkas O., Malick D. K., Rabuck A. D., Raghavachari K., Foresman J. B., Ortiz J. V., Cui Q., Baboul A. G., Clifford S., Cioslowski J., Stefanov B. B., Liu G., Liashenko A., Piskorz P., Komaromi I., Martin R. L., Fox D. J., Keith T., Al-Laham M. A., Peng C. Y., Nanayakkara A., Challacombe M., Gill P. M. W., Johnson B., Chen W., Wong M. W., Gonzalez C., Pople J. A., Gaussian 03, Revision A.1 (Gaussian Inc., Pittsburgh PA, **2003**)

52. Lendvay G., Mayer I., *Chem. Phys. Lett.* **1998**, 297: 365.

53. Pei S., Zajac G. W., Kaduk J. A., Catal. Lett. 1993, 21: 333.

54. Bordiga S., Boscherini F., Coluccia S., *Catal. Lett.* **1994,** 26: 195.

55. Bordiga S., Coluccia S., Lamberti C., *J. Phys. Chem.* **1994**, 98: 4125.

56. Bordiga S., Damin A., Bonino F., Zecchina A., Spanó G., Rivetti F., Bolis V., Prestipino C., Lamberty C., *J. Phys. Chem. B* **2002**, 106: 9892.

57. Zicovich- Wilson C. M., Dovesi R., Corma A., *J. Phys. Chem. B* **1999**, 103: 988.

58. Damin A., Bordiga S., Zecchina A., Doll K., Lamberty C., *J. Chem. Phys.* **2003**, 118: 10183.

59. Bellusi G., Fatore V., *Stud. Surf. Sci. Catal.* **1991,** 69: 79.

60. Davis R. J, Liu Z., Tabora J. E., Wielband W. S., Catal. Lett. **1995,** 34 :101.

61. Limtrakul J., Inntam C., Truong T. N., *J. Mol. Catal. A: Chemical* 2004, 207: 137.

62. Damin A., Bordiga S., Zecchina A., Lamberty C., *J. Chem. Phys.* **2002**, 117: 226.

63. Bordiga S., Bonino F., Damin A., Lamberti C., *Phys. Chem. Chem. Phys.* **2007,** 9: 4854.

7 ALKYLATION OF BENZENE WITH ETHYLENE OVER ACIDIC ZEOLITE

Abstract

A quantum chemical investigation of alkylation of benzene with ethylene over acidic zeolites has been performed using PW91/DNP method. A 5T cluster model been used to represent the zeolie. Stepwise and concerted mechanisms of alkylation reaction of benzene with ethylene are considered. In the stepwise mechanism, ethoxide intermediate is first formed due to adsorption of ethylene on Brönsted site of zeolite followed by the reaction of ethoxide with benzene molecule to produce ethylbenzene. In concerted mechanism, alkylation of benzene takes place in single step without prior formation of ethoxide. The concerted mechanism has the activation energy in between the two activation energies of stepwise mechanism.

7.1 Introduction

Ethylbenzene is an important raw material in petrochemical industry for the manufacture of styrene, which is one of the most important industrial monomers. Worldwide capacity of ethylbenzene production is about 23 million metric tons per year.[1] Conventional methods for industrial production of ethylbenzenes follow the Friedel-Crafts alkylation reaction with $AlCl_3$ or supported H_3PO_4 as catalysts. Unfortunately, these commercial processes present serious ecological problems such as corrosion and disposal of spent harmful catalysts. Now-a-days zeolite-type catalysts mostly replace the aluminum halides, as they offer environmental and economical advantages. The microporous structure of zeolites provides large internal surface area and most important selectivity effects are related to diffusion of reactants and products inside the pore and steric constrains of transition states. In alkylation of benzene, zeolite based catalysts also offer additional advantage to suppress formation of undesired diisopropylbenzenes, n-propylbenzenes and chlorinated products. Experimentally these reactions have been studied extensively.[2-7]

From industrial point of view, elucidation of reaction mechanism of benzene alkylation on zeolite catalysts is of great interest. However, the reaction mechanism of alkylation of aromatics with short-chain olefins on zeolites is not yet clearly understood. Venuto *et al.*[8] and Weitkamp[9] suggested that alkylation of benzene with ethylene over acidic faujasite and ZSM-5 zeolites followed Eley–Rideal mechanism. Corma *et al.*[10] reported the Eley–Rideal mechanism for alkylation of benzene with propylene over MCM-22. While the Langmuir–Hinshelwood mechanism of alkylation of benzene with short-chain olefins has also been reported.[11,12] Recently, Smirniotis and Ruckenstein [13] suggested that the size of the pores of zeolites in combination with the size of the aromatics and the alkylating agents could regulate the alkylation mechanism. In case where the size of the aromatic molecule is comparable to

the pores of the zeolite, alkylation proceeds via the Langmuir–Hinshelwood mechanism. For large-pore zeolites such as faujasite and beta zeolites, alkylation occurs via the Eley–Rideal mechanism. To understand the reaction mechanism, theoretical studies can offer a practical tool that provides insight to the reaction mechanism complementing experimental investigations or, in certain cases, offer an understanding that is not possible by experimental investigations. Numerous theoretical models, including the periodic calculations, have been proposed to study the crystalline zeolites.[14-20] The large number of atoms present in the unit cell of zeolites makes the use of periodic *ab initio* calculations computationally too expensive and even impractical when very large zeolites are concerned. Therefore, electronic properties of zeolites are usually modelled with quantum chemical methods for relatively small clusters where only the most important part of zeolites is focused.[21,22] It has been proved that the course of acid zeolite catalysed reactions can be studied qualitatively using cluster approximations.[23,24] The cluster approach is well-suited to describe local phenomena such as interactions of molecules with active sites or bond breaking and bond formation processes which allows use of high quality theoretical methods on it. Limtrakul *et al.*[25], in their recent studies, investigated reaction mechanism of ethylation of benzene over acidic faujasite zeolites using quantum chemical methods. Clark *et al.*[26] calculated the overlap between Fukui functions of the aromatic and the electrophilic alkyl group as a measure for the tendency of electrons to transfer from the aromatic to the alkyl group. This gives an indication for the probability of reaction.

In this work, density functional calculations were performed to study stepwise and concerted mechanism of alkylation of benzene with ethylene on a 5T cluster of acidic zeolites.

7.2 Computational Details

5T model cluster were taken from the lattice structure of fauzasite to represent active site of the zeolite. Central silicon atom in the zeolite cluster is substituted by an aluminum atom, and a proton is added to one of the oxygen atoms bonded directly to the aluminum atom to preserve electrostatic neutrality. The dangling bonds are saturated with hydrogen atoms. All geometry optimizations were performed without imposing any geometrical constrain. During the geometry optimizations, we look for a local minimum for reactants and products and for a first order saddle point for transition structures. On stationary states, vibrational frequencies were calculated to ensure that the obtained structures have correct number of imaginary frequencies: none for minima and one for transition structures. All calculations were carried out with DMol3 program package, using PW91 functional and DNP basis set.

7.3 Results and Discussion

7.3.1 Alkylation of benzene with ethylene

We performed DFT calculation to study the reaction mechanism of ethylation of benzene with acidic zeolites. The reaction can be considered to occur either by stepwise mechanism or concerted mechanism. In this work thermodynamics of these two mechanisms for the reaction is studied.

7.3.1.1 Stepwise mechanism for benzene alkylation with ethylene

In this pathway, ethylene molecule is initially adsorbed on the acidic site of the zeolite, and an ethoxide intermediate is formed. Subsequently, involves the interaction of benzene with ethoxide intermediate, ethoxide leave the zeolite wall and a C—C bond is formed, resulting in the formation of ethylbenzene adsorbed on acidic zeolite. Figure 7.1 and Figure 7.2 show the stationary points for the formation of ethoxide from ethylene and reaction of

ethoxide intermediate with benzene, respectively. The selected geometric parameters of ethoxide intermediate formation and its reaction are summarized in Table 7.1. The interaction of ethylene double bond with Brönsted acid site of zeolite results in the formation of π- complex. Due to adsorption of ethylene molecule on zeolite, minor changes of geometrical parameters are noticed. It is seen from Table 7.1 that the acidic O_1—H_1 bond distance is increased from 0.97 to 0.99Å and C—C double bond distance of ethylene increases from 1.33 to 1.34Å. This increase of bond distances indicates that adsorption of ethylene molecule on acidic zeolites weakens the C—C double bond and O_1—H_1 bond. A smaller deviation of Si_1—O_1—Al and Si_2—O_2—Al bond angles are also noticed on adsorption of ethylene molecule. The adsorption energy of -7.08 kcal/mol is calculated for adsorption of ethylene molecule on acidic zeolite. Namunangruk *et al.*[25] reported an adsorption energy of -8.73 kcal/mol using ONIOM method. In the transition state for ethoxide formation, the acidic proton is about halfway between the zeolite oxygen atom (O_1) and ethylene carbon atom (C_2). Simultaneously, the other carbon atom (C_1) of ethylene is moving closer to another zeolite oxygen atom (O_2) and hence, the C_1—O_2 bond of ethoxide is formed. At the transition state one imaginary frequency of -583 cm^{-1} is obtained which corresponds to movement of zeolite proton towards ethylene carbon (C_2) atom while C_2—C_1 bond is increased from 1.34 to 1.41Å and carbon C_1 is moving towards zeolite oxygen atom O_2 to form a covalent bond. The activation energy for the protonation of ethylene is found to be 21.52 kcal/mol and apparent activation energy for this step is 14.44 kcal/mol. The activation energy as well as apparent activation energies reported by Namunangruk *et al.*[25] are higher than that of our resulsts (30.6 and 21.33 kcal/mol, respectively).

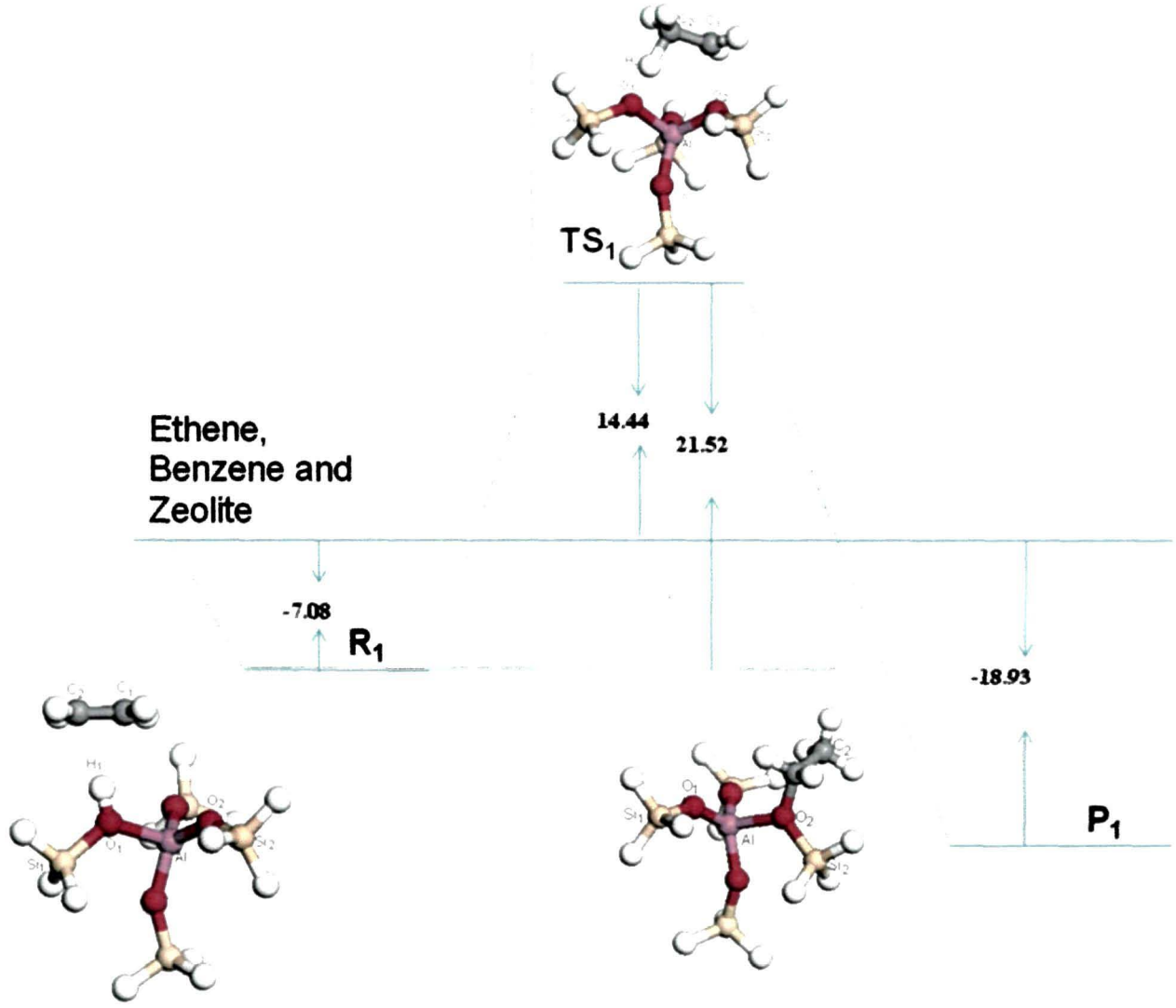

Figure 7.1: Energy profile diagram for the first step of the stepwise mechanism of ethylation of benzene.

However, the activation energy reported by Svelle *et al.*[27] (23.18 kcal/mol) is in reasonable agreement with the activation energy calculated in this work. On formation of ethoxide, a significant geometrical change of the zeolite cluster is noticed. The Al—O_1 bond distance is decreased from 1.93 to 1.72Å, while Al—O_2 distance increased from 1.72 to 1.93Å (Table 7.1). The Si_1—O_1—Al and Si_2—O_2—Al angles are also change significantly due to the formation of ethoxide.

In the next step, benzene is adsorbed on zeolite cluster next to ethoxide group, interacting with the cluster as well as ethoxide.

Table 7.1: Optimized geometrical parameters of ethane adsorption, transition state and alkoxide intermediate. Distances are in Å and angles are in degrees

Parameters	Isolated cluster	Adsorption complex (R_1)	Transition state (TS_1)	Products (P_1)
AlO_1	1.95	1.93	1.83	1.72
AlO_2	1.72	1.72	1.80	1.93
O_1H_1	0.97	0.99	1.38	4.41
H_1C_2	----	2.22	1.28	1.10
H_1C_1	----	2.20	2.14	2.16
C_1C_2	----	1.34	1.41	1.51
Si_1O_1Al	121.2	123.2	128.8	150.0
Si_2O_1Al	150.5	149.3	128.7	119.0

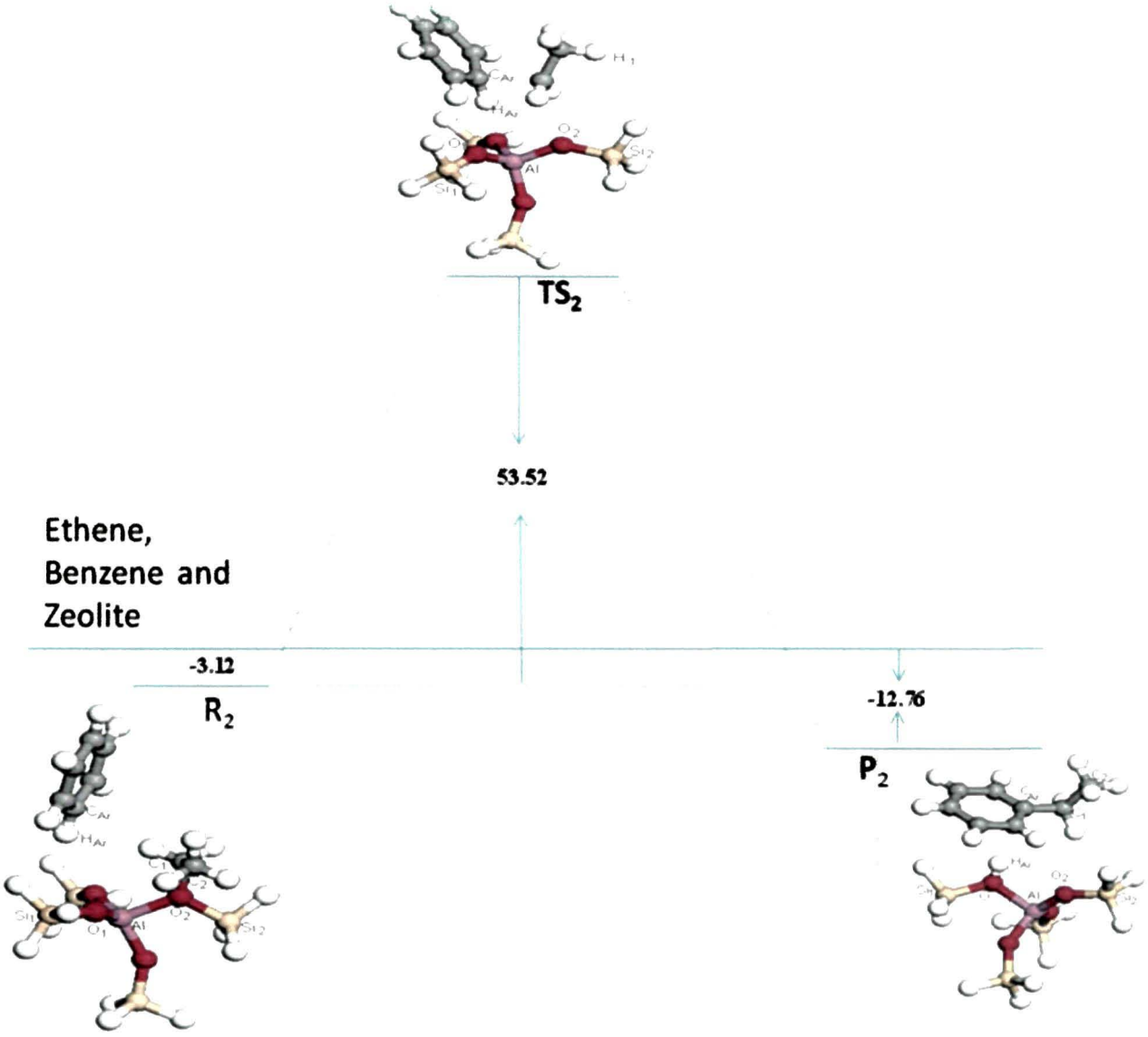

Figure 7.2: Energy profile diagram for the second step of the stepwise mechanism of ethylation of benzene.

The energy profile diagram of benzene adsorption on ethoxide is shown in Figure 7.2, and selected geometrical parameters are listed in Table 7.2. The transition state of ethylation of benzene involves formation of new C—C bond between ethoxide carbon (C_1) and benzene carbon (C_{Ar}) and cleavage of C_{Ar}—H_{Ar} bond, giving the proton back to zeolite framework oxygen. The O_2—C_1 bond, which connects the ethoxide with the cluster, is gradually

stretched and at the same time C_1 moves closer to C_{Ar} carbon of benzene. The activation energy for the step in which new C—C bond is formed is calculated to be 53.52 kcal/mol. This value is higher than that of the corresponding energy reported by Namunangruk *et al.*[25]

Table 7.2: Optimized geometrical parameters of benzene-alkoxide adsorption complex, transition state and product adsorbed ethylbenzene. Distances are in Å and angles are in egrees.

Parameters	Adsorption complex (R_2)	Transition state (TS_2)	Products (P_2)
AlO_2	1.92	1.78	1.73
AlO_1	1.73	1.79	1.94
O_2C_1	1.48	2.85	3.87
C_1C_2	1.51	1.48	1.54
C_1C_{Ar}	3.97	2.38	1.51
$C_{Ar}H_{Ar}$	1.09	1.12	2.53
$H_{Ar}O_1$	2.55	1.85	0.99
Si_1O_1Al	144.8	146.0	122.1
Si_2O_1Al	118.6	140.2	146.0

7.3.1.2 **Concerted mechanism for benzene alkylation with ethylene**

In the one step mechanism, ethylene and benzene molecules are co-adsorbed on acidic zeolite without the formation of ethoxide intermediate. The energy profile of the concerted reaction is shown in Figure 7.3 and the selected geometrical parameters of the reactant, product and the transition state are presented in Table 7.3. The reaction is initiated by co-

adsorption of benzene and ethylene at the acid site of the zeolite. The acidic proton of zeolite is in interaction with π - electrons of ethylene. In the co-adsorbed reactant, the ethylene is adsorbed on the acidic site and the benzene is adsorbed edge on. When the proton attacks C_2 carbon of ethylene molecule, the C_1atom becomes electron deficient and thus undergoes an electrophilic attack with benzene. The co-adsorption energy evaluated for the reaction, 10.06 kcal/mol, is slightly higher than the values reported by Vos *et al.*[28] and Arstad *et al.*[29] (7.3 and 7.8 kcal/mol, respectively). The energy difference might be due to different geometries of the adsorbed state. However, the adsorption energy reported by Namunangruk *et al.* [25] is higher than the values reported in this study.

It is seen from Table 7.3 that no substantial deformation of the zeolites cluster is noticed on co-adsorption of ethylene and benzene. In the adsorption complex the C_2—H_1 and C_1—H_1 distances are found to be 2.22 Å. The benzene H-atom (H_{Ar}) that is closest to zeolite cluster is 2.60 Å far from the oxygen (O_2) atom. This is in agreement with the empirically known van der waals radii of the two atoms. In the transition state, the acidic proton H_1 attacks an ethylene carbon atom C_2, and simultaneously, the other ethylene carbon C_1 starts forming a bond with benzene carbon atom C_{Ar}. In the transition state O_1H_1 distance is elongated from 0.99 to 1.62Å. The C_1—C_2 distance increases from normal double bond distance 1.34 to 1.43 Å, and C_1—C_{Ar} distance changes from the noninteracting distance 3.92 to 2.17Å. This distance is much longer than the normal C—C double bond, but within the van der Waals distance. However, structure of benzene molecule does not significantly differ from that of the co-adsorbed structure except that the distance between H_{Ar} and O_2 atoms. In the transition state, slight deviation of the structure of the zeolite cluster is noticed. The Al—O_1 (1.81 Å) distance is found almost equal to Al—O_2 (1.77Å). The transition state structure obtained in this study is similar to that reported by Arstad *et al.*[29] and

Table 7.3: Optimized geometrical parameters of isolated cluster, adsorption complex, transition state and products of concerted reaction of ethylation of benzene. Distances are in Å and angles are in degrees.

Parameters	Adsorption complex	TS	Products
AlO_1	1.93	1.81	1.73
AlO_2	1.73	1.77	1.93
O_1H_1	0.99	1.62	2.88
H_1C_2	2.22	1.16	1.10
H_1C_1	2.22	2.30	2.19
C_1C_2	1.34	1.43	1.53
C_1C_{Ar}	3.92	2.17	1.51
$C_{Ar}H_{Ar}$	1.09	1.11	2.64
$H_{Ar}O_2$	2.60	2.47	0.99
Si_1O_1Al	122.3	139.5	144.9
Si_2O_1Al	143.3	137.4	122.3

slightly different from values reported by Vos *et al.*[28] in which the acidic proton is completely attached to the ethylene molecule (C_2—H_1 distance is 1.09Å) and the distance between acidic proton (H_1) and nearest oxygen atom (O_1) on zeolite is 3.69Å. In this work, the corresponding distances are 1.16 and 1.62 Å. However, C_1—C_{Ar} distance is found to be 2.17Å which is closer to the value of Vos *et al.*, (2.12 Å) but smaller than that reported by Arstad *et al.* (2.39Å).

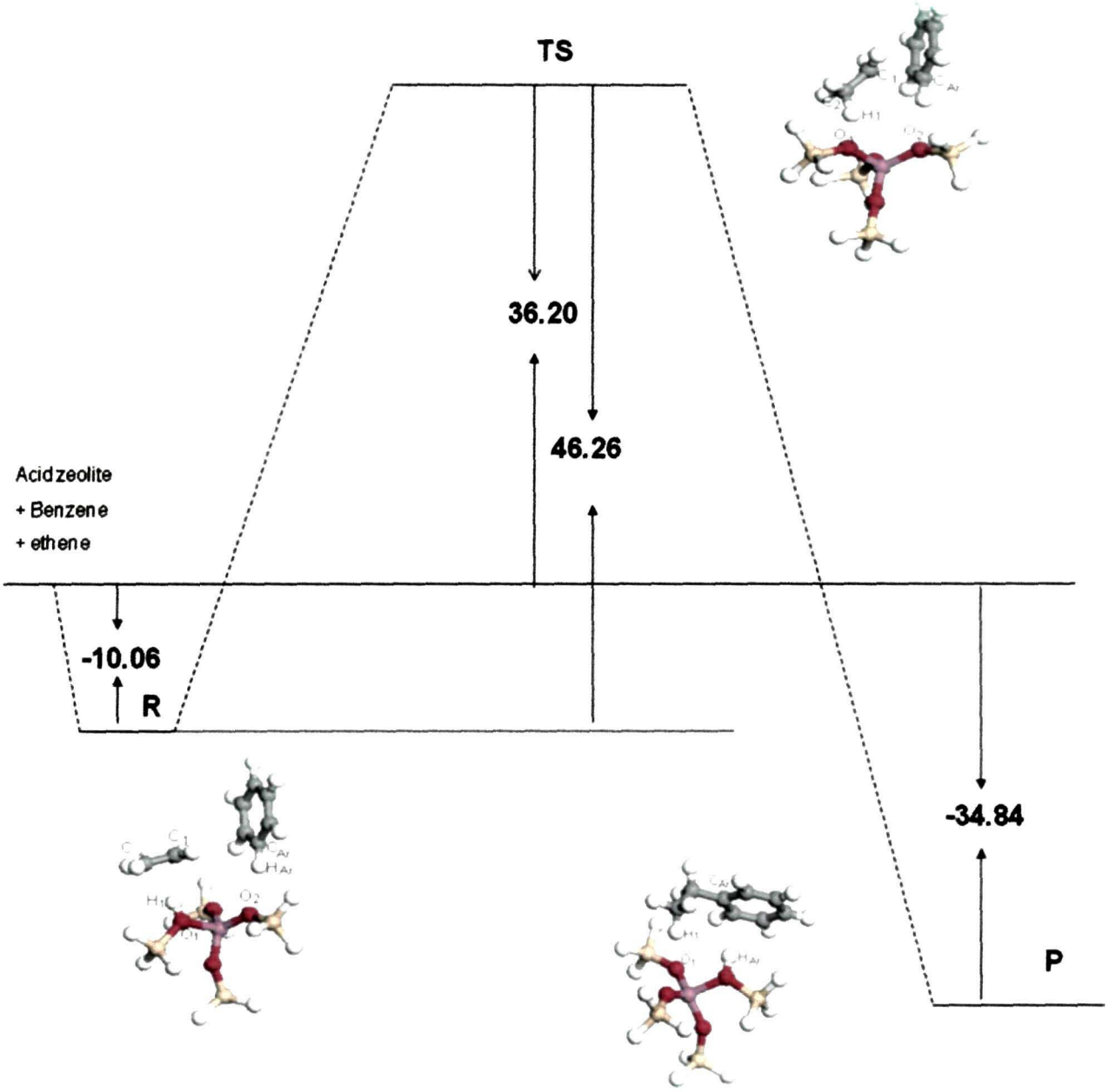

Figure 7.3: Energy profile diagram for the concerted mechanism of ethylation of benzene.

The activation energy for this reaction is calculated to be 46.25 kcal/mol. This energy is higher than the corresponding value reported by Vos *et al.* [28] (31.6 kcal/mol), Arstad *et al.* [29] (31.3 kcal/mol) and Namunangruk *et al.* [25] (33.41 kcal/mol). The reaction ends when the bond between ethyl fragment and benzene is formed (C_1—C_{Ar} =1.51Å) and benzene releases a proton, H_{Ar}, (C_{Ar}—H_{Ar}= 2.64Å) which form a bond with a bridging oxygen atom, O_2, of the

cluster (H_{Ar}—O_2=0.99Å). Ethylbenzene is now adsorbed on an acidic site of the zeolite cluster. The adsorption energy of ethyl benzene on acidic zeolite is -34.82 kcal/mol. The adsorption energy of ethylbenzene reported by Namunangruk *et al.* [25] is close to the value presented in this study.

7.3.2 **Concerted versus stepwise mechanism for benzene alkylation with ethylene**

The first barrier of the stepwise mechanism (formation of ethoxide) is lower than the single barrier of the concerted mechanism, whereas the second barrier of the stepwise mechanism is considerably higher than that of the concerted mechanism. In the stepwise mechanism, the ethoxide formation has smaller activation energy of 21.52 kcal/mol and the reaction between ethoxide intermediate with benzene has the activation energy 53.52 kcal/mol, which is the rate determining step. However, the activation barrier for the concerted mechanism is 46.25 kcal/mol, which is in between the barriers of the stepwise mechanism. With this in mind, one could argue that concerted mechanism should dominate the overall ethylation reaction. However, the stepwise mechanism could also contribute significantly, because activation energy for ethoxide formation is relatively low, hence, ethoxide forms easily. Thus every acidic site of the zeolite is occupied by an ethoxide in the first step of two-step mechanism blocking the route for concerted mechanism. Once the ethoxide intermediate is formed, the stability of the adsorbed benzene ethoxide adduct makes the reverse reaction more difficult and thus leads the formation of ethylbenzene.

7.4 Conclusion

The ethylation of benzene over acidic zeolite has been investigated with 5T cluster using PW91/DNP method. Both concerted (simultaneous protonation and C—C bond formation) and stepwise (via ethoxide formation) mechanism have been evaluated.

Formation of ethoxide has the lowest activation barrier of the investigated reaction steps. The barrier of the second step of the stepwise mechanism, i.e. C—C bond formation step, has the higher activation energy than the single barrier of the concerted mechanism. In the stepwise mechanism, ethylation starts with the protonation of the adsorbed ethylene which leads to the formation of ethoxide intermediate. The ethylation takes place due to the interaction of benzene and ethoxide intermediate. The second step is found to be the rate determining step with the activation energy of 53.52 kcal/mol. In the concerted mechanism ethylation of benzene takes place in a single reaction step with an activation energy barrier of 46.25 kcal/mol.

References

1. Degnan Jr. T. F., Smith C. M., Venkat C. R., *Appl. Catal. A* **2001**, 221: 283.

2. Keading W. W., Young B. L., Chu C. –C., *J. Catal.* **1984**, 89: 267.

3. Keading W. W., *J. Catal.* **1985**, 95: 512.

4. Cejka J., Wichterlova B., Bednarova S., *Appl. Catal.* **1991**, 79: 215.

5. Wichterlova B., Cejka J., *J. Catal.* **1994**,146: 523.

6. Ivanova I. I., Brunel D., Nagy J. B., DerouaneE. G., *J. Mol. Catal. A* **1995**, 95: 243.

7. Corma A., Martinez-Soria V., Schnoeveld E., *J. Catal.* **2000**, 192: 163.

8. Venuto P.B., Hamilton L.A., Landis P.S., *J. Catal.* **1966**, 5: 484.

9. Weitkamp J., Int. Sympos. in Zeolite Catalysis, Siofok, Hungary, *Acta Phys. Chem.* **1985**, 217.

10. Corma A., Martinez-Soria V., Schnoeveld E., *J. Catal.* **2000**,192 :163.

11. Morita Y., Matsumoto H., Kimura T., Kato F., Takayasu M., *Bull. Jpn. Pet. Inst.* **1973**, 15 (1): 37.

12. Becker K.A., Karge H.G., Streubel W.-D., *J. Catal.* **1973**, 28:403.

13. Smirniotis P.G., Ruckenstein E., *Ind. Eng. Chem. Res.* **1995**, 34:1517.

14. Shah R., Gale J.D., Payne M.C., *J. Phys. Chem. B* **1997**, 101: 4787.

15. Jeanvoine Y., Angyan J.G., Kresse G., Hafner J., *J. Phys. Chem. B* **1998**, 102: 5573.

16. Hillier I.H., *J. Mol. Struct. (THEOCHEM)* **1999**, 463: 45.

17. Limtrakul J., Jungsuttiwong S., Khongpracha P., *J. Mol. Struct.* **2000**, 525: 153.

18. Sauer J., Sierka M., *J. Comput. Chem.* **2000**, 21: 1470.

19. Sauer J., Ugliengo P., Garrone E., Saunders V.R., *Chem. Rev.* **1994**, 94: 2095.

20. J. Sauer, *Chem. Rev.* **1989**, 89: 199.

21. Limtrakul J, Chem. Phys. 1995, 193:79.

22. Limtrakul J., Treesukol P., Ebner C., Probst M., Chem. Phys. **1997**, 215:77.

23. Van Santen R. A., Kramer G., *J. Chem. Rev.* **1995**, *95*: 637.

24. Blaszkowski S. R., van Santen R. A., *J. Am. Chem. Soc.* **1997**, *119*: 5020.

25. Namuangruk S., Pantu P., Limtrakul J., *J. Catal.* **2004**, 225: 523.

26. Clark L. A., Snurr R. Q., *Stud. Surf. Sci. Catal.* **2001**, 135.

27. Svelle S., Kolboe S., Swang O., *J. Phys. Chem. B* **2004**, 108: 2953.

28. Vos A. M., Schoonheydt R. A., De Proft F., Geerling P. *J. Phys. Chem. B* **2003**, 107: 2001.

29. Arstad B., Kolboe S., Swang O., *J. Phys. Chem. B* **2004**, 108: 2300.

8 GENERAL CONCLUSIONS

Structure, reactivity and interaction of reactant molecules with the active sites of zeolites are very crucial in understanding their catalytic behaviours. These properties can only be properly described when the laws of quantum mechanics are taken into account. Currently there is growing interest in using molecular modelling techniques, based on quantum mechanics to get insights into the catalytic behavior of zeolites. The development of powerful computational techniques and their implementation in softwares, created a tool of sufficient accuracy for making quantitative predictions. The use of cluster models representing the zeolite catalyst is very popular. However, cluster models do not reflect a specific zeolites framework and neglect the long-range electrostatic interactions. In order to overcome such limitation, hybrid quantum mechanics/molecular mechanics (QM/MM) techniques have been used. With the growing computer power and development of new methods made it possible to investigate the full structure of zeolites. Therefore, complete information regarding the influence of zeolite structure can be obtained.

In this work, these techniques have been used to study the structure and reactivity of cation exchanged and isomorphously substituted zeolites. It has been a long standing issue in the field of theoretical studies on prediction of acidity and basicity of zeolites. We have investigated the effect of alkali and alkaline earth cations on structure and Lewis acidity as well as Brönsted acidity of alkali and alkaline earth cation exchanged faujasite zeolites

successfully. The strength of Lewis or Brönsted acidity depends on a number of factors including the Si—O—Al bond angles, number of next-nearest neighbour Al atoms and the presence of extraframework cations. Location of alkali and alkaline earth cation with respect to zeolite framework depends on ionic radius of the cation. With increasing ionic radii of cations, they move away from plan of the 6T ring.

In this thesis, we have presented Lewis as well as Brönsted acidity of cation exchanged and isomorphously substituted zeolites using DFT based global (chemical potential, chemical hardness and electrophilicity index) and local (Fukui function and relative electrophilicity) reactivity descriptors. These reactivity indices are well suited to predict Lewis and Brönsted acidity of cation exchanged and isomorphously substituted zeolites. For the first time we have successfully reproduce the experimentally observed Brönsted acidity sequence of mixed form of zeolites containing both proton and alkali or alkaline earth cations as charge compensating cations.

A systematic investigation has been carried out to elucidate the structure and location of Ti, Zr and Sn in MFI framework. Substitution energies of Ti, Zr and Sn for Si were evaluated performing DFT calculation on a 10T cluster for each site. The geometrical parameters around TO_4 moiety are in agreement with some experimental data. Calculated substitution energy values revealed that distribution of Ti, Zr or Sn in MFI framework is nonrandom. The calculated substitution energies of Ti, Zr and Sn for Si in MFI framework at different T sites suggest that location of Ti, Zr and Sn atoms in MFI framework is energetically favorable at T4, T8 and T10 sites.

To understand the mechanism of TS-1 catalyzed reactions, it essential to know the adsorption behaviour of small probe molecule on it. We have applied cluster as well as ONIOM methods to study the adsorption of small molecules *viz.* water, hydrogen peroxide,

methanol and ammonia on TS-1. On adsorption of small molecule on Ti-zeolite, local geometry of the cluster changes significantly.

Cluster calculations on geometry of the interacting molecules along with reaction path provide insight into the reaction mechanism. In case of ethylation of benzene with ethylene two path ways are possible. Concerted mechanism, where benzene and ethylene react together and in stepwise mechanism where ethylene is first converted to ethoxide intermediate which react with benzene to produce ethylbenzene. The stepwise mechanism has higher activation energy than concerted mechanism.

List OF PUBLICALTIONS

1. **Reactivity of α, β-Unsaturated Compounds Towards Nucleophilic Addition Reaction: a local Hard-Soft Acid-Base Approach**

   Paritosh Mondal, Kalyan Kr. Hazarika and Ramesh C. Deka, *Phys. Chem. Comm.* **2003**, 6: 24.

2. **Quantum chemical studies on acidity of isomorphously substituted ZSM-5 zeolite**

   Paritosh Mondal, C. Arunabhiran, K. K. Hazarika and R. C. Deka, *Bull. Catal. Soc. Ind.* **2004**, 6: 82.

3. **Structure and stability of titanium atoms in TS-1 zeolite using density functional theory.**

   Paritosh Mondal and R. C. Deka, *Bull. Catal. Soc. Ind.* **2007**, 6: 151.

4. **Density functional studies on Lewis acidity of alkaline earth metal exchanged faujasite zeolite.**

   Paritosh Mondal, K. K. Hazarika, A. Deka and R. C. Deka, *Molecular Simulation* **2008.**

5. **Density functional studies on the Brönsted acidity of alkali cation exchanged faujasite zeolite.**

   R. C. Deka, **Paritosh Mondal**, A. Deka, A. Miyamoto, *Micropor. Mesopor. Matterial.(Communicated)*

6. **Density functional studies on the Brönsted acidity of alkaline-earth cation exchanged faujasite zeolite.**

   Paritosh Mondal, R. C. Deka, *J. Mol. Catal. A* (Communicated)

7. **Structure, location and reactivity of Titanium and Tin in MFI zeolite: A density functional study.**

   Paritosh Mondal and R. C. Deka, *Catal. Lett. (Communicated)*